Flood Fragility of a Cavity Wall

experimental results on the deformations of a window-featured cavity wall due to hydrostatic flood actions and failure of the window-wall interface

M. van Haren

Report

Technische Universiteit Delft

Flood Fragility of a Cavity Wall

experimental results on the deformations of a window-featured cavity wall due to hydrostatic flood actions and failure of the window-wall interface

by

M. (Mick) van Haren

In partial fulfilment of the requirements for the degree of

Master of Science
in Hydraulic Engineering

at the Delft University of Technology,
to be defended publicly on Monday December 13, 2021 at 15:45 UTC+1.

Thesis committee

Chairman	Dr. ir. J.D. Bricker	TU Delft
Mentor	Ir. P.A. Korswagen	TU Delft
	Prof. dr. ir. J.G. Rots	TU Delft
	Ir. G.W.F. Rongen	TU Delft
	Prof. dr. ir. S.N. Jonkman	TU Delft

Student number: 4380673
Department of Hydraulic Engineering
Faculty of Civil Engineering and Geosciences
Delft University of Technology

An electronic version of this thesis is available at `http://repository.tudelft.nl/`.

Acknowledgment cover: Victor van Breukelen, January 2018 Dordrecht

TU Delft

Preface

When my grandmother was still an infant, her hometown Dreumel suffered a major flood event. A dike breach upstream of the Maas river acted as an inlet; allowing the water to rapidly cover vast areas of the region known as 'Land van Maas en Waal'. Although the damages were minor, my grandmother's house still was flooded for a great period of time. The water was present for so long even, that her father felt he should not have to pay rent for the period his family could not live in the residence. This not only shows the financial creativity of my great-grandfather but also his accepting view on the situation.

Living in a river-dominated area the threat of flooding is present every year and it is only due to engineering that such flood events are now labelled as 'uncommon' or even 'rare'. While for most people it seems like standard practice, I certainly am still amazed by the level of security that is provided by the Dutch dikes and dunes.

During her life, my grandmother witnessed, among other things, the construction of the Afsluitdijk, the Amsterdam-Rijnkanaal, and the Deltawerken; all improving the flood risk for the better. In that same period, however, the environment started changing for the worse. The field of flood risk is, therefore, no static subject; full security can never be guaranteed and the probability of a flood event is never zero.

I am very grateful to have had the opportunity to study and contribute to this fascinating field; adding a small piece of new information to the ever-growing understanding of the flood fragility of modern residences and, hopefully, resulting in even better mitigation strategies for people, so that during the unfortunate event of a flood, their only concern would be the rent as well.

Enjoy reading!

M. van Haren
Delft, November 2021

Abstract

Because of the fortunate absence of great flood events in The Netherlands during the second half of the twentieth century, no physical data was added to the structural understanding of flood fragility on walls. Considering that during the same period the cavity wall became standard in the construction of houses, a certain inconsistency can be recognized between the expected and observed (structural) behaviour of a modern wall during flood events. Nevertheless, failure, or collapse, of residential buildings is included in the Dutch flood protection standards as an important cause of damage and one of the main reasons for loss of life. It is generally believed that the developments in terms of building materials translate to a safer residence i.e. less prone to flood actions. This consensus is also found in the trade-off for certain mitigation measures, especially in areas where horizontal evacuation is difficult. An improved understanding of the flood fragility of a modern cavity wall is thus needed to prove the general consensus or to adjust the current mitigation measures to comply with the allowed fatality risks.

A window-featured cavity wall section was constructed at the Flood Proof Holland facility, using calcium silicate bricks, fired clay bricks, and a weaker mortar to partly account for the virgin effect of any newly-built wall. Both inner and outer walls were connected with adequate wall ties. The wall section was subjected to several hydrostatic pressures at both sides. These experiments were performed to physically grasp the deformations corresponding to certain flood scenarios affecting cavity wall sections from ordinary terraced houses. Additionally, the effect of the window was investigated; both on the stability and its contribution to the water height inside a residence.

The experimental data was used to find specific characteristics, which allowed an analytical model to extrapolate the data and find water level combinations that imply failure. To account for the window gap inside the wall, part of the model was featured with lower stiffness. The model gave sufficient results but also showed difficulties for small head differences (< 0.2 m). A second model was created with DIANA FEA to investigate the non-linear behaviour. Both models showed similar results for the linear analysis but with the notion of non-linearity, the finite element model showed failure for lower water levels. As the experiment failed to generate data for the wall ties it was chosen to assign scenarios, or boundaries, in which the wall ties would form (A) a perfect bond between the walls or (B) a poor connection between the walls (but a connection nonetheless).

Computations showed that the cavity wall in a one-way bending configuration starts to show significant cracks between 1.3 and 1.6 meters of outside water level. Because of the brittleness of the masonry, this would imply failure. It was further found that the non-linear deformations would reach 4 millimeters. Considering that for these water levels the internal moments were still far from their maximum capacity, the results suggest that failure occurred due to cracks that were forced to form because of the deformations. This indicates that modern cavity walls are still quite vulnerable for floods and their flood actions. The influence of the hydrostatic pressure, however, can be decreased considerably by a water level inside the residence that acts as a counter force. Contrary to what was expected, the window does not contribute to this inside water level, since its leakages turn out to be negligible. To keep the damages to a minimum and preserve the overall stability, it is advised to seal the residence to a height of 1.0 meter; floods that exceed this sealing should not be countered anymore and rather be allowed to enter the residence.

Samenvatting (Dutch)

Door het uitblijven van grote overstromingen in Nederland tijdens de tweede helft van de twintigste eeuw, is er geen hernieuwde data toegevoegd aan het inzicht in de structurele werking van bakstenen muren ten tijde van een overstroming. Daar komt bij dat in diezelfde periode de spouwmuur werd geintroduceerd in de woningbouw. Hierdoor is er een verschil ontstaan tussen de verwachting en de daadwerkelijke afloop wanneer een moderne spouwmuur wordt blootgesteld aan een overstroming. Desalniettemin, is het falen (en instorten) van woningen ingebed in de Nederlandse overstromingsaanpak en wordt het gezien als een van de meest belangrijke oorzaken van schade en slachtoffers. Er wordt algemeen aangenomen dat de ontwikkelingen in de bouw hebben bijgedragen aan een betere weerstand tegen overstromingen. Dezelfde aanname is terug te vinden in de evacuatie strategie: vooral in grote steden waar evacuatie moeilijk is, worden mensen veiliger geacht in hun woning. Een beter begrip van de huidige kwetsbaarheid van spouwmuren is nodig om, ofwel deze consensus te bewijzen, of de evacuatie strategieën aan te passen zodat weer voldaan kan worden aan de afgesproken risico niveaus.

Daartoe is een levensgrote spouwmuur gebouwd in een basin van Flood Proof Holland. De muur is gebouwd met een kalkstenen binnenmuur en een bakstenen buitenmuur en uitgerust met een raam. De mortel is opzettelijk van lagere kwaliteit om een muur na te bootsen die al langer bestaat. Verder zijn de muren verbonden met meerdere muurankers. De muur is vervolgens blootgesteld aan verschillende waterstanden om op die manier de vervormingen te kunnen meten. Daarnaast is er gekeken naar het effect dat het raam op de stabiliteit heeft en of het raam bijdraagt aan het water dat zich in huis verzamelt.

De verkregen data is gebruikt om karakteristieken van de muur te vinden, die vervolgens zijn toegepast in een analytisch model dat in staat is om vervormingen, toebehorend aan hogere waterstanden, te benaderen. Zwakkere eigenschappen zijn toegekend aan het gedeelte van de muur waar het raam zich bevindt. Hoewel het analytische model aanvaardbare resultaten gaf, bleek het model voor kleine waterstandsverschillen af te wijken van de data. Een tweede model werd gemodelleerd met het DIANA FEA programma om de non-lineaire eigenschappen te onderzoeken. Beide modellen gaven vergelijkbare resultaten voor de lineaire analyse, maar bij de non-lineaire analyse bleek de muur zwakker. Doordat het experiment niet in staat bleek de werking van de muurankers te meten, is er voor gekozen om dit te benaderen met scenarios waarin (A) de ankers een perfecte connectie vormen tussen beide muren en (B) waarin deze connectie geen krachten overdraagt.

Resultaten tonen aan dat de spouwmuur, die niet is ingeklemd aan de zijkanten, scheuren begint te vertonen voor waterstanden tussen 1.3 en 1.6 meter. Door de brosheid van de mortel zullen dergelijke scheuren snel leiden tot instorting. Daarnaast bleken (non-lineaire) vervormingen tot een afstand van 4 millimeter te reiken. De weerstandscapaciteit van de muur is voor bovengenoemde waterstanden nog lang niet bereikt; wat suggereert dat het faalmechanisme een gevolg is van de scheuren die gedwongen ontstaan zijn door de vervormingen. Bovenstaande doet vermoeden dat spouwmuren nogsteeds kwetsbaar zijn voor overstromingen. Om schades in huis tot een minimum te beperken wordt dan ook aangeraden om het water alleen tegen te houden voor waterstanden onder de 1.0 meter. Boven deze limiet doet men er goed aan het water (deels) binnen te laten zodat het (inwaards) drukkende effect van het water afneemt.

List of symbols, terms, and abbreviations

A_b	Bottom surface	$[m^2]$
C_D	Drag coefficient	[-]
C_p	Pressure coefficient	[-]
E	Young's modulus of elasticity	$[MPa]$
f	Water depth	$[m]$
f_b	Brick strength	$[MPa]$
f_m	Mortar strength	$[MPa]$
f'_m or f_c	Masonry compression strength	$[MPa]$
f_{tx}	Tensile strength in standard directions (1,2,3)	$[MPa]$
f_w	bond strength	$[MPa]$
f_{x1}	vertical flexural strength	$[MPa]$
$F_{buoyancy}$	Buoyancy force	$[N]$
g	gravitational force	$[m/s^2]$
G_{f-t}	Tensile fracture energy	$[N/mm]$
$h_T(t)$	Head difference	$[m]$
H	Water height	$[m]$
H_1, $H_{outside}$	Outside water level	$[m]$
H_2, H_{inside}	Inside water level	$[m]$
ΔH	Head difference	$[m]$
I	Moment of Inertia	$[mm^3]$
K	Masonry haracteristic	[-]
M_R	(internal) Resisting moment	$[Nm/m]$
$p_{\gamma,c,t}$	Probability of car collision or tree collision	[-]
$p_{\varphi,c,t}$	Probability of a floating car (or tree) intersecting with a structure	[-]
P	Pressure from flood action x	$[Pa]$
Q_x	Inflow of water through ..(box, casi wall, or clay wall)	$[m^3/s]$
t	Thickness of structure	$[mm]$
t	Time	$[s]$
$u_T(t)$	Efflux velocity of a fluid	$[m/s]$
v	Flow velocity	$[m/s]$
α	Rotation of a building, masonry characteristic	$[circ]$, [-]
β	Masonry characteristic	[-]
γ_m	partial factor for masonry	[-]
δ	Deformations	$[mm]$
Δ	Beam's deflection along the x-axis	$[mm]$
$\eta_{c,t}$	Availability of a car (or tree) in the area of a flood	[-]
ρ_w	Density of (fresh) water	$[kg/m^3]$
σ_v	Compressive stress in vertical direction	$[MPa]$
Ca	Calcium	Element
Fe_2O_3	Iron(III)oxide	Element
SO_4^2	Sulfate	Element

Translated terms

English equivalent	*Dutch equivalent*
Additional framework	Spouwlatten
Brick indication E	Element
Brick indication L	Lijmblok
Brick indication M	Metselblok
Brick indication V	Vellingblok
Code of regulations	Bouwbesluit
Delta Works	Deltawerken
Horizontal mortar joint	lintvoeg
New standard instructed requirement	Modelbouwverordening
Poor insulation execution	Valse spouw
Rail	Raamdorpel
Secondary framing	Stelkozijn
Semi-detached	Twee-onder-een-kapwoning
Sill	Waterslagen (keramieke vensterbanktegels)
Stretcher bond	Halfsteenverband
Terraced houses	rijtjeshuizen
Thread	schroefdraad
Weep hole	Stootvoeg

Abbreviations

CaSi	Calcium silicate
CoV	Coefficient of Variance
DF	Standard big dimensions
FEA	Finite Element Analysis
FEM	Finite Element Modelling
FPH	Flood Proof Holland
IQR	Inter Quartile Range
LVDT	Linear Variable Differential Transformers
NL	Non linear
NPR	Nederlandse PraktijkRichtlijn
RMSE	Root Mean Square Error
SLS	Serviceability Limit State
ULS	Ultimate Limit State
VF	Vecht dimensions
WF	Waal dimensions

Contents

1 Introduction

On January 31st, 1953, the biggest flood disaster of The Netherlands in the twentieth century marked the beginning of new flood policies [31]. Apart from the construction of the well-known Delta Works (Dutch: Deltawerken) and the necessary improvements on dikes, attention was also given to measurements that should reduce the possible damages. Since then, the flood risk assessment in The Netherlands gradually evolved. New definitions of risk were established and not only prevention, but also mitigation, and evacuation became intertwined in the new flood risk assessment.

Exactly 42 years later, on January 31st, 1995, the Dutch rivers started rising quickly. On that day alone, 80.000 people were evacuated from the Rivierenland area and brought to safety in higher elevated cities [41]. The dikes endured nonetheless. Despite the great number of evacuations, not everyone was willing to leave and especially older people refused.

1.1. Problem statement

If the dikes would have breached, a high inflow of water would have led to devastating results. Especially in such regions that are situated at a lower elevation than the river or sea, the area will quickly fill like a bathtub without a direct outlet. Also in other regions, fatalities in the zone with high rise rates can be significant [27]. In The Netherlands, both types of regions are common, with a great number of cities situated below mean sea level.

With this in mind, mortality functions were established to calculate the number of possible casualties within individual 'zones'; each zone defined by its own rise rate and flow velocity.

These functions help give a better sense of the consequences and therefore allows for more decisive ways to mitigate those events; defining the trade-off between horizontal evacuation or vertical evacuation. In densely populated areas, this trade-off is different than in other areas. Here, the vast majority of people can be asked to seek refuge on the next dry floor of their residence, while in rural areas horizontal evacuation might be preferred.

With the structural performance of building materials improving current buildings should be able to withstand a higher water height than before. Yet, adequate information is lacking, since no real flood event has happened in The Netherlands since 1953. Flood events abroad are not representative for the Dutch houses and are therefore difficult to interpret. Without knowing the behaviour of structural elements of modern residences against the forces of floods no clear substantiation for vertical evacuation can be made from a structural point of view.

It was already concluded that modern buildings are able to resist a significant hydrodynamic pressure by investigating the pressure coefficients [20]. By addressing these coefficients together with the hydrostatic pressure virtual damage curves could be constructed. These curves showed the structural stage of a wall as a function of flow velocity and water depth in front of the wall. For this, it was assumed (I) an inside water level of zero and (II) an inside water level equal to the water level outside [20]. The latter case showed that no critical wall stage was reached. Especially during the initial stages of a flood event, the real damage curve will lie somewhere between the two extreme cases. A water level difference will occur until the water reaches the height of a window, after which the water will quickly enter the building and the difference slowly levels out [32]. A different approach is given for coastal residences in England; here a study was performed varying the water level differences and flow velocities and found an average rise rate value of 0.005 m/s [21]. Although either approach seems reasonable, no complete experiment has been performed to investigate the rise rate inside a house, which is highly dependent on the materials used. Nevertheless, the rise rate is an important parameter that can influence the pressure distribution acting on load-bearing walls and may just be the difference between collapse or enduring of the structural element.

A window influences both the structural behaviour of the wall and plays an important part regarding the rise rate inside a house. While windows are usually constructed in walls with no direct load-bearing function, weakening or even failure of such infill walls can still undermine the stability of the residence as a whole; There is evidence that infill walls contribute to lateral stiffness and increase the energy dissipation potential and while this is investigated in the case of seismic action [29][30], one could reason this to be the case with other hazardous events as well.

1.2. Research objective

This research aims to investigate the general believe that modern residences are less prone to flood events and define the inconsistency between the expected and observed behaviour of residential buildings. On the one hand, the leakage through the wall-window interface is analysed to understand the influence on the rise rate. On the other hand, the deformations of the cavity wall itself is studied to understand the structural behaviour of this wall section. In order to do so, a life-sized cavity wall was constructed at Flood Proof Holland (FPH) and subjected to several experiments to investigate both aspects of this research.

The research objective is summarized in the research question:

How does the presence of a window affect the stability of a cavity wall during floods and how does it influences the rise rate of water inside the building?

In an attempt to answer this main research question, a number of related sub-questions are listed, making the overall research more manageable and allow for a broader perspective. Preceded by a literature study on structural aspects and configurations of a window-featured cavity wall, the subsequent questions are formulated below.

1. *What are the out-of-plane deformations of a window-featured cavity wall?*
2. *At what rate does the water infiltrate through the gap and how does the rate evolve through time?*
3. *How do the moment distributions on the walls evolve by including water levels on both sides?*
4. *How does the inclusion of both the window and the cavity influence the structural stages of the wall during a flood?*

Since there are many different design options and construction methods to create a window, it is important to address the configuration that is most common. In-depth knowledge of the construction method and mounting of the window frame allows for a solid introduction of the problem and provides a helpful focus on the research. This is studied in the first part of the research. Next, the outcomes of the hydrostatic pressure acting on the cavity wall are researched. With this, the weakening effect of the window can be quantified. In the third part, the infiltration rate is established. An approximation is made for the rise rate inside the residence by addressing the other infiltration factors. Next, the pressure distributions at both sides of the wall are calculated by approximating the water depths. In this case, there are three different water levels to address: the water level outside, the water level inside the residence, and the water level inside the cavity. In the final part, the water level difference is translated into a so-called damage curve, showing the performance of the cavity wall with window depending on the water level inside and outside.

1.3. Research scope

This project is based on Dutch houses only. It should be noted that the found results are not representative for all residences. Multiple influential parameters and material options were disregarded to find only the most representative of cases. As such, only a small percentage of Dutch modern-day houses can be recognized in the results. For other configurations, the results can be expected to slightly deviate and thus should be treated with care.

In The Netherlands, two mechanisms are thought to be the most relevant for direct damage to buildings. Failure of the walls is one of these mechanisms and results from the forces acting on the wall. The other mechanism is scour [32]. Scour on the foundation due to the flow velocity can undermine the structure and this can also lead to (partial) collapse of the building. However, this research only treats the first damage mechanism due to the boundary conditions of the experiment.

The research treats direct damages only. Damages due to other secondary factors are not taken into account completely. For instance, in time the saltwater attack will affect the brickwork by crystallization. This makes part of the bricks chip off. The same can be observed during wintertime, where freezing of wet bricks can lead to cracks.

1.4. Greater context

This research is one of the projects that is being performed to physically determine the fragility of Dutch masonry buildings against flood events. As such, it is a continuation of previous experiments. More specifically, it is an extension of the masonry wall experiments performed at FPH earlier in 2020. In these experiments, a single-leaf masonry wall was tested against hydrostatic pressure and debris impact. With the addition of a window frame and the alteration to a cavity wall, this research can help form a better understanding of the flood fragility of modern Dutch houses.

1.5. Thesis outline

In the following chapter, the literature study can be found. The information provided in this chapter was used to broaden the understanding and to define the borders that mark the flood fragility of a cavity wall. At first, the notion of flood fragility is discussed in greater detail. The literature study then treats the different elements of a (Dutch) cavity wall and window frame installation. Finally, the chapter focuses on the characteristics of masonry and the different tests needed to find the properties.

In Chapter 3, the acquired knowledge from the previous chapter is translated into a design made up of available materials. Furthermore, the experimental set-up is explained and the protocol for the experiment is treated. Next, the results obtained during the experiments are treated in Chapter 4. Here, also other observations and additional test results are discussed. The data existing of deformations and water levels is used to obtain the leakage rate through the window-wall interface.

Chapter 5 is used to explain the different wall models. The models are computed to extrapolate additional data up to the point of failure. In this chapter the results from the analytical model and the finite element model are discussed and concluding computations are shown; leading to certain water levels that imply failure. Finally, in Chapter 6, the methodology and results are discussed using the gained insight during the project. The research questions are answered and recommendations can be found forming potential new experiments.

2

Flood fragility and relevant wall properties

In The Netherlands, the use of bricks as a building material was partially driven by the fact the then-used materials were vulnerable to flames. With the cities and population growing, the damages due to large fires also increased. There are a great number of cities in The Netherlands and abroad that once got destroyed completely by such a disaster. Although bricks were already introduced long before, the prohibition to use flammable materials for houses made the use of bricks rather popular [36]. While urban conflagrations now belong to the past, numerous towns and cities are still facing an ongoing threat by nature. Often with devastating consequences, floods have been a problem of the past as well as of the present. With collapsing of buildings as one of the main causes of fatalities, the negative effect of water on a structure is indisputable.

Currently, bricks are still the most used materials for facades. In modern houses, the load-bearing function has been taken over by the inner-leaf, while the aesthetically pleasing looks and weather protection are still governed by the outer wall. It is these types of walls that should withstand the forces of the water during a flood.

This chapter introduces a literature study on flood fragility and presents the different structural elements that are used in the construction of a wall, as well as in the installation of a window frame. Rules and regulations are listed in order to design a representative wall section of a Dutch house.

2.1. Flood fragility

In The Netherlands, the method to determine the damages and fatalities due to flood is called HIS-SSM. It is a standard model that is also used to derive the safety standards of flood defences [35]. Note that insurance companies also make use of the regulations to evaluate their policies regarding flood damages. However, the economic damages are outside the scope of this research, so will not be treated here.

The method allows the number of fatalities to be calculated for every flood event, either real or simulated. Generally speaking, the fatalities that are calculated are found in individual zones that are based on characteristics like depth, rise rate, and arrival time. The zones are separated by critical boundaries and have their own thresholds:

1. Breach zone with high flow velocities
2. Zone with a high rise rate
3. remaining zone with large depths

Only causes that are directly linked to the flood event are of influence on the number of fatalities; one of which is the structural failure of buildings. With mortality defined as the fraction of fatalities divided by the total number of exposed people, it is concluded that most of the fatalities can be found in the zone with a high rise rate [27]. Especially smaller areas that are prone to a quick rise of the water i.e. subjected to a high inflow, show high mortality numbers around the 10% [27].

Where high flow velocities are normative (near the breach) the number of fatalities is far less, with some analyses even showing no fatalities [27]. This means that the specific thresholds corresponding to the breach zone are not exceeded in populated areas. It was proposed to alter the thresholds and divide the separate zones more gradually by including a fourth zone: the transition zone. This zone should define the mortality in-between the breaching zone and the zone with a high rise rate and is a linear interpolation between both existing functions. The current mortality functions can be found in Appendix A.

2.1.1. Flood actions

Floods can not only lead to fatalities, they also can do some severe damages to buildings and other structures. In fact, collapsing of buildings is one of the main causes of fatalities. Failure of the structure must therefore be prevented and insight in the 'flood actions' is needed. Flood actions can be categorised in three ranks [23]:

1. High relevance and relatively predictable: hydrostatic and hydrodynamic loading from the water inside and outside a building, and water contact due to rising of the water.
2. Varying relevance and relatively predictable: buoyancy
3. Varying relevance and difficult predictability: capillary rise, debris, waves, turbulence, erosion, and chemical-, nuclear-, and biological actions.

It goes without saying that some of these actions are depending on the location, having a high uncertainty, while others are not.

General assessment

Generally, damages are mostly regarded as a consequence of the first category. While the rising of water is assumed to be slow, meaning no significant height difference inside and outside, the hydrostatic and hydrodynamic forces that act upon a building are assumed to be the dominant effect for damages. Indeed, this becomes clear when looking at the division proposed by Clausen [10].

1. Inundation damage when $v < 2$ m/s or $f \cdot v < 3$ m^2/s
2. Partial damage when $v > 2$ m/s **and** 3 m^2/s $< f \cdot v < 7$ m^2/s
3. Total destruction when $v > 2$ m/s **and** $f \cdot v > 7$ m^2/s

Note the similarity between the last class and the criteria belonging to the breach zone.

Overview of flood actions

Here the flood actions as described by Kelman in [23] are considered in the same order of hierarchy.

Hydrostatic actions

The hydrostatic actions that are set in motion by a flood lead to lateral pressure against a building. The pressure of course is defined as:

$$\Delta P = \rho_w g (H_1 - H_2) \tag{2.1}$$

Here, the water levels at both outside and inside the building are marked H_1 and H_2. So, the pressure will increase if the difference between both water levels gets bigger.

A second consequence of the hydrostatic action is the occurrence of capillary rise; wetting the joints. These effects can already occur in pores between 0.1 μm and 100 μm, for soils as well as for masonry structures [18].

Hydrodynamic actions
Several phenomena are classified as hydrodynamic action. The most obvious is the pressure that is acting due to the flow velocity, which can be approximated by:

$$\Delta P = 0.5\rho v^2 \tag{2.2}$$

Localised effects due to the flow of water at, for instance, corners will impart secondary loads that are also regarded as hydrodynamic action. A third action is turbulence. Turbulence is highly variable and difficult to predict due to the short temporal and spatial scales but can be of great magnitude depending on the circumstances.

As waves at sea are i.a. generated by wind, the same can happen during a flood event, depending on the available fetch. Waves then change the hydrostatic pressure which results in an additional term. When waves are breaking, a fifth effect is observed, again resulting in significant hydrodynamic pressures.

Erosion
Not only does moving water act on surrounding buildings, but also the soil is subjected to loading. While, generally, erosion and scour should be prevented as much as possible, significant damage is observed in terms of months or even years. However, if circumstances do allow the flood event to affect the soil significantly, slipping of slopes or damage due to instability of foundations can become the result.

Buoyancy & Debris
A phenomenon that is difficult to predict, but can have severe consequences is the presence of debris in front of a building. When objects start to float (buoyancy), they are carried by the water and eventually can hit a person or a building, also known as dynamic debris. The effect of buoyancy is not only observed by objects but can also be perceived underneath foundation slabs of buildings as an upward force, acting against gravity. Thus, buoyancy might affect the friction and stability of a building. Buoyancy can be calculated relatively simple when regarding the bottom surface and submerged depth:

$$F_{buoyancy} = \rho_w g A_b H \tag{2.3}$$

When objects start collapsing with other objects, eventually the bed is subjected to a special form of erosion entirely due to the debris, accumulation of these sediments is regarded as a static debris action. Although many objects can become afloat and thus can contribute to the debris to some extent, it is often cars and trees that are regarded as the predominant form of potential debris. In fact, all possible forms of debris eventually can be characterised as a car or a tree by means of parametrisation [25]. By doing so, the relevance and predictability are becoming more accessible in terms of probabilities. Referring to the probabilistic equations, the predictability of debris becomes somewhat more manageable. Below, the probability of a car collision, $p_{\gamma,c}$, and the probability of a tree collision, $p_{\gamma,\tau}$, are shown.

$$p_{\gamma,c} = 1 - (1 - p_{\varphi,c})^{\eta_c} \tag{2.4}$$

$$p_{\gamma,\tau} = 1 - (1 - p_{\varphi,\tau} \cdot p_{r,\tau})^{\eta_\tau} \tag{2.5}$$

Here it shows that the probability of a car collision is expressed as a function depending on (1) the probability of the floating path of a car intersecting with a structure ($p_{\varphi,c}$), and (2) the availability of cars in the area (η_c). The same reasoning applies to the probability of a tree collision, however, here an additional factor is applied referring to the probability of a tree becoming unrooted due to the flood event. This factor is denoted as $p_{r,\tau}$.

It should be noted that objects do not necessarily have to float. When the buoyancy force is not strong enough to set the objects floating, dragging can be the compromise, resulting in erosion and damage nonetheless.

Non-physical actions
Secondary effects leading to structural failure are often difficult to predict and the relevance is different for every situation. While damages due to nuclear actions are obvious, the long-term effects of a flood event are more extensive. Corrosion of structural elements or the building of fungi can be the consequence of flood events. These processes can evolve more rapidly when the water is contaminated.

So, depending on the circumstances and which objects are focused on in the assessment, the relevance of the above-mentioned actions varies. The combination of certain flood actions can result in failure of the one building, while other buildings might still survive the same event.

2.1.2. Local Effects due to Flood Actions

The basic concept prior to the failure of a structural element during a flood is quite simply the acting loads exceeding the structural strength. For a wall element, the sum of the flood actions listed above account for a great deal of the acting loads, but can also be canceled out when the same phenomena happen at the other side of the wall, 'pushing' back. As long as the strength of the element is big enough to counteract the pressure from both sides, the total sum of the acting load will reduce when water is also present inside the residence.
The reach of the flood actions differs spatially and therefore the outcome of such event is highly dependent on the location. By analysing the extent of flood actions locally, the effects on individual residences can become more clear, allowing for possible simulation and further understanding of the loading.

Hydrostatic Loading: Rise Rate
In the previous, it was assumed the rising of the water proceeds slowly and therefore the water inside and outside a residence will be almost identical. Eventually, the difference will be cancelled when the lower level of the window opening has been reached [32]. This just might be the case when the window is open or the glass is broken being subjected to the flood actions described in chapter 2.1.1. In the meantime, the water has multiple other pathways to enter the buildings. For instance, for Easter England residences a typical value of an inside rise rate of 0.005 m/s was found [21]. This could mean the water has risen 30 centimeters in only one minute. Possible inflow pathways are:

1. Doors and windows: when opened, no difference in water level will exist. When closed, still a tight gap can be observed between the door and the frame around. Note that windows are generally situated higher in the wall and contribution to the inflow will therefore happen subsequently.

2. Additional gaps in doors: often doors feature a window frame that begins closer to the floor than windows featured in walls. Additional gaps can exist for hatches that allow domestic pets to enter the residence. Also possible, is a gap specially made for mail, although in modern houses this feature is removed for isolation purposes.

3. Utility lining: nowadays, most of the electrical and sewage enters the house from underneath and thus creates small leakage pathways to enter the residence. Especially the sewage system allows for significant leakage through the pipe, since the diameter of this pipe is generally larger and connected to the outdoors.

4. Porosity: much like the capillary rise the small spaces between particles in the brickwork also allow for water seeping through. Typically this means the water will enter the cavity first, where it is expected to add little to the water already entering from the ventilation holes.

A preliminary investigation showed that the maximum water level difference will be in the order of 0.5 meters and that eventually, the sewage system will act as a direct connection between the water level outside and inside, cancelling out the water level difference that had evolved in the meantime [43].Note that for this difference in height the flow velocity should already be greater than 14 m/s to fulfil the Clausen criteria and initiate destruction, when only regarding the hydrostatic loading.

Hydrodynamic Loading: Pressure coefficients
The hydrodynamic pressure is of great influence too, adding significant pressure to the outside of a wall which cannot be canceled out from inside; simply because such flood actions cannot develop in a residence. Because of the many effects that can be attributed to the hydrodynamic pressure, the quasi-steady component is often a multiplication of equation 2.2 with a so-called drag coefficient, C_D. The purpose of using this drag coefficient is debatable. Research was dedicated to determine the pressure coefficients acting on walls of terraced houses and argued that the drag coefficients are important when assessing flood effects at foundation level, but that failure of, in this case, masonry residences is characterised by failure of individual walls. It was opted to assess the pressure of a single wall instead of using a drag coefficient for the entire structure. As is the case with wind loading, the multiple structural elements of buildings are not subjected to the same force and differ per side. Therefore the pressure coefficient, C_p, is used in such cases, rather than a single drag coefficient [20]. The drag coefficient then can be defined as:

$$C_D = \frac{1}{B}(Bcos\alpha \cdot C_{p,front} - Lsin\alpha \cdot C_{p,left} - Bcos\alpha \cdot C_{p,rear} + Lsin\alpha \cdot C_{p,right}) \tag{2.6}$$

With B and L being the width and length. Here the negative pressure at the opposite side also contributes to the derivation of the drag coefficients. This is because the pressures are both in the direction of the flow. With this the drag coefficient is no longer a single value but rather a combination of pressure coefficients acting on different faces of a building [20].

When scaling the picture to a big city, instead of a single row of houses, one can imagine that the residences are orientated differently throughout the town. The angle of attack and the ability for blockage thus differs per street. While the maximum angle of attack will happen for some terraced houses, during the same event other houses will be subjected to a smaller angle of attack [20].
By implementing the drag coefficient it is possible to compute the water depth at which the different walls started to crack and, as a result, lost bearing capacity. Note that the later possibilities have similarities with the Clausen criteria defined earlier, but mind the loss of stability is already happening at lower values of the water depth and flow velocity. The Clausen criterium acts as an absolute limit.

For modern residences a corresponding water depth of 1.8 meters was found; above this value, the wall is losing its capacity for load-bearing. These results, however, altered significantly when the influence of wall thickness and no water level difference was taken into consideration. By increasing the wall thickness the damage curve shifted towards the right, allowing a greater water depth before significant damage. As already discussed above, the presence of water inside the residence canceled out the effect and no water depth could be found that would lead to minor damage even [20].

2.2. Construction elements of Dutch walls

In The Netherlands, almost every building has a form of masonry. This also includes fences and inner partition walls that are constructed with masonry. Masonry can be defined as a composition of solid units, like bricks, held together with mortar, like paste or glue. Similar to concrete, masonry is strong under compression and weak under tension. 79% of the current buildings in The Netherlands have structural unreinforced masonry (34% clay bricks and 45% calcium silicate bricks) as their main structural system [13]. The percentages can also be found in Figure 2.1. From the same study, it was conducted that 71% of the current buildings are equipped with a cavity wall [13]. The decision to test a cavity wall during this research is hence based on this number.

The selection of both the inner- and outer-leaf can also be reasoned using Figure 2.1. When regarding all possible combinations, it appears that the greatest number of buildings are built with calcium-silicate (CaSi) bricks acting as the structural wall. In the case of a cavity wall, this means the CaSi wall is regarded as the inner-leaf, while the outer-leaf consists of clay bricks with no load-bearing function.

By selecting a cavity wall with an inner-leaf consisting of calcium-silicate elements and an outer-leaf consisting of clay bricks only a quarter of all buildings is represented in the experiment to come [13]. Yet, it is the greatest representation possible in a single wall experiment. Nevertheless, a closer look is needed in the selection of these structural elements as well as the selection of the material used for connecting the elements and the walls.

Structural Walls		Outer Leaf	Floor Type	Percentage
Main Direction	Secondary Direction	(Cavity Wall)		
Calcium-silicate	-	Yes	Concrete	24.8%
Calcium-silicate	Calcium-silicate	Yes	Concrete	14.8%
Clay Brick	Clay Brick	-	Timber	12.4%
Clay Brick	-	Yes	Concrete	10.0%
Clay Brick	-	-	Timber	7.0%
Calcium-silicate	Calcium-silicate	Yes	Timber	5.5%
Clay Brick	-	Yes	Timber	4.3%
Concrete (in-situ)	-	Yes	Concrete	4.0%
Concrete (prefab)	-	Yes	Concrete	3.3%
Steel Braced	Steel Framed	-	-	2.0%
Timber Framed	Timber Framed	Yes	-	2.0%
Steel Braced	Steel Braced	-	-	1.7%
Timber Panels	-	Yes	Timber	1.0%
Calcium-silicate	-	Yes	Timber	0.9%
Timber Panels	Timber Panels	Yes	Timber	0.9%
Concrete (in-situ)	Concrete (in-situ)	-	Concrete	0.9%
Other				4.7%
				100.0%

Figure 2.1: Taxonomy Structural Systems (adapted from: Arup Exposure Database EDB V5 Structural systems by Van Elk and Doornhof (2018)).

2.2.1. Fired-clay bricks

When clay is mixed with water, the plasticity increases and the mixture can be shaped in any form. When dried, the mixture loses its plasticity again but keeps its shape. This process largely determines the quality of the brick, but the used clay material is also highly important. The sedimentary composition of clay is different around the world and the presence or absence of certain metals influences the colour of the clay and eventually the colour of the brick. Even in The Netherlands the colour of the brick can already differ significantly depending on the location. Clay with high calcium, (Ca), content results in yellow bricks and a high degree of iron(III)oxide, (Fe_2O_3), will lead to red bricks. The colour can be manipulated by draining the oxygen supply during the baking process, which will give a darker colour due to the formation of (Fe_3O_4) or FeO on the outside of the brick [36].

In the old brick baking factories, the fire came from below, which resulted in glazed bricks at the bottom and soft bricks at the top. These height differences in the baking process resulted in a number of different types of bricks. Bricks used for roads and water retaining structures came from the bottom at that time. The softer bricks from the top could best be used for non load-bearing inner-partition walls [5]. After the second world war, the grouping of bricks became more straightforward, with six categories ranked from hard bricks to soft bricks [36].

Not only the function of the brick was determined by the baking process, but also the shrinkage, and thus the dimensions, were influenced by the process. Even in the middle ages the ideal ratio of a brick was 4:2:1. The length of a brick should be twice the width, also accounting for a single joint [36]. Nowadays, the fabrication process of bricks is more controlled resulting in more uniform shapes. To reduce the shrinkage and cracking of the clay, sand is added in the process [17]. This sand also increases the strength [36] leading to more uniform qualities. The dimensions of the most used bricks in The Netherlands were recorded in NEN2489:1976 nl:

1. Waal dimensions (WF) (Dutch: Waalformaat): 210 x 100 x 50mm

2. Vecht dimensions (VF) (Dutch: Vechtformaat): 210 x 100 x 40mm

3. Standard big dimensions (DF) (Dutch: Dikformaat): 210 x 100 x 65mm

In the same code, the allowable dimension tolerances are listed in three classes, ranging from class I (2mm tolerance) to class III (4mm tolerance). NEN2489:1976 separates also three areas of application: Inner-walls (A), outer walls (B), and heavy-loaded inner and outer walls (C). These classes are further subdivided based on application. In the case of outer walls with heights below 10 meters, the quality requirements on the brick unit are summarized in class B1. Since the majority of Dutch houses (semi-detached (Dutch: twee-onder-een-kapwoning) or terraced houses) belong in this class the requirements are listed here.

1. Minimum average value for the pressure load: 12.5 N/mm^2

2. lower limit of the pressure load: 7.5 N/mm^2

3. lower limit of the tensile load: 0.3 N/mm^2

4. Upper limit of the sulfate, SO_4^2, concentration: 0.24 %

For the brick units only, European norm EN 772-1 prescribes the characterisation of masonry by means of compression testing.

2.2.2. Calcium silicate bricks

While fired clay bricks used to be the main structural system, many houses now rely on the load-bearing function of calcium silicate units, see Fig 2.1 once more. These units are composed out of fine siliceous aggregates and 10-20% quicklime or well-hydrated lime. This mixture is compressed and moulded into the right size at 170 degrees Celcius [19]. The binding of the brick is due to the reaction of the lime with the aggregate. As such, the calcium silicate hydrate is formed [9]. These CaSi bricks have similar durability as concrete [9] and show isotropic behaviour in terms of shrinkage [7]. The CaSi brickwork is more vulnerable for shrinkage than fired-clay masonry, which can cause cracks on the wall surface [19]. The insulating properties of the calcium silicate bricks get lost when the material is subjected to moisture [38]. The fired-clay brickwork protects the CaSi wall from such weather conditions and the insulation and ventilation features inside the cavity wall will maintain the thermal conductivity of the calcium silicate material.

The low costs and the rate at which the CaSi units can be installed make it a very applicable material. The manufacturing of CaSi blocks began in 1950, after which the material quickly became a suitable element in the utility construction [37]. Generally, CaSi walls are either consisting of bricks, blocks, or elements. Here, the bricks are also divided into standard dimensions:

1. Waal dimensions (WF) (Dutch: Waalformaat): 214 x 102 x 55mm
2. Amstel dimensions (AF) (Dutch: Amstelformaat): 214 x 102 x 72mm
3. Maas dimensions (MF) (Dutch: Maasformaat): 214 x 102 x 82mm

The CaSi blocks are bigger than the bricks and are indicated with an M (Dutch: metselblok), L (Dutch: lijmblok), V (Dutch: vellingblok) followed by their width and height. CaSi elements are the greatest form of structural CaSi. Elements are indicated with E (Dutch: Element) followed by their width. The compressive strength is listed according to the NEN-EN 771-2 code; indicated by CSxx with xx being the compressive strength in N/mm^2.

2.2.3. Mortar

In essence, mortar is the overall term for any material that binds the units. In the case of a structural wall, the units that need binding are the bricks or the CaSi elements. The mortar used for these masonry works can either be a cement paste or glue. Due to the application time, elements are more often treated with glue while for bricks the cement paste suffices [16]. The paste consists of aggregates, water, and a binder. When wet, the paste is workable and is placed on top of a brick course. The water reacts with the binder and after hardening the mortar locks the bricks in place. Classic mortar contained lime as a binder, but now Portland cement is more in use with sand used as aggregates. Ordinary mortar is a mixture in a 4:1:1.5 ratio (sand:cement:water). With the binding of the bricks, the mortar itself must develop a good adhesion with the brick, while also being watertight. This adhesion is partly due to the fact that the bricks absorb some of the water and allow the mortar to bond.

Just as with concrete, the degree of water content in the mixture has a large influence on the strength. If the water to cement ratio (w/c) is too high this leads to a reduction in strength; a w/c ratio that is too low results in a weaker mortar with difficult workability. From experimental results it was found that 'compressive and split tensile strengths are maximum at w/c ratio of approximately 0.6 for cement mortar [..]' [34]. When subjected to tensile strength the mortar shows brittle behaviour similar to concrete. The required performance of factory-made mortar is listed in the NEN-EN 998-2 standard code. Mortar is divided into classes depending on the compressive strength; Mortar with a compressive strength of 5 MPa is classified as M5.

2.2.4. Wall ties

Wall ties form the connection between the inner and outer leaf. To form a solid connection NEN-EN845-1 prescribes the steel ties to be anchored at least 40 millimeters in the outer leaf, but no further than 70 millimeters. Additional requirements prevent the ties from transporting moisture towards the insulation or the inner leaf. To do so, the wall ties are installed with a downward inclination, avoiding the water from moving up. The wall ties are also used to keep the insulation material in place. Furthermore, acoustic insulation can be accomplished by installing the ties separately and connecting them with an additional sound-proof element. The code NEN-EN 1996-2 provides the durability requirements that are prescribed for the wall ties. Class MX1 is used for masonry in dry environments and class MX5 is for masonry in highly chemical environments. In the case of Dutch buildings the masonry can be defined as class MX3.2: subjected to moisture and water combined with frost and thaw, but only on the outside. Class MX4 is also possible. This class describes masonry that is subjected to salty air or seawater. Residences near the coast can thus be classified as MX4. For classes MX3.2 and MX4, the code requires the usage of stainless steel wall ties.

2.2.5. Steel bracket

With walls featuring windows or doors, the brick courses are logically interrupted to allow for the framework. Since mortar is rather weak in tensile stresses, the overlaying courses cannot be carried by the mortar alone. While the structural repercussion of this interruption for the stability of the wall is part of this project, this also means that the framework will need to take over the load-bearing function of the removed courses. However, for wider frames or higher facades, the framework is not capable of taking the weight of the brickwork on top. This then can lead to deformations and damages. In older houses, this problem was solved by placing a wooden lintel over the frame. In this way the weight of the overlying courses was transferred via the lintel to the courses on the side, relieving the window frame from carrying the load. In more modern houses the fired-clay brick wall is now merely used as a facade, which means the forces acting in the clay wall are lower than before. The bulky lintel is therefore often replaced by an L-shaped steel bracket. This bracket allows for a more aesthetic look since the bracket is non-visible; only the flange can be seen from below. The bracket is mounted on the inner leaf and the courses are stacked on the flange. Multiple types of brackets are available, but they all have the same purpose of keeping the courses in place and transfer the weight to the sides. The introduction of the bracket also enabled multiple options regarding the way of stacking the bricks. Occasionally, houses are equipped with a row of vertically or diagonally stacked bricks above the window. There are also brackets that are not connected with the inner leaf. Such brackets are C-shaped and feature a couple of rows in-between the flanges.

2.2.6. Concrete lintel

Although a steel bracket is a useful alternative from an aesthetic point of view, it cannot be used for load-bearing walls and as such is only applicable on the outer leaf of a cavity wall. A lintel is thus still needed for the inner- CaSi wall to carry the floors and courses of the CaSi bricks. In this way, the lintel relieves the window frame from taking these loads. Most lintels are either made of wood or cast in concrete and span the window frame and a small section of the courses on the side i.e. an overlap of at least 10 centimeters at each side. For convenience, the lintel usually has identical width and height as the bricks in the same course to guarantee an easy fit in the wall. Since the CaSi wall is often plastered and finished with paint or wallpaper the lintel will not be visible from the inside.

2.3. Window frame installation and insulation aspects

An obvious interruption in a (cavity) wall would be the presence of a window. Not only is it expected the window will have a weakening effect on the wall, but the window also is expected to allow multiple pathways for the water to leak through the wall. In order to make the final results as useful as possible, the window frame and its installation should be representative. A small investigation in the window-wall interface is therefore carried out to find the characteristics of a representative window section that is commonly used in cavity walls in The Netherlands.

2.3.1. Window-wall interface

A solid window-wall interface should include four critical barriers: The water-shedding surface, the exterior moisture barrier, the vapor barrier, and the air barrier [33]. The first two barriers should prevent the water from entering the building and consists of the glazing and the frame of the window as well as the sealing between the components, see Figure 2.2.

The installation of a window frame determines the water migration into the opening; a window can be installed either as a water barrier or installed to allow drainage [33]. When installed as a water barrier, the sealant inside the window-wall interface is completely closed; water that may leak through the wall itself cannot be countered afterwards. When installed to allow for drainage the sealant features channels to drain the water penetrating the wall. In the latter case, the water-shedding surface is thus situated further inwards. In this case, an interior seal is present, preventing water from intruding into the building.

For masonry walls, the window should act as a barrier rather than allow for drainage. In this case, the drainage channels could only be created on the surface of the wall, which would deteriorate the exterior moisture barrier otherwise [33].

Other possible sealants of the window-wall interface were also researched. Although this investigation revolved around the airtightness of the interface, some similarities with water tightness can be reasoned. Significant air losses, indicating possible leakage pathways, were observed with mineral fibre and spray-in-place foam because these materials were unable to completely close off the joint and would therefore create an inconsistency in the moisture barrier [3]. Airtight membranes also showed losses. These losses were situated in the corners of the wall gap, which is due to the folding of the membranes here [3]. However, during the construction of older houses, these materials were not yet used, which indicates the air losses, or leakage pathways, are more prominent in these sorts of houses.

2.3.2. Window sill

Often the case with masonry walls, the thickness of the wall itself is hard to cover completely with the window frame. Not only will it increase the needed material significantly, but it also would not have an aesthetic look either. For that matter, the frames are placed slightly inwards which results in two niches at both sides of the wall. The inside niche is often covered in plaster and a sill is placed on the lower plane of this niche to allow for decorative elements. The outside niche is subjected to the weather conditions; to prevent (rain)water from accumulating on the lower plane here a sill should be placed as well. This sill (Dutch: waterslagen) features an inclined top plane that directs the water further downwards and avoids the water to concentrate near the sealants of the window-wall interface. The outside sill is thus actually part of the first water-shedding barrier. To prevent the water from seeping over the wall surface a small notch is present at the bottom of the sill. This will make the droplets fall a few centimeters in front of the wall. Modern-looking sills can be a one-piece composed of stone, concrete, or metals. Older sills consist of a number of ceramic tiles that are placed under an angle.

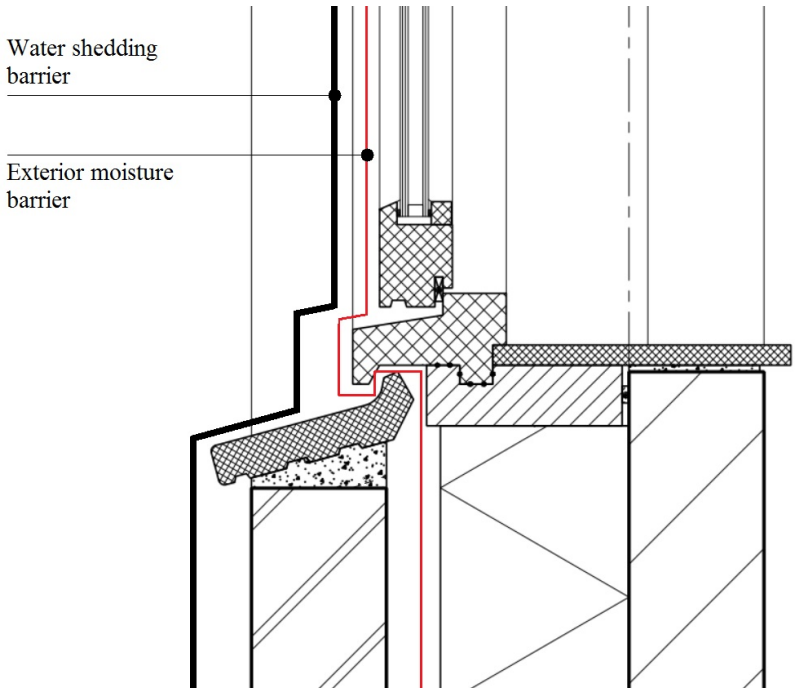

Figure 2.2: The water shedding-and exterior moisture barriers of typical window-wall interface (according to (Salzano et al, 2010). Figure obtained from Rockwool B.V. (2017) and adapted for this report.

2.3.3. Window frame

The current trend to make residences more climate-resilient affects the conventional configuration of a cavity wall greatly [12]. Cavities are being insulated and windows are equipped with double or even triple glass. To reduce the amount of heated air leaking through the wall, even the window-wall interface is regarded with more care; hence the research on the airtightness of multiple sealants. Because of this trend, window frames are no longer solely made out of wood. Aluminum frames or plastic frames are popular alternatives that require less maintenance. Still, wooden window frames are the most favoured as they are cheaper and traditionally more compatible with brick walls. Almost all wooden window frames are made out of hardwood i.e. either Meranti or Oregon pine. Other types of wood that are of lesser quality are being modified by thermal processes. This thermally modified wood also has a positive influence on the environmental performance [40].
Wooden window frames have standardised sections with dimensions 67x114mm. The section for a bottom part of the frame, called a rail (Dutch: raamdorpel), also features an inclined top plane, just like a window sill. Again, the reason is to prevent water from accumulating near the sealant. The glass itself is placed against the flanges of the sections and wooden stiles are placed over the edges of the glass to seal the window. In case the window should open the glass itself is placed in a secondary frame and this secondary frame is placed in the wooden window frame. Here a rubber band is used to seal the space between the secondary frame and the primary frame.

2.3.4. Installation

The overall dimensions of a window can be any size; meaning that limitations are due to the properties of the glass. In more modern houses, windows can stretch the entire height of one storey. In older houses, this too can be realised, but here the non-bearing walls are often equipped with radiators that are part of the central heating system of the residence. Because of this, windows are placed higher in the wall at a height of 850 millimeters [4], so people can still look outside when sitting down. On higher floors, windows are placed at different heights. When the design requires the window to be installed at floor level the code (Dutch: Bouwbesluit) obliges the use of safety glass.

Mind that through the years the height of one storey has increased from 2.40 meters in 1992 to 2.60 meters in the current code. The height of a window therefore could increase simultaneously to allow an aesthetically pleasing connection between the window and ceiling.

A window frame can be mounted in multiple ways, using mounting brackets or by placing an additional plywood framework inside the cavity. The mounting brackets are attached to the CaSi wall and keep the window frame in place. The additional framework (Dutch: Spouwlatten) is attached in-between both walls either with screws or other material. The window frame is then placed inside the additional framework, locking the window inside the cavity. Window frames that are not made out of wood often require a second set of additional framing (Dutch: Stelkozijn). This additional framing is placed against the inner-niche and the wooden frame inside the cavity. Next, the final window frame glides into place, covering the framing from the front and sealing the window-wall interface.

Whenever the cavity is too wide to be closed off by the frame itself, so-called cavity closers are used first to cover the cavity. These closers act as a seal and prevent the water vapour from reaching into the building. The cavity closer is mounted on the silicate inner-leaf by means of an overlapping flange and the other side is connected with ties in the mortar bed of the fired-clay wall. With cavity closers, the window should be installed using mounting brackets and any interaction between the window frame and the cavity is lost. This system is therefore regarded as a major source of water ingression; without the interaction of the wall, the window-wall interface is weaker [11].

2.3.5. Insulation

A wall should not only be able to keep the local weather conditions out but the inside climate should also be maintained. It is already made clear that the advantageous thermal conductivity of the calcium silicate brick gets lost when the bricks get wet. The fired-clay wall prevents the CaSi bricks from getting wet, but cannot prevent the warm air from leaking through possible joints and holes in the CaSi wall. To avert the unnecessary loss of heated air modern houses are well-insulated during construction. Conventional walls can be insulated for the same economical and environmental reasons, although existing walls require different insulating techniques.

The fired-clay bricks are well capable of preventing outside water from entering the cavity, as this wall is part of the water-shedding surface. Nevertheless, water can accumulate inside the cavity. This water originates from inside i.e. the main system of air convection between the inside room and the cavity. When the warm air from inside leaks through the CaSi wall and reaches the cold surface inside the cavity the air starts condensing. The moisture that is generated by the condensing can reduce the thermal conductivity of the brick for the worse, resulting in more convection and more condensation. Finally the moist will lead to the growth of fungi and rot of the structural materials.

To block the warm air from entering the cavity, insulation material is placed inside the cavity against the inner leaf. To prevent secondary airflow along the insulation material it is important to make sure the insulation panels are well-connected, see left image of Figure 2.3. By means of the wall ties, the insulation can be kept in place. When a panel is not connected tightly or the wall ties fail to keep the insulation in place (Dutch: Valse spouw) the insulation properties decrease considerably, see centre image of Figure 2.3. When done right the moisture barrier behind the insulation is uninterrupted and condensation is avoided. The thickness of such insulation panels can differ considerably and can result in cavity thicknesses of 15+ centimeters.

2.3.6. Ventilation

The cavity is not entirely filled with insulation material, rather a small cavity of around 5 centimeters is left for ventilation. This free space allows fresh air to enter from the bottom and moist air to leave from the top, thus keeping the cavity dry and preventing the air from condensing even further, see right image of Figure 2.3. The fresh air enters the cavity through weep holes (Dutch: Stootvoeg), which are vertical joints left open. To keep out insects and rodents a small grill can be placed in the weep hole. The fresh air then flows vertically upwards to the ventilation vents where the moist air leaves the cavity. These ventilation vents are also vertical joints left open. Weep - and ventilation vents are placed every meter or after each stretch of 5 bricks depending on the ventilated area.

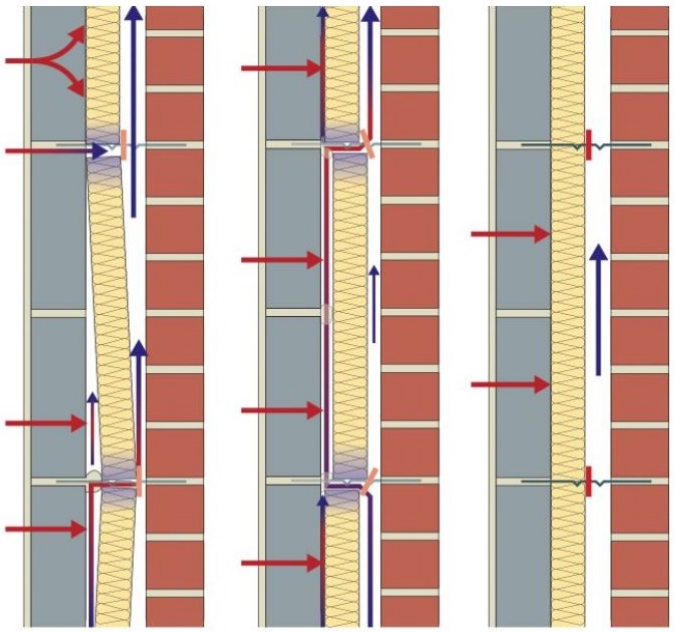

Figure 2.3: Left and centre: failure of the ventilation properties due to displacement of insulation material, leading to secondary airflow and moisture problems. right: adequate placement of insulation material. The airflow will ventilate the cavity, preventing moisture problems

2.4. Wall properties

To counteract possible torsion of the building, and to seal the residence, infill walls are part of the construction of the modern residence. Usually, these walls can be found at the front and back of a residence, where big windows and doors are placed. The infill walls are built after the construction of the load-bearing walls and concrete floor [30].
Current trends for cavity walls feature a 100 mm wide outer wall of clay-brick, while the inner wall is constructed using 102 mm wide calcium-silicate blocks, leaving a gap of 100-200 mm for insulation and air.

2.4.1. Masonry Properties

The properties of masonry are different in different directions. While high compression stresses can be endured, the walls show brittle behaviour when subjected to tensile strength. This can be dealt with by reinforcing the masonry wall. The brick itself has different properties than the assembly of the wall; shear between bricklayers can lead to failure of the mortar and bending or settling can lead to tensile stresses. Masonry compression strength, f'_m or f_c is defined as:

$$f'_m = K \cdot f_b^{\alpha} \cdot f_m^{\beta} \tag{2.7}$$

Here, the mortar strength, f_m, is depending on the water/cement ratio and the properties of the aggregates used. The mortar is tested with cube or cylindrical testing and is subdivided into different (strength) classes. The brick strength, f_b, depends on the material and dimensions and therefore bricks should always be tested during an experiment. Note that the K, α, and β values are characteristic values that are listed in a table and differ per brick type and joint thickness.

Flexural strength can have different directions with a turning moment around the vertical axis and a moment around the horizontal axis parallel to the wall. Also here, characteristic values exist for different types of brick and mortar. Elasticity can be approximated using the masonry compression strength defined above, like:

$$E = K_E \cdot f'_m \tag{2.8}$$

Where the first parameter can be obtained through characteristic tables or Eurocode standards. Tables also exist accounting for friction between masonry and different type of materials. This table shows that steel has the least potential attaching to masonry.

Thermal expansion can lead to significant damages when not accounted for. Especially bricks can absorb water and therefore expand. Opposite of this, calcium silicate bricks may shrink after construction, leading to possible cracks. Dilatation joints are often included in a big wall to allow the material to expand. For this different design, requirements are listed as well as deformation properties for unreinforced masonry walls. Some design requirements are available allowing deflections depending on the position and configuration of the wall. Vertically the maximum deviation during construction can be 50 mm for a three-storey building, showing the importance of solid and detailed execution.

Because of the high deviations that exist throughout the properties of masonry, safety factors are in order to decrease the probability of failure. In the Netherlands, the partial factor for masonry is $\gamma_m = 1.7$, which is quite a significant factor. The same can be observed for load factors, showing the vast uncertainty of the properties.

2.4.2. Masonry characterisation

To evaluate properties of masonry it is important to classify the material properties which are also needed in the design of new structures. It is important to know the strengths and above all the

weaknesses of the used material. In order to do so, it is necessary to characterise the following properties:

1. Compression and the structural stiffness corresponding to the elastic properties, the structural resistance corresponding to the strength properties, and the toughness properties in case of cracking. The latter is mostly used in numerical analyses, while the first two are used in preliminary assessments and analytical formulations.

2. Shear; which is relevant for the resistance of lateral forces. In case of failure, the wall can start to slide off horizontally (in between rows of bricks) or diagonally where the crack exists in horizontal and vertical joints. The strength is therefore depending on the normal stresses on the joints.

3. Tension (originating from bending), which is relevant when regarding buckling and overturning can lead to out-of-plane loading and in-plane loading. In this case, the joints are the most vulnerable aspect of the wall and are therefore often the place where cracks start to form. Usually, horizontal tension can be endured to a higher extent with the force reaching two to four times the amount needed for failure in the vertical direction.

Note that the combination of tension and torsion, with bending, could lead to out-of-plane failure and thus once again marks the importance of understanding the different properties of the masonry material.

2.4.3. Testing

Often the case with structural testing, most properties reveal themselves by destructive testing. Nowadays, some structural properties and quality of the masonry can also be found and determined by means of slightly destructive testing and even non-destructive testing, like rebound hammers or ultrasonic testing. Although these tests can provide useful information, destructive tests are still needed to require insight into the material properties. A vast set of standard tests exist to compare the properties throughout the material. Some norms and requirements are composed and summarized in the following European codes:

1. Units: EN 772 I (compressive strength)

2. Mortar: EN 1015 XI (flexural and compressive strength)

3. Masonry: EN 1052 I (compressive strength), II (flexural strength), III (shear strength), IV (shear strength), and V (bond strength)

For the testing of the first two categories, units and mortar, guidelines prescribe compression tests to determine the compressive strength. In addition, a three-point bending test is prescribed to determine the flexural strength of the mortar. Masonry itself is tested more extensively with multiple prescriptions and configurations corresponding to the orthotropic behaviour of the wall.

Compression tests are performed on either wallets or prisms. Both can show the compressive strength of masonry, but additionally, the elastic modulus can also be obtained when the testing rig is assembled as a wallet, which can be seen as a small fragment of the wall. When applying a displacement-controlled test, rather than a force-controlled test, one can also determine the toughness, that starts to develop at the cracking stage. As mentioned earlier horizontal tension can be endured to a higher degree; the same applies for horizontal compression where the stress-strain diagrams show the wallet can resist greater normal stresses and greater strains, although to a lesser extent than tension.

Flexural properties can be investigated by performing out-of-plane bending tests. Bending tests are also performed to study the in-plane behaviour because often it turns out the masonry is too brittle to perform uniaxial tensile tests. For instance, the flexural bond strength, f_w, can be determined by performing a bond wrench test. This test applies a lever arm force to find the properties.

Shear characteristics of the masonry can be investigated by stacking three units like a prism. Applying a force on the second unit will generate shear in the bed joints. This triplet test is also regarded as a force-controlled test, but with displacement-controlled tests, the residual friction can be determined in addition to the shear properties.

3

Designs and experimental method

To find the behaviour of a cavity wall being subjected to hydrostatic pressure, a life-sized cavity wall was constructed in the basin at Flood Proof Holland (FPH). The wall features a window, which is generally believed to have a weakening effect on the wall. This effect can become evident from out-of-plane deformations and leaking rates. The current lack of appropriate data highlights the need for a physical experiment, which afterwards can become a starting point for further research by either performing additional experiments or by including proven theory. A physical experiment gives a high level of control and allows multiple situations to be tested at once. Yet, it also is vulnerable to errors and can lead to artificial situations [2]. An experiment should thus be representative and should be performed with great diligence to be able to become the starting point of any future research.

In this chapter, the experimental set-up is presented. Furthermore, the theoretical configuration of Dutch walls in Chapter 2 is translated to available and practical materials that, assembled together, make up the design for a Dutch cavity wall. Lastly, possible inaccuracies originating from the construction of the cavity wall are elucidated in this chapter.

3.1. Experimental set-up

The experiments took place in the largest basin at the FPH facility at the south of the TU Delft campus, between the Delftse Schie canal and the A13 highway. The basin can be filled to a controlled water level of around 1.50 meters and is filled with water flowing from the higher-laid main reservoir. The water level can be lowered by a pump, after which the water is discharged on a small lake outside the FPH facility.

The cavity wall has been constructed with the same set-up as the earlier single-leaf masonry wall that was tested. As such, the main dimensions of the cavity wall are similar to the dimensions of the single-leaf masonry wall i.e. 2600 x 2600 mm. The steel rig that acts as the wall support was placed in the deepest corner of the basin, in front of the pump. The steel rig forms a framework consisting of multiple steel beams and columns with varying lengths, ordinary sections of 300 x 300 mm, and flanges with a thickness of 20 mm, see Figure 3.1. The beams are perforated repeatedly in both the flanges and the web, except for the larger top and bottom beams which are only perforated in the flanges. The rig is supported by additional beams forming the 'legs' of the set-up. The top beam is attached to the rig using four threads (Dutch: schroefdraad). Springs are attached at the bottom of these bars to mimic and control the lateral forces acting in the wall. To counteract the possible uplift, ordinary sandbags of 25 kilograms each are available at the basin and can be placed in-between the flanges of the beams.

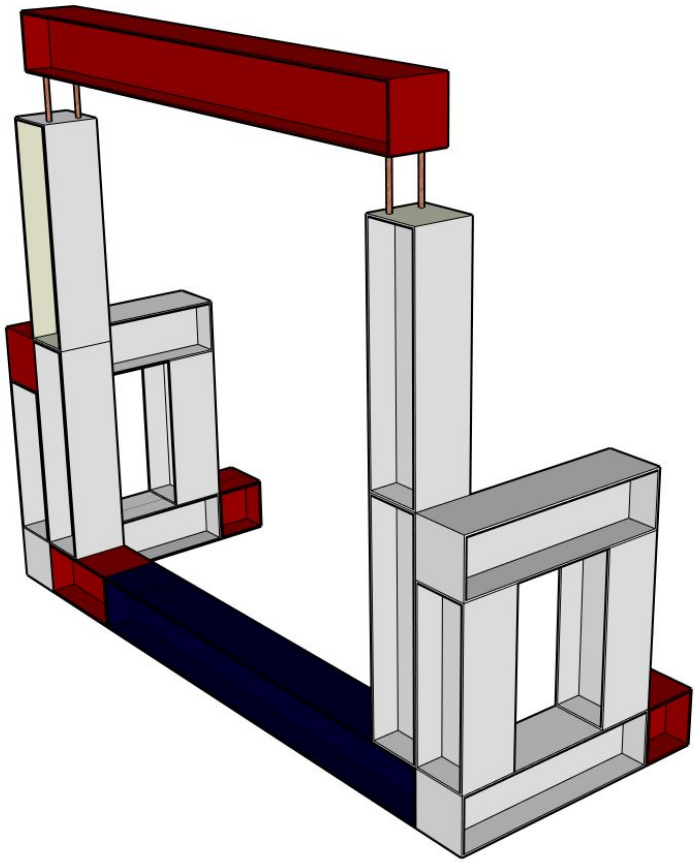

Figure 3.1: Illustration of the steel rig present at the Flood Proof Holland Basin and used in the experiments.

3.2. Translation of theory into practice

It was tried to construct the wall as a representative section of an ordinary Dutch house. Yet, materials that are very common on construction sites can be very rare or expensive for private use. Construction techniques that are nowadays routine were unusual in the seventies and eighties; the period in which the cavity wall became a standard requirement due to new instructions (Dutch: modelbouwverordening) [39]. To account for this mismatch, some alternatives were needed in order to construct a wall that was indeed comparable to the real situation.

3.2.1. Materials

Here the (alternative) building elements are listed that were used in the construction of the cavity wall. The choice for these specific materials is reasoned below. A brief overview of the materials can be found in Appendix B.

Fired-clay brick

The Eurocode requires the bricks of the outer walls (Class B1) to have a minimum tensile strength of 0.3 N/mm^2 and a minimum compressive strength of 7.5 N/mm^2, but there are no clear requirements for the dimensions. The previous single-leaf wall, tested in the summer of 2020, used reddish bricks of the Waal dimensions. These bricks were originally chosen because they best mimicked the behaviour of the bricks used in residences in the Groningen province. The bricks were, therefore, initially used in Earthquake related research before the remainder of the units was used in the wall experiment of 2020.

To be able to compare this current research with the results from before, the reddish bricks are once more used as units in the facade of the cavity wall. The same stretcher bond (Dutch: halfsteenverband) is used as well. The tolerances of these bricks are classified as class II; the bricks can deviate 3 millimeters from the standard size. Furthermore, the average value for the pressure load is said to be 35 N/mm^2, see Figure 3.2.

Calcium silicate brick

The CaSi bricks available at FPH are 214 mm in length, 102 mm in width, and 72 mm in height i.e. Amstel dimensions. Again, the reason of choice for these particular bricks can be traced back to the initial Earthquake related research. Nevertheless, CaSi bricks are still quite common to use in the construction of houses, while in non-residential buildings greater (less time-consuming) elements are preferred. The convenient choice to use the same bricks in this specific research is thus justified. The manufacturer has indicated the compressive strength of these specific bricks, CS16, in accordance with the NEN-EN 771-2 code. Additional information can be found in Figure 3.2.

Mortar

The binder used in the experiment is a cement-based mortar. This mortar is used to bind the fired-clay brick units as well as the calcium silicate units. For larger CaSi elements it would have been more representative to glue the elements, but bricks are often treated with the cement paste.

A newly built wall has not been subjected to the outside weather conditions and as such is expected to be stronger than older walls that have been wearing out for much longer. To account for this effect a weaker mortar was used for the experiment. Any mortar is weakened when it is not handled before the expiration date; meaning the compressive strength of the finalized product has been reduced. This is due to the ingression of water. When water has infiltrated the bag before use, the cement has started a full or partial reaction. This results in crystallization of the cement; hard rocks are present in the powdered mortar.

The mortar delivered at FPH went expired in 2018. The bags are sealed and prevent the rainwater from entering. The bags contain a pre-mixed product with cement, hydrated lime, and fine sand and according to the manufacturer need approximately 3.7 liters of water per 25 kg of mixture. To determine the current tensile strength of the expired mortar couplets were made that were subjected to bond-wrench tests.

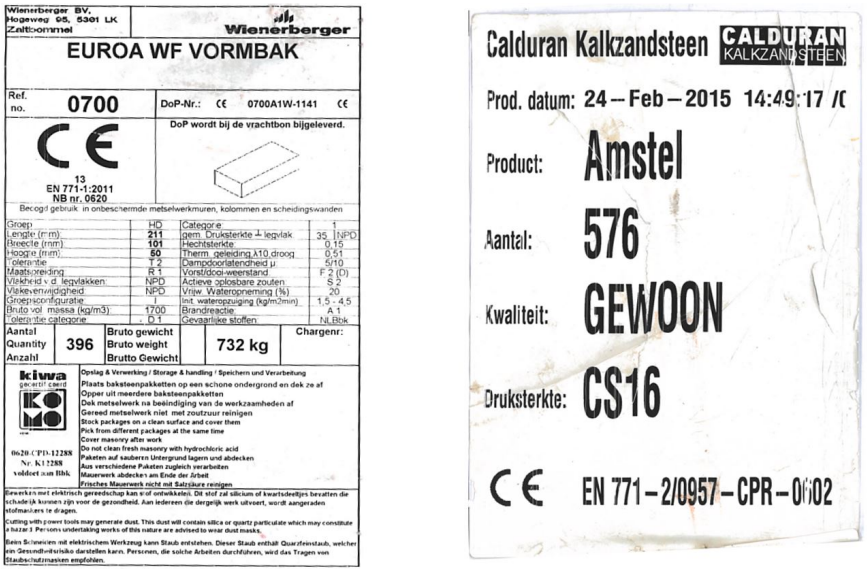

Figure 3.2: Specifications of the bricks present at FPH. Left: fired-clay brick. Right: CaSi brick.

Wall ties
The ties form the connection between both walls and to make sure the ties do not exceed the maximum 70 millimeters anchoring distance the wall ties should have a maximum length of 200 millimeters. The acoustic aspects are not treated in this research, which reduces the number of optional wall ties appropriate for this experiment. The code further requires the use of stainless steel, although the ties used in older walls are not necessarily made of stainless steel. In fact, to account for the corrosion effect of these 'older' ties, the diameter of the ordered wall ties was chosen purposely thinner. Only one available type of wall tie satisfied the required length and diameter i.e. an L-shaped tie with dimensions: 200x30x3.6mm. These ties are galvanised rather than made of stainless steel; meaning they actually do not meet the NEN-EN 1996-2 code. However, for the duration of the experiment, the galvanised wall ties suffice.

Steel bracket
The steel bracket is needed to transfer the loads right above the window frame. The bracket carries the bricks stacked on top and either transfers the forcing to the CaSi wall via the wall brackets or directly on the below courses. For the latter, an overlap of at least 10 centimeters is needed at both sides of the span.

The dimensions of the experimental rig inflict a boundary on the thickness of the cavity and as such also bounds the overall width of the steel bracket. Since the simulated cavity is more narrow than authentic cavities, ordinary brackets would be too wide and would protrude the fired-clay wall. Therefore, the bracket cannot be mounted on the inner-leaf in this case. Instead, an L-shaped bracket with equally wide flanges was chosen that transfers the loads to the sides. The dimensions of this bracket are 90x90x3x980mm; allowing the fired-clay bricks to cover the bracket. With a thickness of 3 millimeters, the bracket can be implemented smoothly in the horizontal mortar joint (Dutch: lintvoeg) and the minimum overlapping of 10 centimeters can be realised.

Concrete lintel
On the 19th of February, the lintel that is part of the CaSi wall was cast in the Stevinlab of the Civil Engineering and Geosciences faculty. To ensure a sufficient overlap at each side of the window the total length of the lintel was designed to be 88 centimeters i.e. the total span plus twice an overlap of 10 centimeters. The height and width of the lintel were set identical to an Amstel-sized CaSi brick. The mould used for casting was constructed earlier and satisfied the dimensions for this research as well.

The concrete mixture consists of cement, sand, gravel, water, and air. As can be seen in Table 3.1, the mixture meets the 10-20-30-40 Rule of thumb quite well; 10% of the mixture should consist of cement, 20% should be air and water, 30% should be sand, and the final 40% is gravel. The cement is classified as CEM III/B, in which the Roman numerals indicate the amount of portland cement and the alphabetical script indicates the amount of slag. The compressive strength [MPa] that is reached after 28 days of hardening is also noted behind this code; in this case 42.5 MPa.

Two rebars with a diameter of 8 millimeters were placed on the bottom of the mould after which the concrete mixture was poured into the mould and vibrated into place. A plastic sheet was placed over the concrete to trap the water and the lintel was left to harden. After three days the mould was removed and the lintel was placed in the fog room to harden even further. The lintel has spent 28 days in the fog room and was removed when construction of the wall started.

Material	Mass	Volume	Fraction V/V
Cement *CEM III/B 42.5 N LH HS*	2.52 kg	0.86 L	10.7%
Sand *0/4mm*	6.38 kg	2.42 L	30.2%
Gravel *4/8mm*	8.52 kg	3.19 L	39.9%
Water -	1.42 kg	1.42 L	17.7%
Air -	-	0.12 L	1.5%
Total	18.89 kg	8.00 L	100%

Table 3.1: The total mixture of the concrete lintel listed in mass, volume, and fraction.

Window sill
Window sills are well-accessible in ordinary DIY stores and have standardised sections. To match the aesthetic the sills are finished with a glazing look; often brown or red. Rather than installing a one-piece sill, for this research, the ceramic tiles are preferred, since these are more suitable for older houses i.e. houses that were build in the early eighties.

The chosen tiles each have a width of 105 millimeters, a length of 160 millimeters, and a thickness of 30 millimeters. The sills are connected with mortar, resulting in a number of joints. These type of sills are always placed after the window has been installed.

Window size
An important aspect of the experiment is the featuring of a window that is expected to lower the resistance of the wall against any hydrostatic pressure. The size of the window can therefore have a large impact on the experiment. The choice of dimensions should not lead to uncommon shapes; yet, for the window size also the boundary conditions of the steel rig should be taken into consideration.

Once again the reasoning is depending on the knowledge that the experiment should represent an infill wall present in ordinary houses built around 1970. At that time the heating systems imposed a boundary at the lower side of the window; windows were placed at a height of 850 millimeters. The upper side of the window was limited by the ceiling at 2400 millimeters. A window would therefore have a calculated maximum height of 1500 millimeters.

Considering that the wall is placed on a steel beam, allowing a distance of 850 millimeters at the downward side of the window would mean only 35 centimeters of water can act on the window before the maximum water level of the basin is reached. In the design, the window is therefore lowered entirely to make sure a sufficient water level is guaranteed acting on the window.

For convenience, the size of the window frame was rounded down to the nearest course of bricks, so that no bricks should be cut in the horizontal direction. To guarantee a smooth transition from the fired-clay wall to the CaSi wall, both sections have the same height. Four courses of fired-clay bricks have the same height as three courses of CaSi bricks (including the joints). This also means the total height of the frame is a multiplication of four courses at the front and a multiplication of three courses at the back. Finally, this results in a height of 1450 millimeters.

The width of the frame is chosen based on the height. While squared windows are not uncommon, a rectangle shape is a more fitting choice in this case for this configuration. The wall itself is 2600 millimeters wide (a distance of twelve clay bricks). It is reasoned that a width of 660 millimeters (a distance of three bricks) results in an ordinary window shape while also allowing a sufficient length of bricks to be uninterrupted at either side of the window.

Framework and glass
A window frame can be constructed with ordinary sections as explained in 2.3.3. The available profiles are made from Meranti wood and are cut precisely to fit the dimensions. The profiles are already treated with a primary layer of paint.

For safety reasons, the glass is replaced by plexiglass (polycarbonate). This plexiglass has a tensile strength of 50 MPa and is much tougher than glass. Ordinary glass would probably not be able to resist the hydrostatic pressure, which would disturb the experiment and final results. The plexiglass has a thickness of 8 millimeters to counteract the pressure and to also resemble the thickness of ordinary glass.

Ventilation
The weep holes are essential in any wall section and therefore should not be neglected. The holes form a crucial pathway into the cavity and as such play an important role in this research. To understand if and how the water seeps through the window-wall interface the influence of these weep holes should be investigated. Afterwards, the effect of weep holes can either be ruled out or it turns out that the pathway through the cavity forms an important addition to the leakage. It is therefore important that the weep holes can be closed off in-between experiments. Ordinary weep vents are difficult to close off and therefore the weep holes are resembled by PVC-pipes. These pipes are much easier to close and re-open. The total area of one weep hole (3.8cm^2) is replaced by the area of two small pipes (4.0cm^2). The steel rig is too narrow to facilitate a cavity that features both the ventilation and insulation aspects. Therefore the insulation was neglected and this research focused on the open ventilation space instead.

3.2.2. Wall and window design

The wall and window were designed separately with the regulations and availability of the materials in mind. For the clay wall, a joint thickness of 10 millimeters was assumed in both the vertical and horizontal directions. With a brick height of 50 millimeters, the fired-clay brick wall was designed to feature 44 courses i.e. a total height of 2630 millimeters. For the CaSi wall, the joint thickness was assumed to be smaller, because the height of the used CaSi bricks is 72 millimeters. For convenience, the joint was assumed to be 8 millimeters. In that way, the CaSi wall could feature 33 courses of bricks which would also result in a height of 2630 millimeters.

Just like the clay brick, the courses in the CaSi wall were laid in stretcher bond. However, the CaSi bricks were slightly longer than the clay bricks, which would have led to too small pieces of brick near the window edge. In the design, this was prevented by cutting the bricks that were placed before the edge pieces, so that the edge pieces still all had a length of 10 millimeters i.e. the size of the header. The calcium silicate wall was constructed first, with wall ties placed in the mortar before hardening. For the locations of the wall ties see Figure 3.3. To allow for some tolerance at both sides of the cavity wall the cavity thickness was designed at 70 millimeters. Note that the steel rig has a total width of 300 millimeters. With both brick types having a width of 100 millimeters, a small niche of 15 millimeters could then be realised at both sides. For the final design and construction report of the wall see Appendix C and the accompanying blueprint Figure C.1.

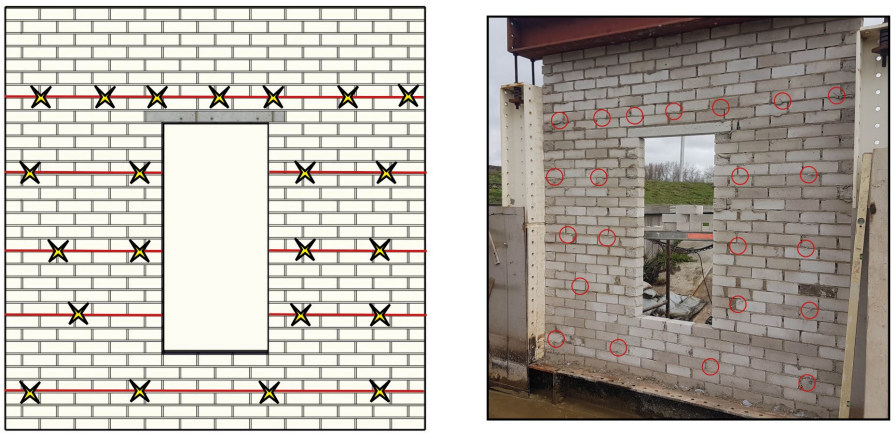

Figure 3.3: Illustration of the placement of the wall ties.

The window frame was designed with ordinary sections (67x114mm). The top and bottom profiles would cover the total width of the window space, while the lateral profiles should be cut to fit in-between the top and bottom profiles. The glass was replaced by polycarbonate and grills were placed inside the niche; locking the polycarbonate in the profile. To place the window into the wall, a secondary ordinary framework was designed. This secondary framework was placed inside the cavity. Afterwards, the window frame was screwed on the additional framework, see Figure 3.4. For the final design and construction report of the window see Appendix C and Figure C.2.

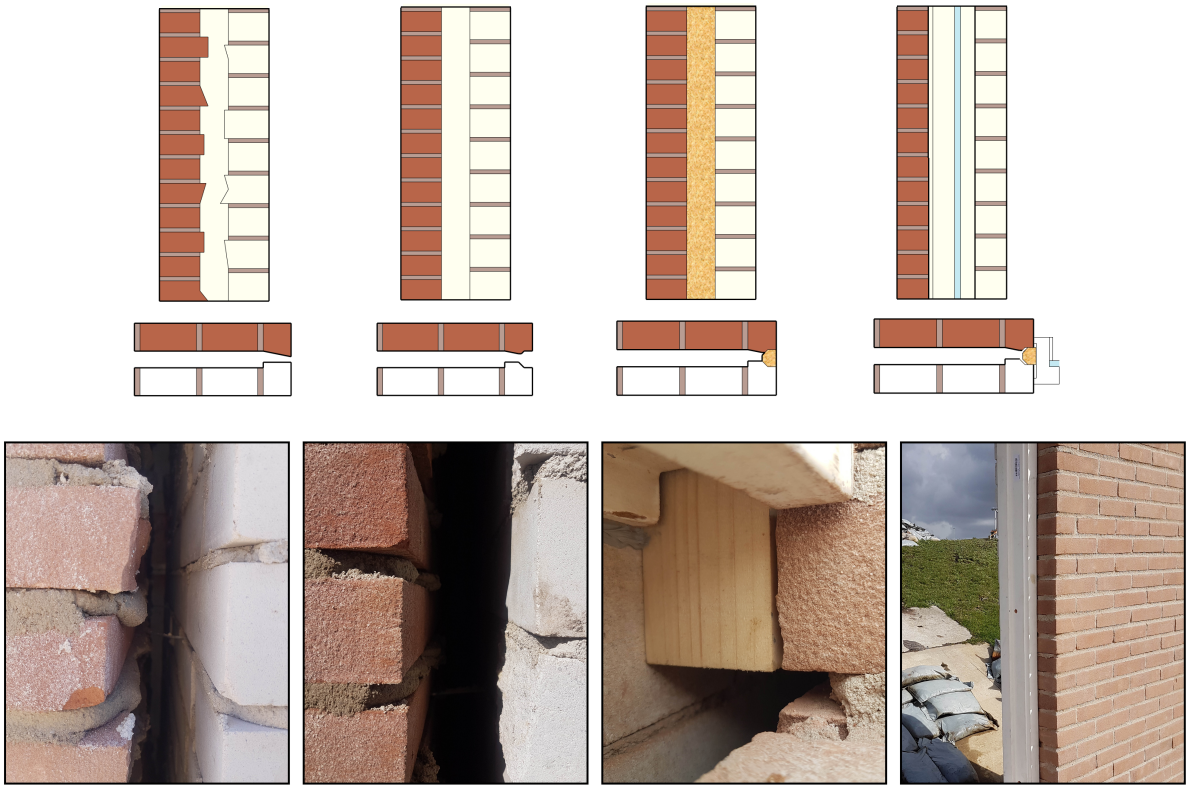

Figure 3.4: Illustration of the method of placement for the secondary framework. Top: Side view of the wall. Bottom: Top view of the wall. The grinder could only reach a couple of centimeters inside the cavity. The corners of the wooden framework were sanded to mitigate the problem. The framework was pulled into the rebate by tightening the screws.

3.3. Protocol cavity wall experiment

The life-sized cavity wall was build to investigate both the possible leakage through the window gap and the deformations (and potential failure) of the wall itself. To that extent, it was important to assure the experiments were arranged to do just that. To make the most out of this research a protocol was prepared that specified the order of the experiments and the tasks needed to obtain adequate data throughout the physical study. Before the final protocol, several assumptions were made. Below the underlying thoughts of the protocol are explained. Furthermore, attention is given to the additional equipment needed to obtain the data in a tolerable manner.

It should be noted that in order to find useful results, the cavity wall was subjected to destructive loads. From calibrated models from the previous experiment, it was predicted that a single masonry wall (constrained only at top and bottom) would fail at a water depth of around 90 centimeters [24]. Although in this research the wall is no longer single-leaf, the weakening effect of the window can still have a significant impact on the fragility of the wall. With 'failure' often collapsing of the wall is envisioned, however, failure can already become evident when cracks in the mortar withhold the wall from doing its structural need. Note the similarity between Ultimate Limit State (ULS) and Serviceability Limit State (SLS). Permanent damage arising from early tests can ruin the outcomes of the next. For that matter, the order of tests was important; not only to obtain decent data but also to get as much data before failure. Since in this case the water level differences were assumed to be the main loads, the smaller loads were tested earlier.

One can imagine the load distribution to be different when water is present inside the cavity. To find the behaviour of this empty space in-between the two walls, it was needed to keep the cavity dry; hence, the replacement of ordinary weep vents by two small pipes that could be closed-off in a more convenient manner (as discussed in 3.2.1). Closing off the cavity also allowed the leakage through the window-wall interface to be more noticeable. If the water started to collect in the cavity even though the weep holes were closed, this could only be attributed to the seepage through the interface. Of course, this meant the effect of a dry cavity would slowly die out when the cavity filled due to seeping water. It was, however, important to test the real situation. For that matter, the experiments with the artificial 'dry cavity' were sacrificed to grasp the real seepage rate. Note that clogging of the weep holes is a common problem, but also note the small probability of the weep holes all being clogged at the same time; hence, the dry cavity is to be labelled as an artificial experiment.

The same reasoning that was applied for the cavity was also applied to the backside of the wall i.e. the inside of a residence. During a flood event, the presence of water at the front side i.e. the clay brick wall is expected, but the rise rate inside the residence varies depending on multiple parameters. While the rise rate inside the cavity was regulated real-time by the weep holes, the presence of water at the backside of the wall had to be regulated manually during the experiments. This was due to the many parameters influencing the rise rate that were not accounted for in the set-up. The water levels that were recreated in the basin ranged from + 0.0 meter to +1.2 meter, with steps of 30 centimeters. These water levels could be present both at the front and the back of the wall, but with the notion that an inside water level could never be higher than the outside water level. These tests thus showed the behaviour of a cavity wall during a flood with (different) water levels at both sides of the wall.

Similar to the experiments revolving around the cavity, in some of the experiments the backside of the wall was kept dry to grasp the possible leakage through the window-wall interface. Again, this meant the artificial situation of no water inside the residence was sacrificed to find the seepage.

Finally, a last set of tests was envisioned to show the different behaviour of both walls individually. Closing the weep holes once more with water levels at both sides would take away any counteractive forces. This situation was assumed to be artificial as well but it would have given insight into the behaviour of the walls individually, which would have helped deduct possible causes of the recorded deformations. This set of test, however, failed. The division of the experiment is shown in Table 3.2.

	Weep holes are open	Weep holes are closed
Water level present at the front side	I	II
Water levels present at both sides	III	IV

Table 3.2: The four different sets of tests are divided into four categories depending on 1. the location of the water (one-sided or two-sided) and 2. the pathway into the cavity (open or closed).

With the water present at one side only, four possible water levels could be tested: +0.3m, +0.6m, +0.9m, and +1.2m, see Test I and Test II in Figure 3.5. With the weep holes open the water would enter the cavity and the water level inside the cavity would rise to an equal height as outside, although the rate of rising could differ depending on the head difference. With the weep holes open the hydrostatic pressure would thus act on the CaSi wall, since both sides of the clay wall would be partially submerged. When closing off the weep holes, the overall water pressure would transfer to the clay wall, since, in that case, the water would only act on the front side of the clay wall. While the CaSi wall was glued to the steel rig to mimic the connection with the structural frame of a house, the clay wall was attached only with mortar to mimic the facade properties. For this reason, the clay wall was assumed to be weaker than the CaSi wall. For the progress of the experiment it would be convenient to test the open cavity first since the water inside the cavity had a favourable effect; reducing the pressure acting on the clay wall.

Test		Water levels [cm]			Duration [h]
		Outside [h_I]	Inside [h_{II}]	Cavity [h_{III}]	Duration [T]
I	.a	30	0	≈ 30	1h
	.b	60	0	≈ 60	1h
	.c	90	0	≈ 90	1h
	.d	120	0	≈ 120	1h

Test		Water levels [cm]			Duration [h]
		Outside [h_I]	Inside [h_{II}]	Cavity [h_{III}]	Duration [T]
II	.a	30	0	0	1h
	.b	60	0	0	1h
	.c	90	0	0	1h
	.d	120	0	0	1h

Test		Water levels [cm]			Duration [h]
		Outside [h_I]	Inside [h_{II}]	Cavity [h_{III}]	Duration [T]
III	.a	30	30	≈ 30	1h
	.b	60	30	≈ 60	1h
	.c	90	30	≈ 90	1h
	.d	90	60	≈ 90	1h
	.e	120	30	≈ 120	1h
	.f	120	60	≈ 120	1h
	.g	120	90	≈ 120	1h

Test		Water levels [cm]			Duration [h]
		Outside [h_I]	Inside [h_{II}]	Cavity [h_{III}]	Duration [T]
IV	.a	30	30	0	1h
	.b	60	30	0	1h
	.c	60	60	0	1h
	.d	90	30	0	1h
	.e	90	60	0	1h
	.f	90	90	0	1h
	.g	120	30	0	1h
	.h	120	60	0	1h
	.i	120	90	0	1h
	.j	120	120	0	1h

Figure 3.5: Overview of the planned experiment. Four different sets of tests show both the deformations and leakages depending on the different loading schemes. Note that for the categories with an open cavity (I, III) the water level in the cavity, denoted as h_{III}, is assumed to be equal to the outside water level, denoted as h_I, but with a lower rise rate. Hence, the notation with: ≈

Next, with water also present at the backside of the wall the combinations of hydrostatic loading were expected to be more extensive, which becomes obvious looking at category IV in Figure 3.5. Again, it was assumed that water inside the cavity would rise to a similar level as the water level outside. For this reason, it would not make sense to test the combinations where the water levels inside the cavity, h_{III}, and in front of the wall, h_I, are equal to the water level behind the wall, h_{II}. In that case, the complete cavity wall would be submerged in the same depth, which takes away any head differences. Note though that this would be the ideal situation during a flood event regarding the structural aspect. The third category is therefore stripped from the unnecessary combinations, which left a total of 24 different tests.

The duration of a flood event can have a significant impact too. Creep and relaxation can lead to redistribution of the acting stresses. To account for that, and to save water, multiple tests were carried out during the same recording. Within the protocol, it was tried to get as much data as possible for all four categories.

The order of tests was therefore arranged according to the following rules and resulted in the order as shown in Figure 3.6. Firstly, the order of experiments depended on the inclusion of all four categories. Secondly, the order was arranged depending on the water level differences between both sides of the clay wall i.e. the opening or closing of the cavity. Next, the order of experiments depended on the water level differences between both sides of the total cavity wall. Finally, the order of experiments depended on the amount of water lost with lowering the water level in-between experiments.

			Water levels [cm]			Expected water level diff. [cm]		
	#	Test	Outside	Inside	Cavity	Clay	CaSi	Total
TEST	A	0.a	30	0	0	30	0	30
	B	0.b	30	30	0	30	30	0
	C	0.c	0	30	0	0	30	-30
Open	1	I.a	30	0	→30	0	30	30
Closed	2	IV.a	30	30	0	30	30	0
	3	II.a	30	0	0	30	0	30
Open	4	III.a	60	30	→60	0	30	30
	5	I.b	60	0	→60	0	60	60
Closed	6	IV.c	60	60	0	60	60	0
	7	IV.b	60	30	0	60	30	30
	8	II.b	60	0	0	60	0	60
Open	9	III.c	90	60	→90	0	30	30
	10	III.b	90	30	→90	0	60	60
	11	I.c	90	0	→90	0	90	90

			Water levels [cm]			Expected water level diff. [cm]		
	#	Test	Outside	Inside	Cavity	Clay	CaSi	Total
Closed	12	IV.f	90	90	0	90	90	0
	13	IV.e	90	60	0	90	60	30
	14	IV.d	90	30	0	90	30	60
	15	II.c	90	0	0	90	0	90
Open	16	III.f	120	90	→120	0	30	30
	17	III.e	120	60	→120	0	60	60
	18	III.d	120	30	→120	0	90	90
	19	I.d	120	0	→120	0	120	120
Closed	20	IV.j	120	120	0	120	120	0
	21	IV.i	120	90	0	120	90	30
	22	IV.h	120	60	0	120	60	60
	23	IV.g	120	30	0	120	30	90
	24	II.d	120	0	0	120	0	120

Figure 3.6: The order in which the different testing occurred as part of the experimental protocol. For completeness, the expected water level difference is shown as well to clarify the order. The fact that the water level inside the cavity will rise to the same level as outside is denoted with: →

3.4. Equipment and completion of the set-up

In order to retrieve the data as contemplated above, the experiment was accompanied by multiple sensors and additional materials that were attached to the wall. In the following section, these materials are listed and the utility of this equipment is explained.

3.4.1. Catchment box and cavity closers

An important aspect of this experiment was to capture the wall's behaviour during a flood event; especially when the water level outside is more significant than the inside water level. To regulate the water level at the back separately from the general water level in the basin, it was needed to cut off the backside of the wall from the water supply. Previously, this was tried with an artificial sandbag dike. Although the sandbags turned out to be sufficiently water-tight, water still entered the backside. This was mainly due to the gaps between the concrete plates on the floor of the basin. Eventually, the piping phenomenon occurred that carried the sand particles in its flow and lowered the tiles; allowing the water to flow in from underneath the steel rig [24].

With the heavy steel rig firm in its place, an alternative was needed. Mitigating the piping problem would be too difficult and possible seepage through the window-wall interface could go unnoticed by these ordinary leakages. The alternative therefore should not only keep the water out but also keep the water originating from the window-wall interface in. Additionally, the alternative could not counteract or intervene with deformations. Eventually, a solution was found by placing a box around the perimeter of the wall. This catchment box allowed the wall to deform without constraining it and with this, the seepage could be recorded as well.

The plates of the box were cut in such a way that flanges were created that could protrude into the I-shaped profiles of the steel rig, see Figure 3.8 for the result. The details can be found in Figure C.3. A silicone substance was put on these flanges and by hammering wedges in-between the profile, the box' flanges were pressed against the flanges of the rig. When the overall water level in the basin rose the water pressure started pressing the wooden flanges tighter against the rig. The same silicone was used to make the edges and corners of the box watertight. By constructing the box, the possible 'length of failure' is shortened extensively and unwanted leakages can be solved more conveniently. Although the problem of piping was now averted, a new possible failure mechanism was introduced i.e. buoyancy. With buoyancy depending on the surrounding water level its behaviour is well-predicted and described by Archimedes' principle. Buoyancy could thus be accounted for during the experiments by weighing down the box with a number of sandbags.

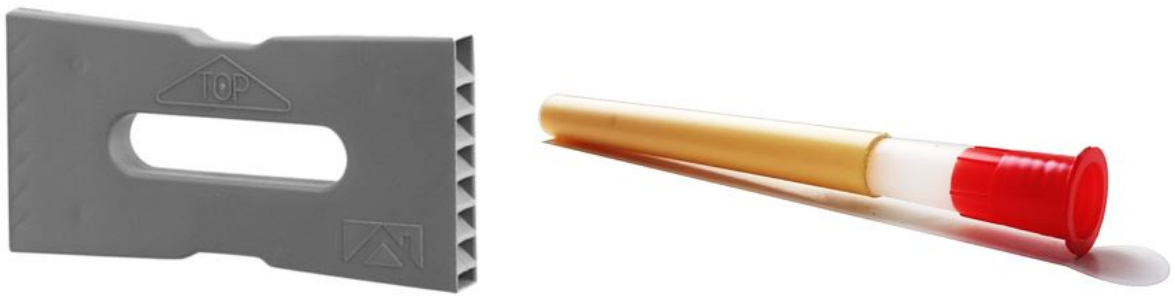

Figure 3.7: Left: Typical weep hole grills that are currently used on building sites. Note that, although the grill covers the complete joint, the possible discharge through the grill is significantly lowered due to the recess in the middle.
Right: The cavity closers used during the experiment. The cone-shaped plugs are marked red for visibility.

Figure 3.8: Left: The catchment box during testing. A small pump located inside the box is used to empty the box when needed. Centre: The small pipes used to mimic the weep holes. Right: location of the springs.

As explained earlier, recreating water levels at the backside of the wall was done separately from the remainder of the basin. A small gap in the bottom of the box was conceived to have the same rise at both sides of the wall. However, still, a pump was needed to allow the realisation of certain water depths in the catchment box independently from the basin.

The direct pathway between the outside and the cavity that exists in both the set-up and any real situation eliminated the need for artificial control of the water level. Yet, for the experiments, it was needed to completely disconnect the cavity from the basin. For that matter, the weep holes were replaced by pipes in the design. The pipes were cut 15 centimeters each to make sure they would protrude into the cavity. To determine the number of pipes to be fitted as one weep hole the area was investigated. Although the area of a joint would be close to 500 mm^2 (which would be 2.5 times the area of a pipe), the design of certain weep hole grills implies a much smaller area; see the left image in Figure 3.7. For convenience, it was therefore chosen to install two pipes at each weep hole, see corresponding Figure 3.8. The pipes have a diameter of 5/8" which roughly translates to 16 millimeters. To close the four pipes use was made of cone-shaped plugs. With the water level in front of the wall always being higher or equal to the level inside the cavity the plugs were forced into the pipes instead of outwards; creating a water-tight boundary; see the right image in Figure 3.7.

A final task required the springs at the top to be activated (Figure 3.8). The springs were tightened to exert a total of 25 kPa on the wall as to mimic the weight from an overlaying floor. A wall will start deflecting under pressure. To allow this deflection the bricks will have to turn slightly in the vertical plane. This second-order effect is resisted by the weight of the floor. Because of this, the beam was lowered onto the CaSi wall only and the two corresponding springs were pressed. The springs each had a stiffness of 1.18 kN/mm. The springs were pressed 5.5 millimeters each. The remaining two springs at the front were pressed only slightly (« 1 millimeter) to maintain contact with the steel rig.

3.4.2. Sensors

For the collection of the data, use was made of two different types of sensors: pressure sensors (employed to measure the water depth) and linear potentiometers or pot. sensors (to measure the deflections). The sensors were prepared in the Stevinlab at the faculty of Civil Engineering and Geosciences. The changes in voltage observed by the sensors were converted into pressures and displacements; both in the order of millimeters with a resolution of 1 μm. Each sensor was calibrated individually to account for non-linear effects.

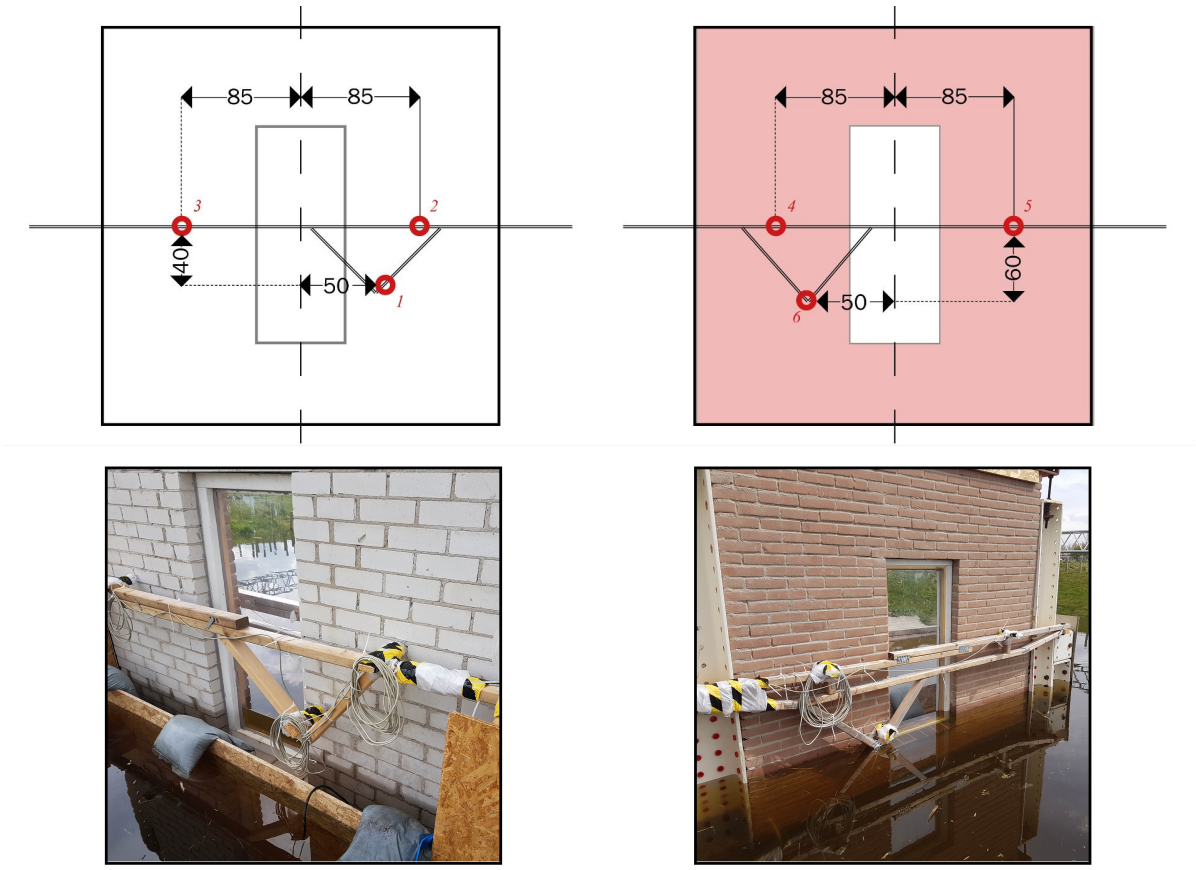

Figure 3.9: Left: Back view of the locations of sensors 1,2, and 3 relative to the centre lines of the CaSi wall.
Right: Front view of the locations of sensors 4,5, and 6 relative to the centre lines of the fired-clay wall. Note that, while the image may suggest otherwise, the timber structures are in fact mirrored.

After transportation to FPH, the sensors were placed on two separate timber structures at both sides of the wall as shown in Figure 3.9. When greater water levels were realised in the basin sensors 1 and 6 were moved up to keep the sensors from getting wet. To make sure the potentiometers actually measured the deflection of the wall instead of an irregularity in the masonry, the potentiometers were placed against a small piece of polycarbonate which was glued to the wall beforehand. Note that the potentiometers at the front were already pressed to their maximum since the clay wall was expected to deform in the backward direction.

The sensors were then connected to three network cables with eight wires each to allow the PC and the Measurement and Control Unit (data acquisition box) to be placed inside. To divide the wires over the sensors some of the network wires were shared. The data was stored in the MP3 software, proprietary to the lab; every 30 seconds the software sampled a new data point for each sensor. Additional specifications on the sensors and the wiring of the cables can be found in Appendix D.

4

Results

During the experiment, results were obtained that describe the displacements of six points on the cavity wall. The recordings of these points indicate certain movements of the wall as a whole. The wall moves to withstand the loading that is governed by the hydrostatic forces of the water. A description of the water levels is provided by the pressure sensors that recorded the levels during the experiment at both sides of the wall as well as inside the cavity. By combining both sets of recordings numerous parameters are obtained that characterize the masonry. These can be used to assess existing structures, but here they are used as input for the analysis to come. Not all the needed characteristics could be found in this manner and as such small-scale tests were performed on the couplets to partly complement the list of characteristics. A final set of parameters is obtained from literature.

This chapter firstly presents some general observations during the tests as they have changed the course of this research. Secondly, results on the deformations inferred from the data are presented. Next, the results of the bond-wrench tests are treated. The final section of this chapter treats the seepage through the window-wall interface.

4.1. General observations

After the first test, it became clear that the water was slowly leaking into the catchment box. Although the pump could handle the amount of water with ease it became difficult to keep the water level inside the catchment box at a still. Of course, the higher the water levels became, the quicker the water-filled the box. While it was tried to find the origin of certain leakages, the main source of the water came from inside the cavity. At every new level, the water came seeping through new holes in the joints of the calcium silicate wall. While this can certainly be the case with ordinary houses also, the thin layer of plaster that is often found on the walls prevents the water from having a direct pathway. At water levels of 1 meter, finally, the capacity of the pump was reached and the box no longer could be emptied.

A second problem was found when the cavity closers were installed. Although the closers worked adequately, the cavity could not be kept dry. In fact, the water was entering the cavity through the connections of the steel beams at the bottom. At high water levels, however, the holes in the CaSi joints became a useful way to pump the cavity to a lower level. By installing the cavity closers, the biggest contributors to the discharge into the cavity were blocked. The remaining water was leaking through the CaSi wall and eventually removed from the catchment box. In this manner, the water level inside the cavity could be kept half of the original water level.

Test	Cavity	Waterlevels	Additional precompression	Remarks
A	closed	40 cm	25 kPa	*Failed to keep the cavity dry*
B	open	70 cm	25 kPa	
C	open	90 cm	25 kPa	*box deformed and touched sensor P1*
D	open	110 cm	25 kPa	*Rupture of the sealant between steel and wall*
E	open	110 cm	25 kPa	
F	closed	110 cm	≈0 kPa	
G	open	110 cm	≈0 kPa	*Installment of new sensor framework and replacement of pump hose*
H	closed	110 cm	≈0 kPa	
I	open	110 cm	≈0 kPa	*A second pump was added to drain the box more quickly*
J	both	110 cm	0 kPa	*The top beam was loosened further*

Table 4.1: Overview of the short tests performed at FPH. The combinations varied throughout the tests and included the installment of the cavity closers, the maximum water level, and the additional precompression of the springs.

While it was expected that uplift would be a severe problem, it turned out not to be. According to Archimedes' principle, every new raise of water (30 centimeters) would require eight more sandbags of 25 kilograms to be placed. Indeed, the weight of the box itself was not accounted for and reduces the amount of counterweight needed. However, it is most likely that the biggest reduction for the uplift can be attributed to the connection to the steel rig. Since a quarter of the total width of the catchment box was embedded in the steel beams a significant forcing could be transferred to the steel columns. The remaining bending moment then was reduced by the placement of the sandbags on the outer edge of the box.

4.2. Deformations of the wall

The sensors recorded pressure and deflections every 30 seconds. In addition to the values for the nine sensors, the files also contain an index column, date, and time. With time present in all the recordings the six displacements can be related directly to the water levels measured by the pressure sensors. After the data collection, the values of the potentiometers at the front (P1, P2, and P3) were reversed so the coordinate systems of both sides of the wall are now identical. With this coordinate system two main directions are introduced: inward movement of the wall and outward movement of the wall. The directions correspond to the perception of residents; during a flood event an inward moving wall would end up being pushed into the living room, while an outward moving wall would be pressed onto the streets. Do note that these directions are merely used to indicate the different deformations and that it does not necessarily represent the failure mode of the wall. The wall is expected to fail due to the exceedance of the internal bending moment or due to great displacements. The main directions are illustrated in Figure 4.1.

4.2.1. Preliminary results

Eventually, ten tests have been performed that are listed in Table 4.1. Next to these recordings, three long tests were performed throughout the measuring campaign. The long tests recorded the natural oscillations of the sensors without the presence of water in the basin. The oscillations are the (partial) result of the temperature variations and can have amplitudes of 2 mm (see Appendix D).

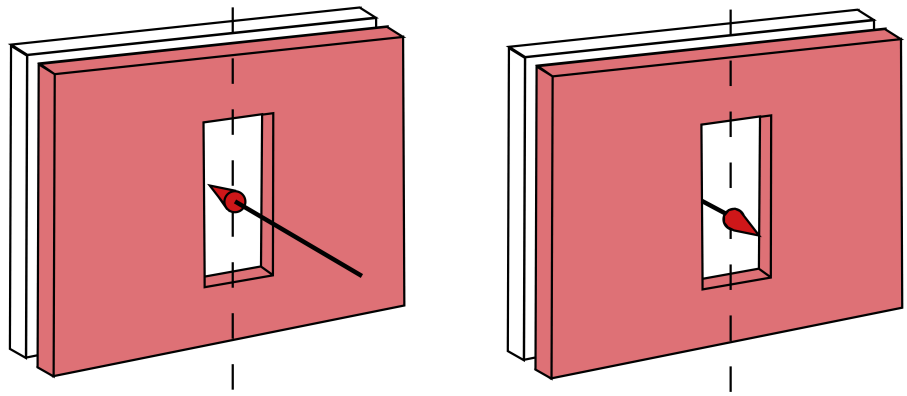

Figure 4.1: Left: illustration of inward movement of the wall. The sensors are pressed and measure positive deflections. Right: illustration of outward movement of the wall. The sensors are released and measure negative deflections.

The initial analysis of the results is based on the graphical representation of the data. These graphs are shown in Figure 4.2 and Figure 4.3. For a clear overview, the graphs showing the water level data are toned. The corresponding deformations are shown right next to the water level graphs to have a pairwise comparison between the two data sets (A-1, B-2, ..., I-9, J-10).

During the experiments, the catchment box was emptied by a small pump and then slowly filled again. This sawtooth behaviour can be seen clearly by the green line of the toned graphs (indicated as 'back side' in the corresponding legend). Whenever the water level at the back of the wall reached a near-zero value, the head difference was maximum. This difference is assumed to be the impetus of the deformations of the wall. Clearly, it can be observed that the deformations become greater when the head difference increases. Yet, some recordings show an outward movement, which is highly unlikely given the fact that the net force is identical to 'what would be' the inward direction. For the sensors at the front (P4, P5, and P6), this effect almost explicitly occurs at the end; when the basin is drained. For the sensors at the back, the outward movement occurs at the start; during the basin fill. While for most of the data this error lies between [0, -0.2mm], the errors in graph 2 and graph 6 grow to -0.5 millimeter. In Appendix D it is shown that the sensors are sensitive to temperature changes, but this sensitivity cannot be related to the errors measured here.

Almost identical situations in terms of water levels do not necessarily result in identical deformations. This can be attributed to permanent damage or hysteresis. Especially regarding the smaller water levels, the latter seems the most plausible. When cracks do start to form the internal forces will redistribute which eventually leads to permanent damage, but at levels lower than 80 centimeters this cracking is not yet severe. Hence, the sensors show some memory, meaning that they are also dependent on their own 'history'. This can be seen clearly in graphs 2 and 7; the deformations do not return to their initial zero and as such increase every time the backside water level is lowered. Although the graphs suggest the deformations are increasing the relative displacements are in fact similar. For graph B-2 the relative displacements are checked for the identical situations, namely at T=2000, T=4000, and T= 5100. At these moments the water levels are equal (see graph B) and the expected deformations would be zero. The subsequent increase in hydraulic pressure, resulting from lowering the water table at the back produces an increase in deformation (graph 2). The relative displacement is defined as this increase in deformation. For the three situations, the relative displacements are 0.24 mm, 0.21mm, and 0.20mm; indicating significant hysteresis of the sensors.

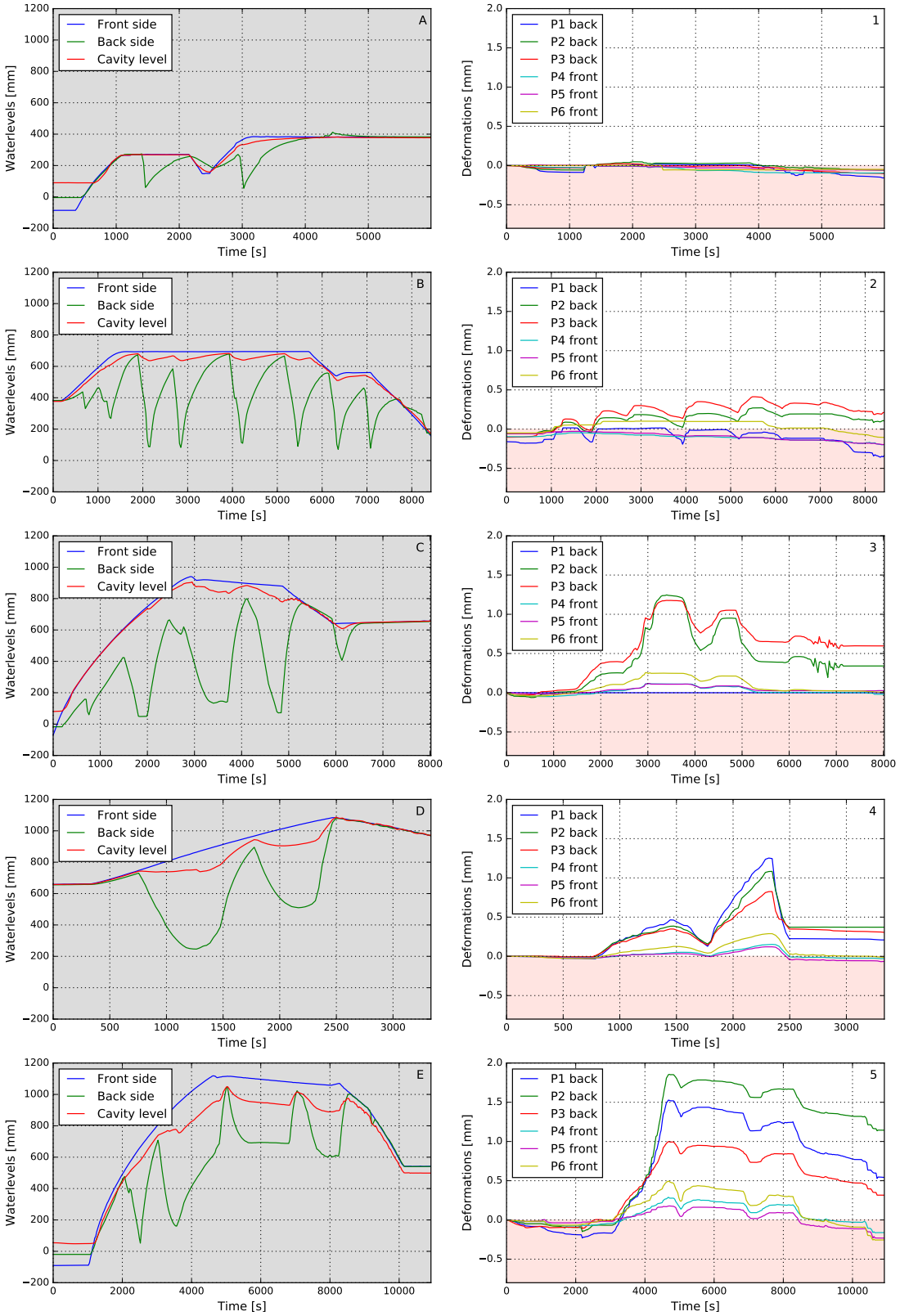

Figure 4.2: Graphical representation of the first five test rounds. If the sensors indicate an outward movement of the walls the individual lines enter the negative regime. This is indicated by the red area visible in the graphs denoted by the Arabic numerals. The graphs denoted by capital letters show the water levels.

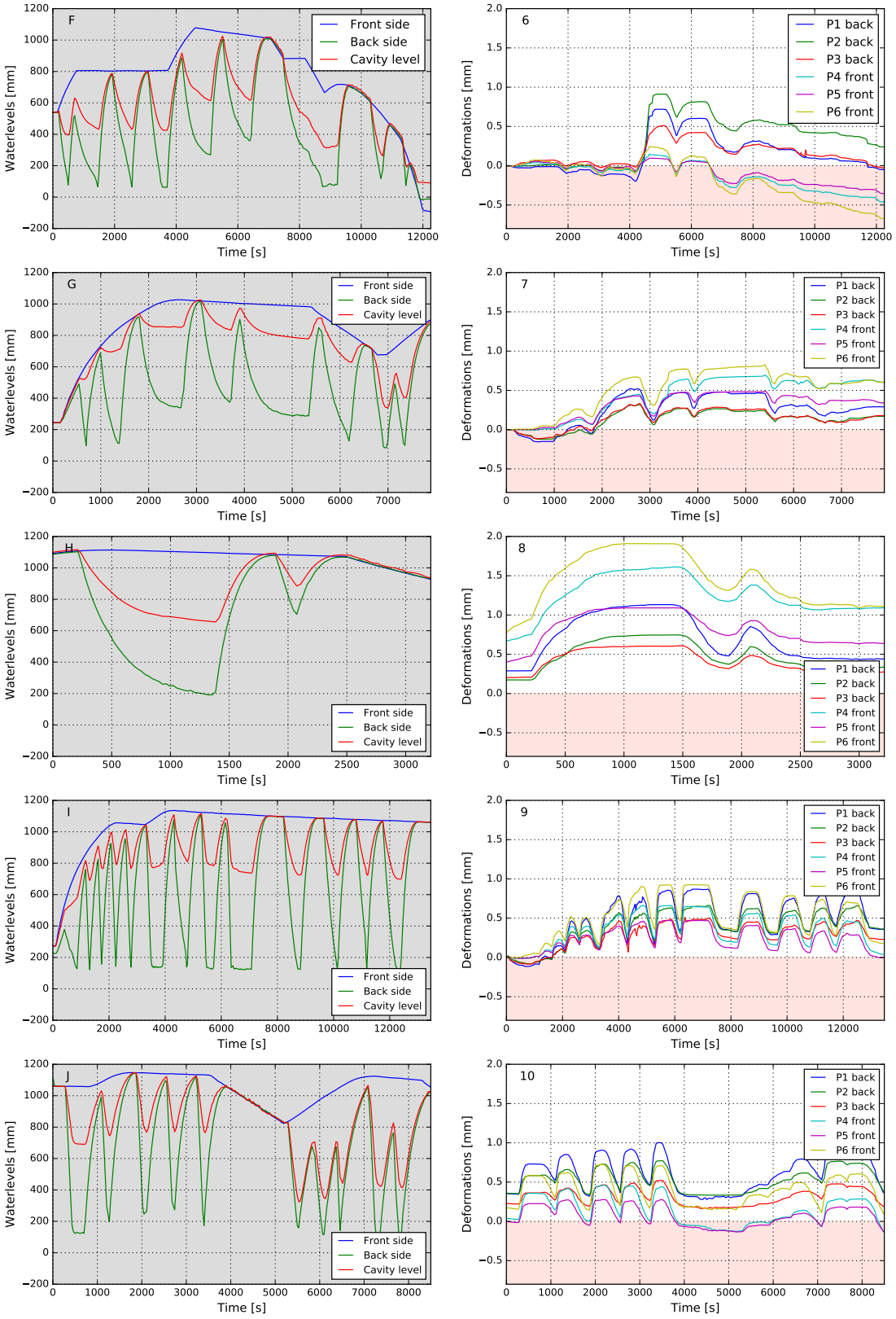

Figure 4.3: Graphical representation of the final five test rounds.

In all recordings, but the final four, the displacements of the sensors at the back are greater than at the front. This seems to be coherent with the water levels. In Figure 4.2 the head difference at the CaSi wall is far greater than the head difference at the clay wall. Note that the head difference for the CaSi wall is defined as the water level difference between cavity level and backside, while the difference between the front side and cavity level defines the head difference at the clay wall.
However, these obvious differences in head diminish in graph E (Figure 4.2) and F (Figure 4.3). Yet, the corresponding deformations still show a greater value for the CaSi wall. This can indicate that the back sensors are measuring interference from the catchment box. It was expected that the box was pressed onto the steel rig whenever the box was drained. However, the flanges were expected to prevent the box from moving in or outward. From afterward observations, the flanges seem to be slightly crushed, which corresponds to the outward moving of the box and would result in an additional pressing of the sensors.

After the initial measuring campaign a new framework was welded and installed. This new steel frame facilitated the back sensors. It was installed on the steel rig rather than the catchment box. With this, the interference of the box was removed. This resulted in the final four recordings (G-7, ..., J-10). As expected, with the new framework, the back sensors show smaller deformations; suggesting that the box was indeed interfering.

Throughout the experiment, the sensors P2, P3, P4, and P5 did not change position. Note that these four sensors were placed at a horizontal distance of 85 centimeters from the centre at a height of 135 centimeters. Although the results from P4 and P5 started diverging more at the final recordings they were quite in sync with their measurements. This indicates that there were no second-order movements and that the wall deformed similar left and right. From recording C-3 and onward sensor P6 was relocated at the same height but 50 centimeters from the centre, see Figure 3.9 once more. This sensor almost consistently measured greater displacements, which raises the question if the window allowed the wall to deform more significantly.

From the back sensors (P2 and P3) it can be concluded that they were not in agreement. However, neither one of them is consistently showing greater deformations than the other one. Looking at the final recordings the measurements of both sensors are quite similar. Since in these tests the interference from the box was excluded, the results are deemed more trustworthy. Therefore it is concluded that the CaSi wall also deformed similar left and right. At the beginning of test D-4 sensor P1 was placed at the same level as the other two sensors, but closer to the middle as well (50 centimeters). Also for this sensor, no consistent bias can be observed. From test G-7 and onward the back sensors were relocated onto the new framework. The distances from the centre line were all kept the same, with only the distance from the bottom deviating a few centimeters. From these two tests again it can be concluded that the deformations near the window (P1) were greater.

The results in Figure 4.2 and Figure 4.3 reveal that some deformations increase even though the head difference decreases. This behaviour can be found in graph 4 and graph 5. While this seems contradictory in fact it is a consequence of the upward movement of the net force. Due to the rising of the water at the backside, the net force decreases, but the leverage distance from the steel support increases. The net force is therefore applied closer to the middle of the wall. From mechanics, it is known that a beam supported at both ends has a maximum deflection when a force is applied to the centre of the beam. To obtain a clearer relationship between water and deformations it is ought to convert the water levels to an equivalent bending moment.

4.2.2. Equivalent bending moment

To combine the water levels at both sides of the wall, the hydrostatic pressures are translated into one equivalent bending moment. The hydrostatic pressure is of course depending on the water depth; this gives it a triangular shape. The point load therefore can be found at one-third of the total water depth. The bending moment is a multiplication of the triangular area times the moment arm. Different water levels at both sides of the wall, therefore, lead to different bending moments. With linear superposition, the two moments can be converted into one equivalent bending moment. The results are found in Figure 4.4.

From Appendix F it is deducted that the average rank correlation coefficient between the water levels and the deformations for the CaSi wall is only 0.395, while the rank correlation between bending moments and deformations becomes 0.501. For the clay wall, these values respectively become 0.544 and 0.659. This shows that indeed the equivalent bending moment is stronger correlated with the deformations than the water levels are.

Looking at the graphs in Figure 4.4 it becomes clear that it is the clay wall that has been subjected to much greater bending moments per unit meter, while the bending moment acting on the CaSi wall stagnates at 1000 Nm/m. The maximum bending moment that has acted on the CaSi wall was recorded during test 9 (Graph I, Figure 4.4). Here the moment originating from the water was 1139.798 Nm/m which translates to a total inward moment of 2963.475 Nm. The maximum bending moment that has acted on the clay wall was recorded in the final test and reached 2184.67 Nm/m i.e. an inward equivalent bending moment of 5680.142 Nm total, which is roughly twice the moment that acted on the CaSi wall.

For better understanding, the relationship between force and deformation is investigated further. Although the inclusion of water levels would seem more logical, the correlation coefficient clearly suggests otherwise. Therefore the bending moment is plotted against the deformations. It was already determined that the sensors left and right were not measuring differently and as such the sensors are combined for these plots. The plots are shown for both walls in Appendix G. In the plots, the hysteresis phenomenon is once more visible, with multiple deformations corresponding to the same momentum value. Although blurry, the plots on the clay wall show a more 'sharp' behaviour while the force-displacement plots of the CaSi wall behave more 'circular'. This 'circular' effect indicates greater displacements and possibly permanent damage to the mortar. Especially in the earlier tests, the sensors recorded a significant increase in displacements for the CaSi wall, while the bending moment hardly increased. In none of the plots do the deformations return to the start value; often indicating permanent damage.

For a more obvious overview of the stiffness of both walls, the initial slope of the plots is collected and compared. Note that this fit is extrapolated for the experiments where small water levels were tested. Due to scaling the effect would otherwise not be visible (see the first and second plots of both walls in Appendix G once more). The linear fits are shown in Figure 4.5. For both the clay wall and the CaSi wall degradation of the stiffness is visible, with test 1 and test 3 regarded as outliers. The stiffness for the clay wall reduces after the fourth test. The fourth test was the first test where water levels above 1.0 meter were reached. After the sixth test, the CaSi wall starts recording lower stiffness as well. Note that the new sensor frame was installed before test 7. It shows that afterwards, the stiffness did not change significantly and that the slopes are quite similar. Generally, the calcium silicate wall seems to have a lower stiffness compared to the clay wall. Although the degradation could indicate that the walls endured permanent damage throughout the experiment, the sudden similarity of the final four tests might also show the previous results are somewhat distorted.

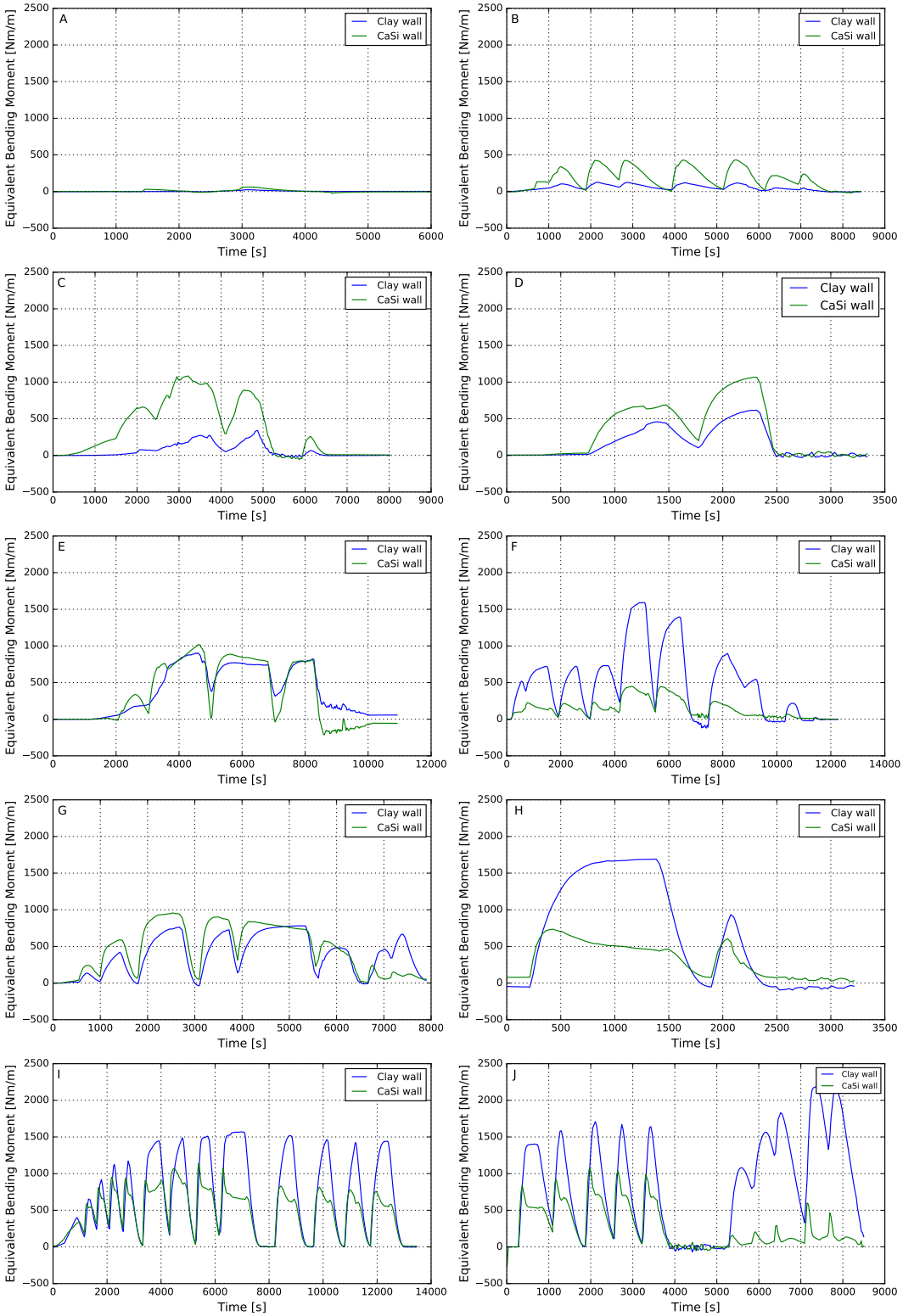

Figure 4.4: Equivalent bending moments. The hydrostatic pressures from both sides of the individual walls were subtracted by the superposition principle. The outcomes show the bending moment acting on the CaSi wall as well as on the clay wall. Note that the capital letters correspond to the previous graphs to maintain the pairwise comparison.

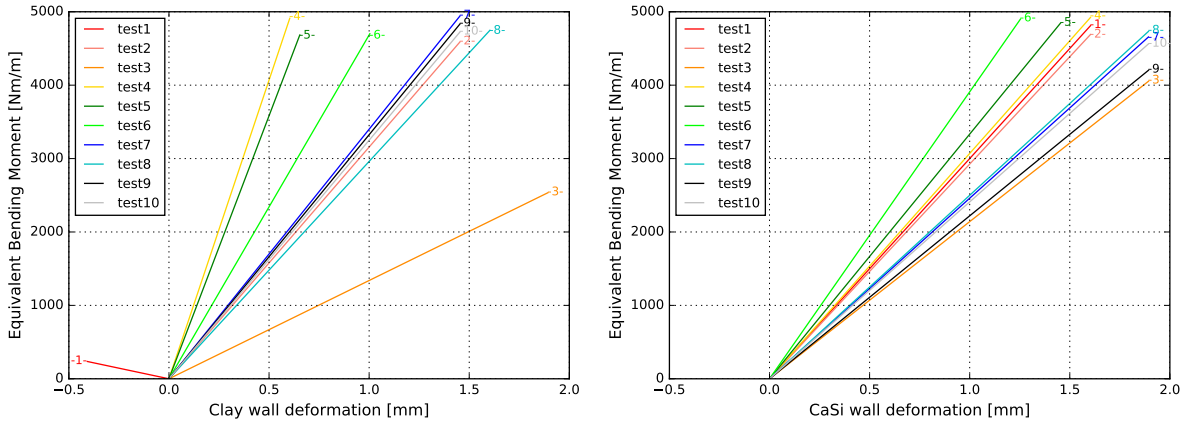

Figure 4.5: Left: the different slopes obtained from the force-displacement plots regarding the clay wall. Note that a negative slope does not make sense and that this is a consequence of extrapolating the results of test 1. Right: The slopes obtained from the CaSi plots.

For the final four tests, an additional investigation is performed in the sensors installed closer to the window gap. In the final configuration, all sensors were placed at the same height, yet one at both sides was placed at a closer horizontal distance. Again the initial stiffness is computed by a linear fit. Here, no degradation effect is visible. The results consistently show an increased stiffness on the calcium silicate side. The stiffness at the clay wall has increased too, albeit only slightly. This can hint that the window frame is acting as a solid body. During the installation of the window, the frame was placed and attached neatly in the CaSi wall, while no real connections were made with the clay wall. Yet, the secondary framework placed in the cavity created a solid (wooden) connection between both walls. This would at least partly explain the increase in stiffness in the wall areas closer to the window.

4.3. Bond wrench test results

Several additional parameters are necessary to model masonry failure due to out-of-plane bending. These parameters are revealed by small-scale (destructive) tests. For both brick types, nine couplets were constructed on the same day as the wall. The couplets were placed next to the wall to have the same meteorological conditions, see Figure 4.6. After eight weeks of hardening, the couplets were transported to the lab where they were used for bond wrench tests. Two couplets broke during transportation (one for each brick type). This standard test reveals the flexural bond strength, f_{x1}, which is then used to determine the tensile strength in the vertical direction. The tensile strength cannot be obtained directly through tests due to the fragile nature of the couplet.

During a bond wrench test, the bottom brick is restrained inside a framework to prevent the couplet from moving. A wrench is attached to the top brick that is used to exert a moment on the joint. The eccentric self-weight of the wrench acts as a second moment with a lever arm of 53.1 mm. The first moment is created by a jack forcing on a distance of 460 mm of the tension face. Two linear variable differential transformers (LVDT) are placed over the longitudinal joint, measuring the opening between the bricks. The vertical displacement of the jack is also measured. Due to the constant computer-controlled rate at which the couplet opens up the tensile fracture energy can be computed as well. Note that this configuration only leads to the vertical tensile strength, f_{t1}. The horizontal strength, f_{t2}, would be revealed by shear tests. No shear tests were performed, however. The results on the bond strength , f_w, and tensile fracture energy, G_{f-t}, are listed in Table 4.2. Further details and results obtained during the bond wrench tests can be found in Appendix H.

Specimen	Bond strength [MPa]	Tensile fracture energy [N/mm]
Clay_A	-	-
Clay_B	0.17	0.009
Clay_C	0.01	0.001
Clay_D	-	-
Clay_E	0.03	0.001
Clay_F	0.37	0.046
Clay_G	0.03	0.001
Clay_H	0.19	0.012
Average	*0.13*	*0.012*
st. deviation	*0.14*	*0.017*
c.o.v.	*1.02*	*1.49*

Specimen	Bond strength [MPa]	Tensile fracture energy [N/mm]
CS_A	-	-
CS_B	0.005	0.0004
CS_C	0.005	0.0014
CS_D	-	-
CS_E	0.007	0.0008
CS_F	0.002	0.0006
CS_G	0.009	0.0010
CS_H	0.006	0.0007
Average	*0.006*	*0.0008*
st. deviation	*0.003*	*0.0003*
c.o.v.	*0.470*	*0.41*

Table 4.2: Lab results on the bond strength and tensile fracture energy. Note that for both types of brick specimen A and D broke during installation and as such are not used in further calculations.

The results show a clear difference in bond strength between the CaSi bricks and clay bricks. Both types of bricks are showing outliers, although the results for the clay bricks are deviating more significantly from the average value (see the coefficient of variation). The same can be concluded from the values on the tensile fracture energy. Nevertheless, the average bond strength originating from the CaSi bricks is extremely low. It is certainly possible the CaSi bricks used for the couplets were too dry, absorbing the water from the mortar. The meteorological data (Appendix E) shows that during the construction of the couplets, and the clay wall, the sun was shining almost contiguously. Perhaps this weakened the mortar even further. Because the clay bricks have a lower absorption this could partly explain the difference in bond strength.

Previous tests using the same batch of bricks and mortar show an average bond strength of 0.09 MPa (2017) and 0.08 MPa (2018). Both values were obtained with a sufficiently low c.o.v. of 0.35 and 0.32 respectively [24]. These values are similar to the characteristic value in the Eurocode for baked clay: 0.1 MPa. While for calcium-silicate bricks this characteristic value is half the value for baked clay, this still is ten times larger than the bond strength found in the test results. Additionally, mean values obtained from the Dutch NEN-codes (NPR, Nederlandse PraktijkRichtlijn) show tensile fracture energy values of 10 N/m. The test results reveal a fracture energy of 12 N/m and 8 N/m for clay and CaSi bricks respectively. While a rule of thumb suggests the flexural strength in the vertical direction should be around similar to the bond strength, results from earlier experiments indicate that the vertical strength should be around twice the bond strength [24].

Figure 4.6: The couplets were left to harden next to the wall for the same duration.

4.4. Seepage through the window-wall interface

It should be emphasized that during a flood the wall is subjected to multiple flood actions; of which hydrostatic pressure is just one. The impact of hydrostatic pressure can be mitigated or averted by a counter-pressure from inside, while, for instance, flow velocities and wave actions are hard to mitigate. Most flood actions are difficult to predict and depending on the situation the relevance can also differ significantly [23]. The hydrostatic pressures at both sides of a wall, along with the flow velocity, are regarded as the most relevant flood actions [23]. From Section 4.2 the importance of having a counter pressure is once more underlined, albeit that the bending moments originating from these two water levels can affect the wall for the worse. The water levels inside and outside a residence should be (approximately) the same to confine the influence of the hydrostatic force. Note that during a flood event the wall would still be subjected to the outside flow velocity and other hard-to-predict flood actions.

The amount of water inside a house is difficult to predict with numerous factors influencing the seepage into the residence. Residences with wooden floors can have significant water flow through the bottom, while residences with a separate mailbox avoid having an additional gap in the front door. Utilizing the experiment it is possible to find a leakage rate of the window-wall interface. Below the possible pathways into a residence are listed [43].

1. Sewage system and other utility lining for cables
2. **Window-wall interface**
3. Door-wall interface
4. Gaps in the front door: mailbox, animal hatches
5. Brickwork porosity

The catchment box allowed the water leaking through the CaSi wall to be recorded. From observations, it is known that the box itself had leakages as well. The seepage through the window-wall interface is therefore hidden in the recordings and can be found by subtracting the contributions of the leakages.

4.4.1. Torricelli's law and box leakages

From graph A (Figure 4.2) it can be deducted that no water was transported from the cavity to the box below a level of 270 millimeters. When the pump was turned on the water level in the box dropped, but the levels at the front side and in the cavity stayed the same. Indeed, prior to the official experiment, the testing round (water levels of +0.3m) revealed all leakages in the CaSi wall below the +0.3-level. These holes left by the masons were filled with silicone sealant. Yet, the porosity of the brickwork cannot be excluded. A study shows that the porosity of the mortar and bricks can lead to a leakage rate of 0.15 m^3 per hour for every meter of wall. This rate is however corresponding to a water level difference of 1.0 meter [14]. This indicates that a small amount of water could have spilled through the masonry and was replenished by the front level; this was however not visible during observations. It is therefore that all water present in the box at this moment is attributed to leakages from the box.

To model the water level in the box use is made of Torricelli's law. The law states that: "the efflux velocity of the fluid equals the velocity the fluid would acquire if it were to fall from the free surface of the reservoir to the opening" [15]. This theory is described by the following equation:

$$u_T(t) = \sqrt{2 \cdot g \cdot h_T(t)} \tag{4.1}$$

With g being the gravity constant and $h_T(t)$ the head difference of a given moment in time. Energy losses are not accounted for in this equation; neglecting the dissipation and overestimating the total velocity. Often a correction factor, μ, is therefore applied [15]. This discharge coefficient accounts for a more realistic curvature of the streamlines; without this coefficient, the streamlines are assumed to make an unrealistically right angle. The final leakage rate is described by the discharge into the box. For that matter, the efflux velocity, $U_T(t)$, is multiplied by an unknown leakage area.

Model description

The efflux velocity is simply calculated by using the head difference between the water level outside the box (front side) and the water level inside the box (+backside). This head difference then drives the water into the box. By first assuming a leakage area of 0.0001 m^2 the leakage rate is calculated; multiplying the efflux velocity with the area. Dividing this discharge by the bottom area of the catchment box then gives the rise rate per second inside the box.

The measured water levels were recorded every 30 seconds and as such the rise rate is multiplied to match the same interval. The resulting parameter describes the increase in water level averaged over the interval. To make the model describe the actual water level inside the box a start value is required, which is obtained from the actual data. Logically, the start value is the lowest water level recorded. By then consequently adding the increases in water levels a Torricelli-based description of the water level is constructed, see Figure 4.7. The leakage area is found by changing the initial value and regarding the difference between the modeled water level and the observed water level. The Root Mean Square Error (RMSE) is then used to calculate the area giving the lowest error.

The leakages are known to be situated at the bottom corners of the box, where the connections between the different beams were not sufficiently tightened; clearly resulting in failure of the sealant (see Figure 4.8). Since the leakages are at the bottom, the flow is governed by the actual head difference. If leakages were to be present higher in the box the efflux velocity would be the result of the distance between the free surface of the basin and the leakage opening. That is until the water level in the box has surpassed the opening, after which the velocity is again described by the head difference.

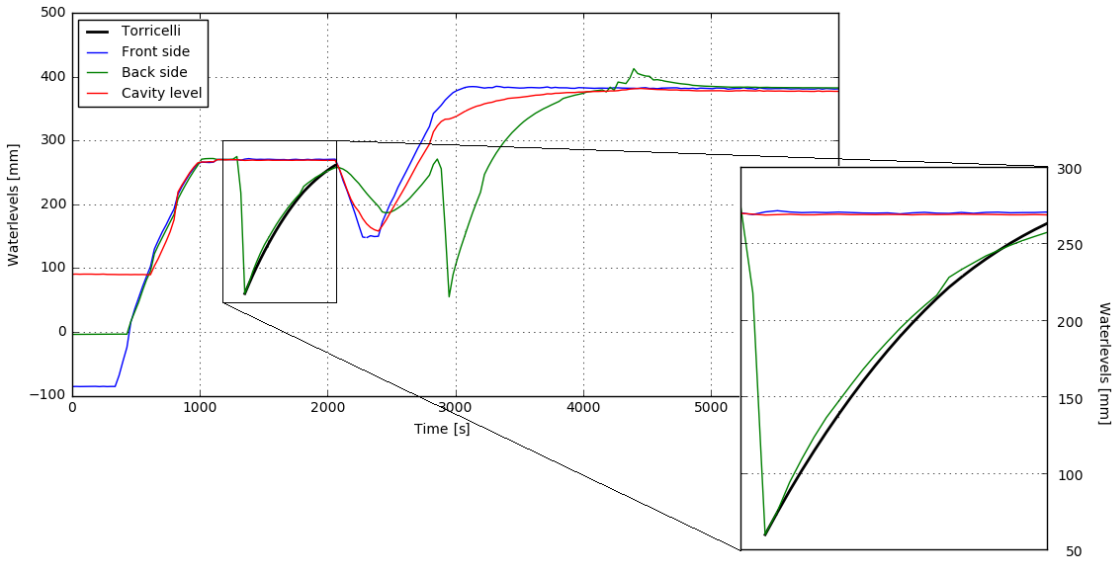

Figure 4.7: Graphical representation and detail of the observed water level and the water level described by the Torricelli theory.

Figure 4.8: Photographs of the box leakages at the bottom of the box. In the corner three beams connect insufficiently; forming a pathway for the water to enter the box. At the locations where the box meets the steel rig also water was observed. It was tried to seal these points, but the water came through anyway.

For a total leakage area of 0.000276 m^2 the RMSE is the smallest: 4.5 mm. This means that the actual leakage area is larger; with the found area being vena contracta. Throughout the experiment, the box has not been altered near the bottom. For the remainder of the investigation, it is thus assumed that the leakage area of the box is 2.76 cm^2. Furthermore, the description by Torricelli's law is accepted to model the discharge seeping through the bottom corners of the box.

4.4.2. Additional leakages CaSi wall

The gaps in the mortar joint above the initial 30 centimeters were not revealed in the test rounds and as such were not sealed before the experiment. Indeed, in Figure 4.8 the cavity level begins to deviate at a level of 33.1 centimeters, while the front side level still rises (at time is 2993 s). This can indicate that there are small gaps in the mortar and sealant that form a pathway into the box. However, it can also mean less water is seeping into the cavity. Considering the sudden change in steepness of the cavity level, the first option seems more reasonable.

With the increased water level in the basin, the discharge seeping through the bottom corners of the box has increased as well. However, the water level inside the catchment box is not only the result of these leakages, as can be seen in Figure 4.9. The black line indicates the water level if the model was only based on the leakages in the catchment box; underestimating the observed water levels. Although this might indicate that throughout the test the leakage area suddenly increased, both relevant drops were only 15 minutes apart and the water level only increased 11 centimeters. Long-time effects are thus excluded to be the cause of this increase and erosion of the wood near the leakages due to the increase in head seem trivial. Based on observations and the comments above, it is clear that additional leakages are present. Water from the cavity is seeping through the CaSi wall.

Additional model description

By including the water that is seeping through the wall, a connection is made between the two system elements with storage capacity: (1) the cavity and (2) the catchment box (see Figure 4.10. The cavity itself is nourished by leakages in the clay wall. This adds another branch, connecting the cavity with the basin. The highly dynamic nature of the cavity in this case eliminates the static calculation of the efflux velocity. Instead, both inflow and outflow of the cavity should be considered. The discharge through the wall can be obtained by consulting the data. Considering the slope of

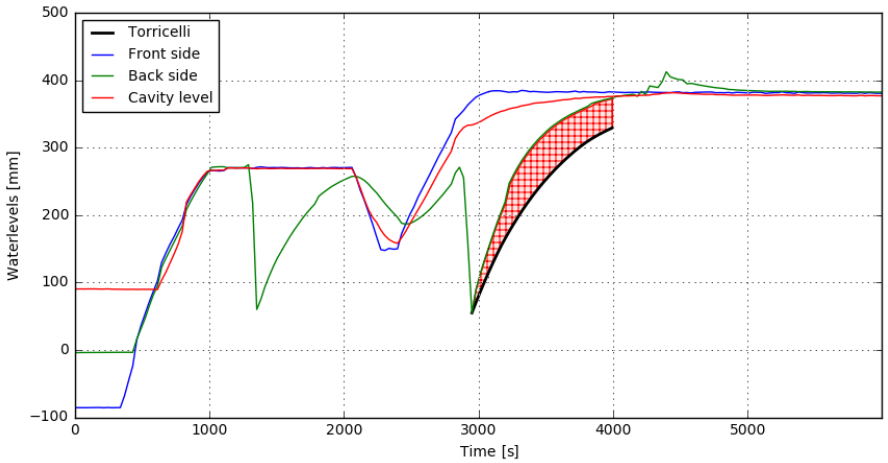

Figure 4.9: Graphical representation of the observed water level and the water level described by the Torricelli-modeled discharge seeping through the bottom corners of the box. The discrepancy between the two water levels is marked red. This red area is attributed to the leakages in the wall which together make up for the second and final discharge into the box.

the actual backside water level and considering the bottom area of the box, the discharge can be obtained for every data point. By subtracting the inflow from the corner leakages (Q_{box}) from the data, the total discharge through the CaSi wall (Q_{casi}) is obtained. Note that Q_{casi} is considered an outflow component of the cavity. It is the result of the initial storage in the cavity and the discharge coming through the facade and flowing into the cavity: Q_{clay}. The cavity level rises when the inflow exceeds the outflow i.e. when $Q_{clay} > Q_{casi}$ and drops when the outflow is greater than the inflow i.e. when $Q_{clay} < Q_{casi}$.

4.4.3. Leakage areas

The gaps in the CaSi wall between +0.3m and +0.38m allowed 0.01 m^3 of water to leak into the box in 1170 seconds. This indicates that on average 0.008 liters of water is seeping through this stretch of the wall every second. However, it is important to acknowledge that, just like the box leakages, the amount of water seeping through is not described linearly. For that matter, an equivalent area is computed that allows the same volume to seep through, depending on the water levels described in Figure 4.10. Considering the fact no water was seeping through the wall below a level of +0.3m this leakage area is situated at 0.33 meters. A combined area of 0.279 cm^2 results in an identical volume leaking through the wall. Note that at this point the window has not yet contributed to the rise rate.

The amount of water seeping through the CaSi wall can only exist like it does if the cavity is nourished by leakages in the clay wall too. Although in this case, water could have been seeping through the connections between the lower beam and the two pillars; this cannot be ruled out.

One vital difference between the catchment box and the cavity that should be noted is the fact that the cavity is not emptied by a pump whereas the box is. Only the leakages in the CaSi wall allow the water level in the cavity to decrease. The water level in the cavity, therefore, does not reach low levels. From the above, it can be deduced that the gaps in the clay wall have a great chance of staying permanently flooded throughout the test; even though the water table lowers a bit. The seepage into the cavity is thus governed by the head difference only instead of the distance between the water table and a certain 'dry' gap situated above a second water table. This means that the location of the leakages in the clay wall does not influence the discharge as long as the flow is governed by the head difference.

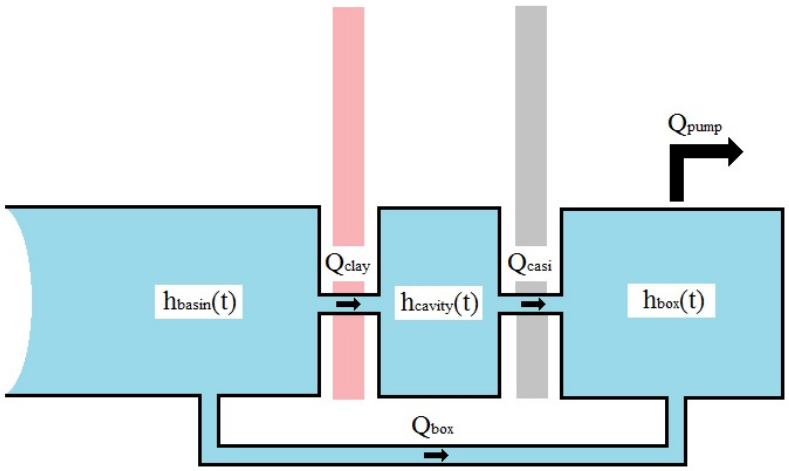

Figure 4.10: The hydraulic system that is used to obtain the discharges through the walls. The leakage pathways are presented as single canals while in fact there are multiple pathways. Note that inertia originating from the small pathways is neglected and that loss factors are not accounted for. The water level in the basin, although slightly changing, is assumed constant because of the large area.

To find the contribution of the window gap on the overall rise rate a recording is needed in which the water reaches a level above 47 centimeters. At this level, the bottom part of the window starts. Knowing the leakage areas from the box and the wall below 0.38 meters, the remaining amount of water is attributed to leakages in the wall above 0.38 meters (of which the window gap is expected to be the main cause). In Figure 4.11, a recording is shown of a test where the water level indeed exceeded the bottom part of the window. Furthermore, this test was performed on the same day as Figure 4.9; so no alterations were constructed in the meantime. Two similar situations can be observed, where the basin level was constant at 700 millimeters and the box level was allowed to increase all the way to the basin level. Both peaks can thus be used to find the amount of water seeping through as a means to verify the observed area. For the first (marked) peak, an additional 0.133 m^3 of water is needed to mimic the backside water level. For the second peak, this amount reduces to 0.13 m^3. This can be explained by the fact that at the second peak still a difference between the cavity level and the box level was present when the big pump was turned on again. As such, the cavity level did not get the chance to discharge the remaining amount of water through the wall. When translated to areas, both volumes can be realised by similar values; respectively 1.649 cm^2 and 1.653 cm^2.

For simplicity, the area is assumed to be 1.65 cm^2. This value is significantly larger than the 0.279 cm^2 found for the leakages at the bottom section of the wall. Therefore, it seems that the window gap is indeed contributing to the volume and area. Yet, the considered stretch of wall is much larger than before. While the 0.279 cm^2 leakage area was found between +0.30m and +0.38m, the second area reached from +0.38m to + 0.70m. Although the latter area is partly filled by the window, still the masonry part of this stretch of wall is 3.2 times larger. It would therefore be wrong to assign the found leakage area completely as a result of the window gap. As there is no indication to assume otherwise, an average leakage area of 0.0000279 m^2 per 0.208 m^2 of CaSi brickwork is accepted for this specific wall specimen. In comparison, literature suggests an overall leakage area of 0.000025 m^2 per 1 m^2 for well-constructed wall parts [14].

According to the reasoning above, only 55 % of the water can be traced back to the brickwork. This means that the window-wall interface allows the other 45 % of water to leak through i.e. the window-wall interface has a total leakage area of 0.75 cm^2. Combining this with the wetted circumference of

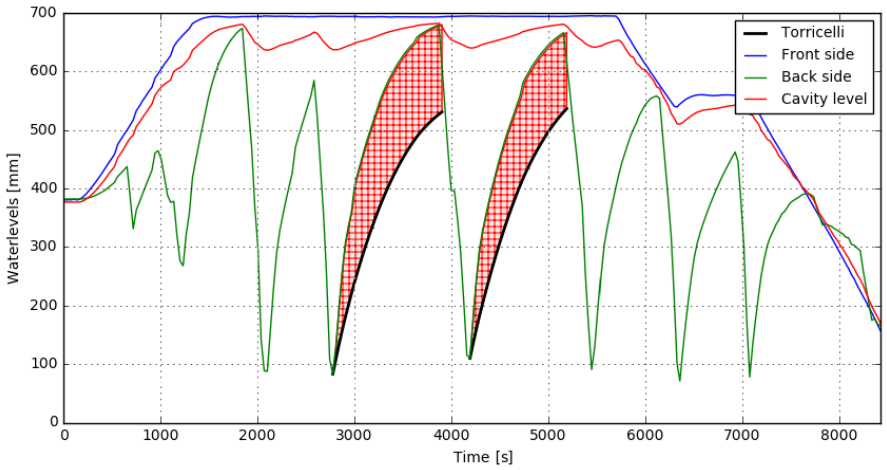

Figure 4.11: Graphical representation of two similar observed water levels and the water level described by the Torricelli model. The black line is a combination of the discharge seeping through the bottom corners of the box and the leakage found previously. The discrepancy between the two water levels is marked red. This red area is attributed to higher leakages in the wall and the window-wall interface.

the window, the interface only has a thickness of a tenth of a millimeter.

During the next tests, the box was altered with an extra plate mounted on the top to allow higher water levels, introducing a new pathway for the water to leak into the box. Also, additional sandbags were placed inside the box changing the inside area. Assuming the leakages in the box did not change over the course of several weeks would be very wrong. On top of that, the sealant between the wall and the steel rig began to wear out with a single rupture observed near the bottom. The static approach that is used in the previous would introduce multiple errors and as such, it was chosen not to take further recordings into consideration.

4.4.4. Rise rate contribution of the window-wall interface

Observations showed that the Meranti wooden window profiles did not suffer significant damage. The primer paint started to deteriorate but no wood rot was observed. For the sake of this research, the leakage area of the window-wall interface is thus considered as a constant.

As so, it is possible to visualize the contribution of the window to the overall rise rate inside a residence. The 'leakage rate' through the window-wall interface is defined by four separate segments that are bounded by the water levels at both sides of the wall i.e. the outside water level and the level inside a residence. Additionally, the height of the window, d_{window}, limits these segments, resulting in the following:

1. $Q_{leak} = 0$ if $h_{outside} < d_{window}$
2. $Q_{leak} = \text{constant}$ if $h_{outside} > d_{window}$ **and** $h_{inside} < d_{window}$
3. $Q_{leak} = f(h_{outside}, h_{inside})$ if $h_{outside} > d_{window}$ **and** $h_{inside} > d_{window}$
4. $Q_{leak} = 0$ if $h_{outside} = h_{inside}$

Whenever the water level does not reach the pathway underneath the window, no amount of water will seep through. However, when the flood exceeds the height of the window, water can seep through and does so at a constant rate as there is no significant water level yet to counteract. As the residence slowly fills with water the water level inside reaches the height of the window as well, after

which the leakage rate becomes a function of both water levels. The linear behaviour disappears and the rate is governed by the head difference. When the water level inside has reached the same level as outside, the head difference diminishes and water will stop leaking through the window-wall interface.

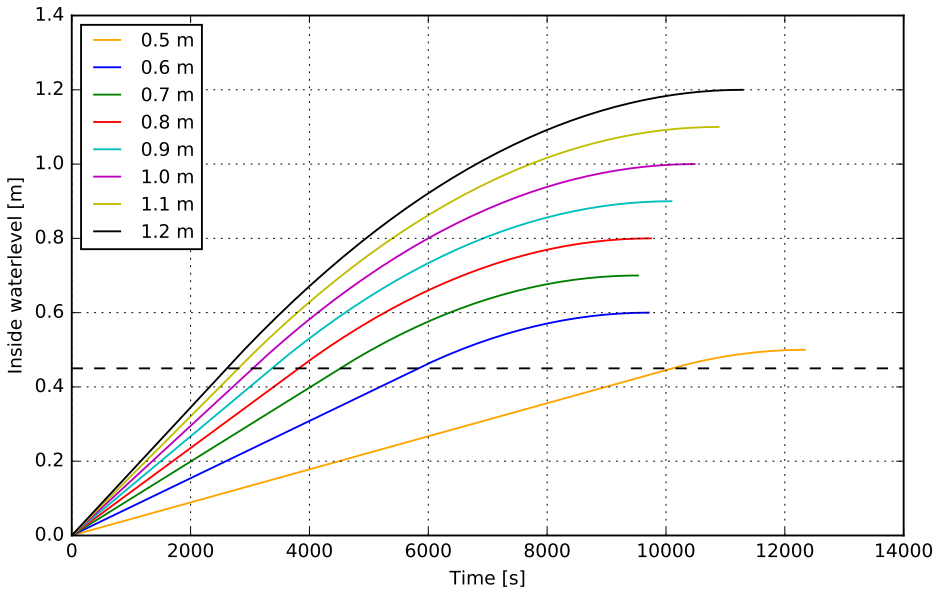

Figure 4.12: The rise rate for different values for $h_{outside}$ for a unit area. The vertical dashed line indicates the height of the window. Clearly, the linear trend of the leakage rate can be observed below this window level. Note the asymptotic behaviour present for outside water levels close to the window height.

For the leakage area found above multiple rise rates were computed for a unit area, 1 m^2, for different outside water levels, see Figure 4.12. Remember the window was placed at 47 centimeters. For large water levels present the segment defining the constant rate shows similar slopes. The smaller the initial height difference between the outside water level and the window height is at the start, the longer it will take before the inside water level has reached the same level. This is a direct consequence of the efflux velocity that the water has acquired as a result of the distance between the surface and the leakages. For small distances, this efflux velocity reduces significantly. Yet, when the inside water level has surpassed the window gap, the head difference damps the obtained rate. For higher water levels this damping goes slower since the current head difference is still significant. Eventually, this results in greater timescales for greater water levels. As can be seen in Figure 4.12 it would take 11.500 seconds for an outside water level of 1.2 meters to fill the inside unit area to the same level.

It does not matter if a head difference of 10 centimeters appears at 1.2 m/1.1m or 0.4m/0.3m. The head difference near the end is therefore identical for all possible water levels; evident from the parallel slopes in Figure 4.12. However, for water levels close to the gap itself the gentle slope has a significant influence on the total timescale. Because of this gentle slope, asymptotic behaviour is noticeable at the height of the window. Because of this behaviour it would take the same time for an initial water level of 0.8 meters to fill the inside unit area as it would take a water level of 0.6 meters; around 9580 seconds. This asymptotic behaviour is present at all window heights, but zero. If the window is placed lower in the wall the behaviour is 'sharper'. Only water levels that are close to the gap will show greater time scales than expected. For all water levels, the needed time to fill the unit area has decreased.

Exactly the opposite can be observed for windows that are placed higher in the wall. The asymptotic behaviour is milder, with almost identical timescales for 0.9 meters, 1.0 meter, and 1.1 meters. The timescales also increased. For greater water levels the timescale only increased a little, whereas for the lower levels the increase is significantly larger.

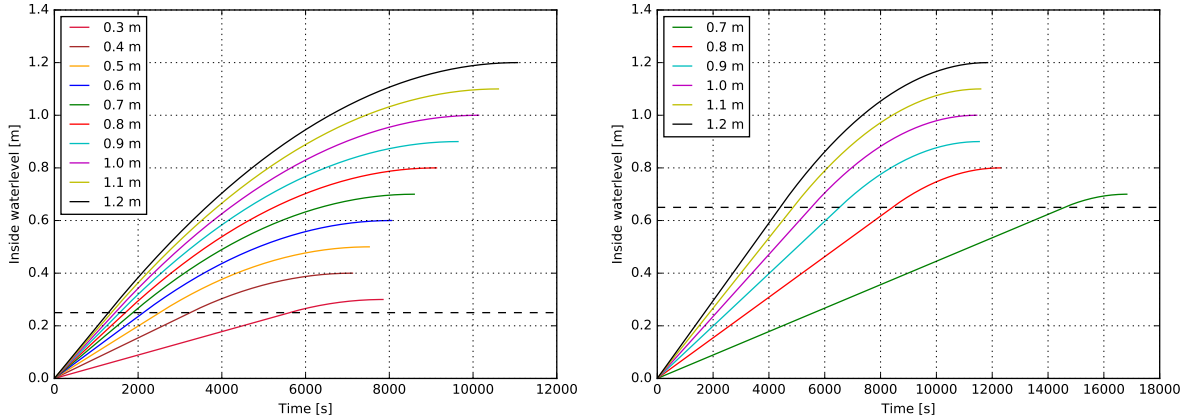

Figure 4.13: The rise rate for different values for $h_{outside}$ for a unit area. In this case, the window is placed lower and higher than before. The height of the window influences the asymptotic behaviour, although this is still present for both cases.

Depending on the strength of the glass, it can be concluded that failure of the window-wall interface will hardly contribute to the rise rate inside a residence. It would take the constructed window at least three hours to completely fill a unit area. Considering that the ground floor of a residence is significantly larger, a vast number of windows could still not make a serious contribution regardless of the window location. During a flood, the majority of water present inside a house must therefore be traced back to pathways other than the window-wall interface. Although failure of the glass cannot be ruled out as such a possible pathway, there is evidence that modern glass can endure great forces [6].

5

Computed Wall models

While the results obtained from the sensors already reveal a great part of the deformations, they only show the deformations at one certain height. For a complete insight into the behaviour of a wall, a great amount of (water-tight) sensors is needed, which, in this case, is unfeasible. To still obtain sufficient insight into the behaviour of the cavity wall, two models are computed. The models possess similar characteristics that were revealed during (lab) testing. As such it is possible to extrapolate additional information from the models and use it to close the knowledge gap left by the experiment. For this research two models were computed: a fast and simple analytical model and a more detailed model obtained by finite element analysis (FEA). Below the models are explained and used to obtain a limit curve that describes the different parameters as a function of the inside and outside water height.

5.1. Analytical model

For the analytical model, both walls are described as a slender structure i.e. relative to their dimensions. As such, they can be analysed with Euler-Bernouilli bending. This theory assumes small beam angles and neglects any out-of-plane curvature, which is valid for cases without significant shear stresses. The equation that governs the Euler-Bernouilli theory is presented below.

$$\frac{d^2\Delta}{dx^2} = \frac{M}{EI} \tag{5.1}$$

Here the left term represents the second derivative of the beam's deflection along the x-axis, Δ, and M being the internal moment. Furthermore, Young's modulus and the moment of inertia are the material property and shape property; represented by E and I respectively.

5.1.1. Model description

The slender structures are subjected to a rotational stiffness that is originating from the steel beams. The model then treats three different wall sections: (I) the bottom part where (hydrostatic) pressure is present at both sides and the resulting force is rectangular-shaped, (II) a middle part where pressure is only coming from the front i.e. outside with a triangular forcing, and (III) the top part where no hydrostatic pressure is present. The deflections are found by expressing the hydrostatic (q-)load as a function of x. By calculating the fourth-grade integral of this function, a new function is created describing the deflection. Since there are three different wall sections, there are also three computed deflection functions. In terms of continuity twelve boundary-and interface conditions are needed. At the connections with the steel beam, two boundary conditions in terms of displacement and rotational stiffness can be found at each side. The remaining constants are found at the interfaces between wall sections 1 and 2 and wall sections 2 and 3. Here, the interface conditions treat

equal deflection and rotation as well as the equal moment and shear force. As a slender structure, the window gap is difficult to model. The wall section where the window is situated is governed by a lower stiffness, simply because at that section, the masonry is interrupted by the gap. For that matter part of the model is given a lower EI-constant, meaning that the uniform beam becomes non-homogeneous and additional wall sections and interface conditions are defined. The top section is therefore divided into two parts and the lower half is given a lower stiffness. The same holds for the bottom section; here a small part is changed to a lower stiffness as well. For the middle part, the stiffness changes entirely. This finally results in the analytical model shown left in Figure 5.1

In a few situations, the water level inside could also be near zero. To compute for these situations the model is altered, resulting in the removal of one wall section, see right Figure 5.1. In essence, both models are identical, albeit that the second model is governed by four wall sections i.e. sixteen boundary-and interface conditions, while for the first model five sections and twenty conditions are defined. Due to the definition of e (and o), the most extreme water levels these models can compute are limited to a height of 2 meters. Water heights above this level would mean a negative length for section d (respectively m) and would also subject a force to the top section, which would require additional interface conditions. Likewise, because of the definition of a and k, the model works best if a minimum of 0.4 meters of water is present because below this level the shape of the force changes.

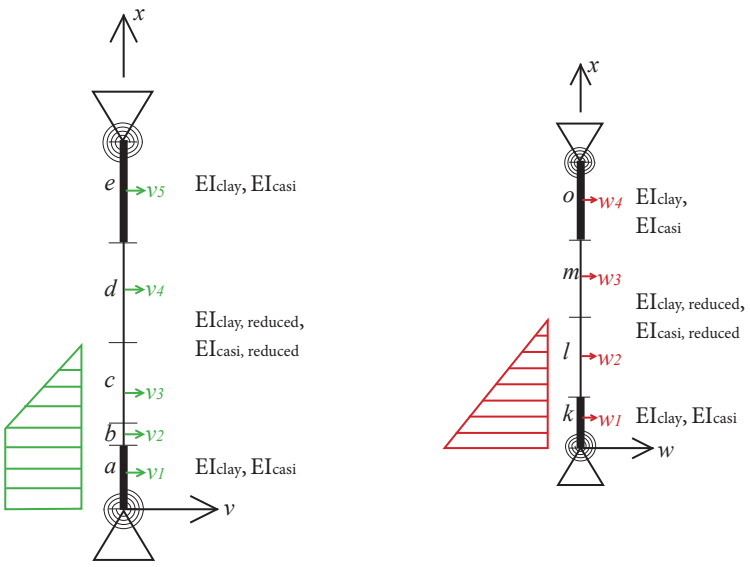

Figure 5.1: Left: analytical model for the cavity wall being subjected to pressures from both sides. The pressure inside the residence reduces the total forcing, which results in the trapezium-shaped pressure. Right: analytical model for the cavity wall subjected to hydrostatic pressure from outside only.

Note that the lengths of sections b and c (and also l for the second model) are depending on the occurring water levels. These wall sections are governed by a reduced wall stiffness, $EI_{reduced}$, that is defined as a fraction of the stiffness belonging to the solid wall sections a and e: EI. While the actual value is unknown the reduced stiffness is implemented as being $0.5-0.8EI$. It is checked which value performs best and computes the most uniform result for the stiffness. Additionally, input values are defined for the rotational stiffness: 250 kN/rad (originating from the steel beam below)[24]. The complete script and definitions for the loads can be found in Appendix I.

5.1.2. Sensitivity of values

The model is computed and improved in terms of deformations. This does not necessarily mean that the analytical model will behave identically to the experimental wall. In fact, it is tried to mimic the behaviour within the boundaries of an analytical model. The choice for certain parameters can influence the results from the analytical model. Therefore, it is important to grasp this influence and understand the sensitivity of numerous parameters. In this case, especially the reduced wall stiffness and rotational stiffness can change the outcomes of the model, see Table 5.1. It seems a zero rotational stiffness does not lead to unrealistic values but still has a significant influence.

Rotational Stiffness	**Reduced EI-value**	**Max.deform. 0.5m - 1m**
250	*0.5EI*	1.178
250	*0.65EI*	0.996
250	*0.8EI*	0.892
0	*0.5EI*	1.769
0	*0.65EI*	1.467
0	*0.8EI*	1.277
∞	*0.5EI*	0.341
∞	*0.65EI*	0.306
∞	*0.8EI*	0.274

Table 5.1: Sensitivity of relevant parameters for the analytical model. For this analysis the inside water level was 0.5m and outside 1.0m. Increasing or decreasing the water height also has influence on the deformation, but this influence is independent of the rotational stiffness and EI-value.

In addition, the relevant properties of the wall section where the window is present are studied further by computing the structural stiffness for all data points. The results are summarized in boxplots, see Figure 5.2. From the figure, it can be deduced that the wall itself needs to have a high stiffness if the window section is governed by a much lower factor. Secondly, the results are more scattered. If for instance, the window section has only half the stiffness of the other sections the overall stiffness value would lay around $1.51 * 10^6 Nm^2$. It can be seen that the overall stiffness gradually decreases if the reducing factor increases. Yet, if the factor gets too high the overall wall stiffness reduces significantly; for $EI_{reduced} = 0.8EI$ the average EI-value for the other sections is only $0.86 * 10^6 Nm^2$. Considering both trends, it is chosen to use a factor of 0.7 to describe the mid-sectional stiffness i.e. the presence of the window reduces the stiffness of this section by 30%.

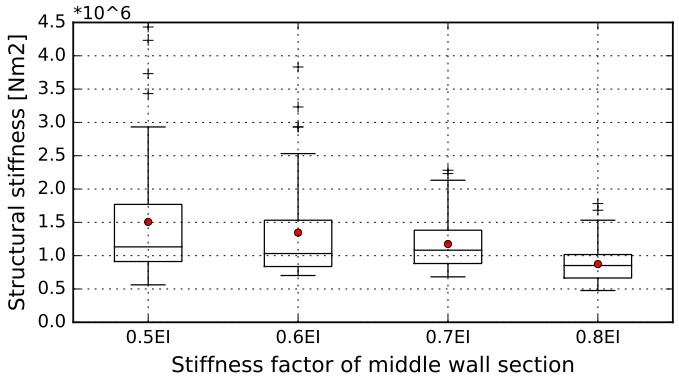

Figure 5.2: Boxplots of the overall stiffness required to describe the measured deformations compared to different $EI_{reduced}$ factors describing the middle section of the wall. For low $EI_{reduced}$ factors, the results become more trivial ranging significantly, while for high factors this trend reduces; resulting in a weaker wall.

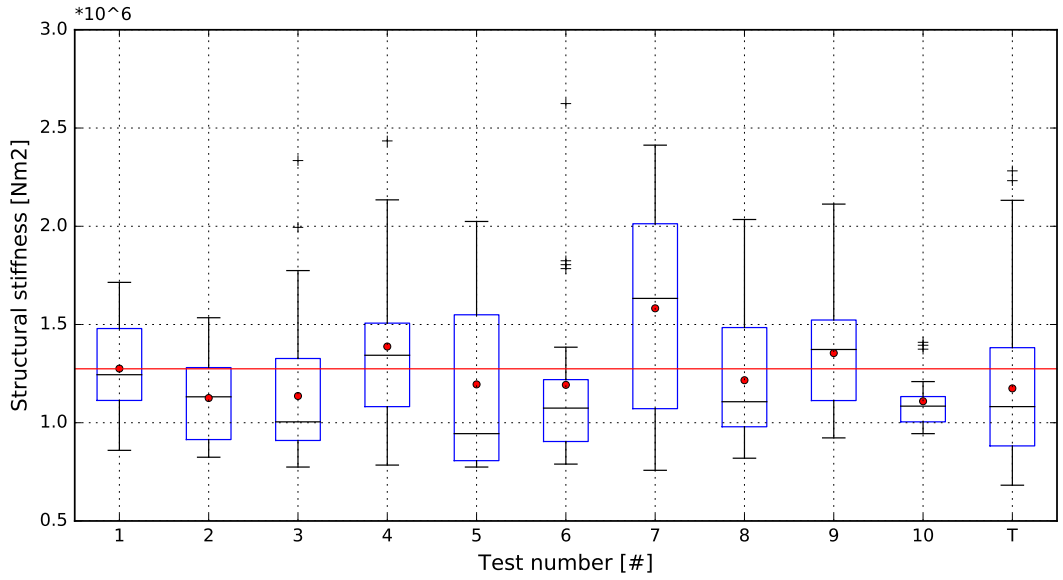

Figure 5.3: Boxplots of the found stiffness for different water level combinations per performed test. The boxplots are computed with data from the first three deflection sensors. The red dots mark the average value of the specific test, while the median (Q2) is indicated by the black line. The total average value is indicated by the red line. Test T indicates the boxplot for all tests combined and is identical to boxplot '0.7EI' in the previous figure. Note that outliers are defined with two times the standard deviation.

5.1.3. Wall stiffness

The data recorded by the pressure sensors during the experiment is used as input values for the water levels inside and outside. The water levels are rounded to the nearest millimeter and identical combinations of inside and outside water levels are averaged to reduce possible errors. The deflections computed by the models are then validated with the averaged deflection of sensors P2 and P3 (CaSi) and sensors P4 and P5 (Clay); both on a height of 135 centimeters. These sensors can both be averaged since there is no evidence that one side of the wall is behaving consistently differently than the other side. Therefore, the difference in measurements seems arbitrary, and averaging both sides is justified.

For each separate test, the found values for the structural stiffness are included in a boxplot as shown in Figure 5.3, with also a separate boxplot for all the values combined (indicated by T). Especially during test 5 and test 7, the stiffness values ranged significantly, which becomes obvious by the Inter Quartile Range (IQR) i.e. the length of the box. Also in other tests, significant values are found resulting in long whiskers.

It should be noted that for the final test (test 10) the top beam was lifted. This could, at least partly, explain the reduction in stiffness; the average value of the total experiment (red line) exceeds the entire boxplot of test 10, with only two outliers above it.

While the average values seem to be similar throughout the tests, the final four tests (with a new sensor framework) are indicating a decrease in stiffness. Regarding the interference of the catchment box in earlier tests, it is possible that the obtained values are consistently too low and the degradation in stiffness already happened before. At that time the wall already endured several 'floods'. Yet, it is also possible that test 7 was an outlier, as the other boxplots tend to agree with each other. From Figure 4.5 it can also be concluded that eventually, the wall reacts similarly throughout the experiment. As there is no real proof a structural stiffness of EI = $1.27 * 10^6 Nm^2$ seems a reasonable value for the analytical model.

5.1.4. Structural limits and influence of wall ties

With water at both sides of the wall, the moment distribution for a single wall is different for different combinations. Eventually, a water level difference will be reached that will exert a moment force that exceeds the capacity of the wall. In this on-way configuration the resisting moment is found by the following:

$$M_R = \frac{I_{zz}}{z} \cdot \sigma_t \rightarrow \frac{b \cdot t^2}{6} \cdot (f_{x1} + \sigma_v) \tag{5.2}$$

For symmetrical (rectangular) shapes, distance z is equal to half the thickness of the structure, t; resulting in the section modulus as a first term. In this case, the resisting moment is thus a function of the vertical flexural strength (obtained by bond wrench test), f_{x1}, and the compressive stress in vertical direction,σ_v, originating from the top beam. In Chapter 4 it was already found that the flexural strength should be around 0.3 MPa. It should be noted that the springs were tightened to exert a stress of 25 kPa.

The notion of a unit width (b=1) cannot be used here, since the presence of the window gap will negatively affect the available moment capacity. Instead, the middle section is governed by a 'wall width' that is only 2 meters, rather than the total width of 2.6 meters. The two transition points from the bottom section to the middle section and the middle section to the top section mark the vulnerable area where the capacity suddenly reduces by 23%.

However, due to the wall ties, a connection between both walls is made which is expected to increase the internal capacity of the cavity wall. Although the exact influence of the wall ties is unknown due to experimental flaws, upper and lower boundaries can be reasoned. In the experiment, the cavity wall had a total thickness of 0.27 meters. Yet, using this thickness might lead to an overestimation of the total capacity, since the cavity wall is hardly a solid structure in terms of thickness. To acknowledge the structural behaviour of the wall ties an equivalent thickness can be found using Steiner's (Parallel axis) theorem; resembling the cavity wall as an I-profile and translating the found second moment of inertia back to a single thickness. In this case, the ties form a perfect connection, while the opposite might occur as well; forming a poor connection. Then, the total capacity can be reasoned using the capacities of both walls separately, with a vertical compressive stress for the CaSi wall only. A lower bound is found using the capacity of a single wall only, where the thickness is reduced to a value of 10 centimeters. These scenarios are summarized in Figure 5.4. It can be reasoned that the actual behaviour of the ties would be found somewhere between the second and third scenarios.

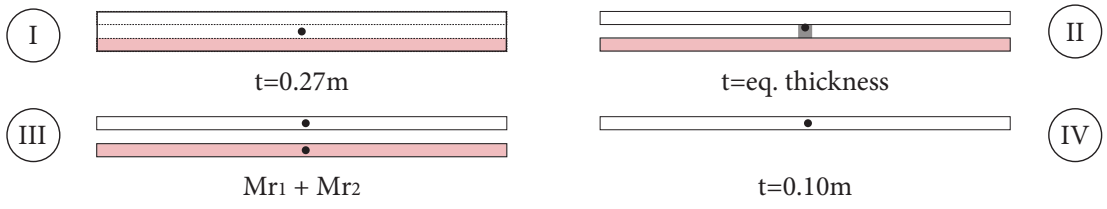

Figure 5.4: Different scenarios to acknowledge the influence of the wall ties. The upper boundary is governed by a cavity wall having a thickness of the total structure, while the lower boundary only features the CaSi wall. Centres of mass are marked by a solid dot.

5.1.5. Limit curves

There are multiple ways in which the capacity can be reached and exceeded for the different wall ties scenarios. Using the analytical model to compute the maximum moments that act inside the masonry it is found that for the lower bound the subjected moment will exceed the resisting moment for the first time at an outside water level of 1.38 meters. However, if both leaves of the cavity wall will react to the hydrostatic pressure, a water level of 1.7 meters can be withstood before exceeding the internal moment. For scenarios III and IV, the results found using the analytical model are summarized in the left plot of Figure 5.5. In this plot, the curvature of the internal moment is visible depending on the combination of inside and outside water levels. The lower bound for scenario IV is shown as a red line, while the contours are originating from scenario III. For this one-way configuration, it seems like the cavity wall could quite easily withstand outside water levels of 1.5 meters. Above this level, the moment moves quickly in the >90%-regime. For higher water levels the maximum moment is found below the inside water level, meaning that initial cracks and damages will occur below the water table. It is important to note that there is only a minor overlap where failure occurs below the inside water level; in most cases of failure, water is only present at the outer side of the joint.

For the scenarios where the wall ties will form a perfect solid connection, the limit curves will move away perpendicular from the centre line because the capacity increases. Not only will the 'safe' regimes become wider, but the (red) exceedance curve will also move upward and disappear from the plot. This indicates that water levels of 2.0 meters can be withstood with ease, see Figure 5.5.

The Euler-Bernouilli method of the analytical model makes it difficult to translate the contour plot of Figure 5.5 in terms of (linear) elasticity. At a certain moment in time, the capacity is reached at specific points, after which the wall enters the non-linear regime. Cracks begin to form and forces are redirected to interfaces that are still intact, which cannot be computed by this model.

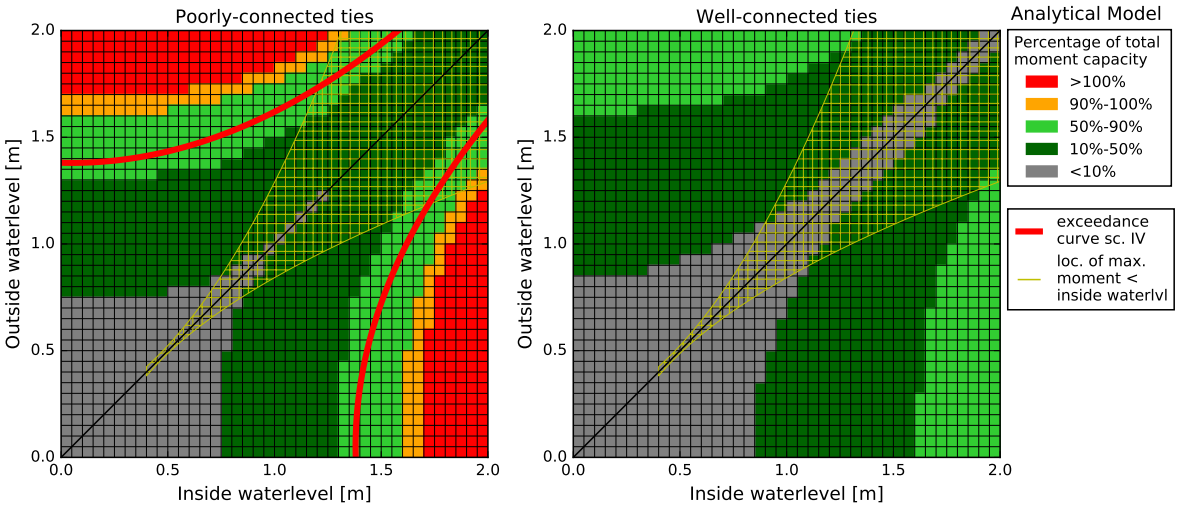

Figure 5.5: Analytically computed results on the occurring internal moments as a function of water levels at both sides of the wall. The Figure shows the results for the upper and lower boundary i.e. for poorly-connected wall ties (left) and well-connected wall ties (right). The maximum capacity is calculated by Equation 5.2 and is denoted as 100%. The colour gradient shows the occurring moments as percentage of the maximum allowable moment. For both plots, the imagery is mirrored in the x=y line; assuming that the wall will behave identically in both ways. Additionally, the area in which the maximum moment is found below the inside water level is marked yellow for both plots.

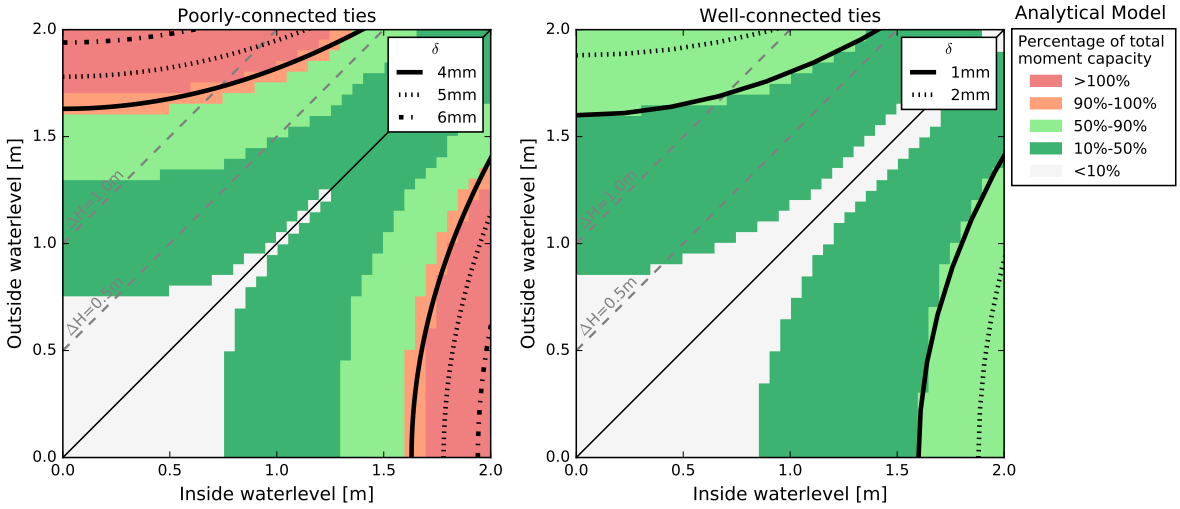

Figure 5.6: Analytically computed results on the occurring deformations as a function of water levels at both sides of the wall. Several exceedance lines for the deformations are projected on the previous obtained momentum behaviour as to have a comparison between both failure modes. Note that the results are again separated to account for the different wall tie-approach. Both plots show small deformations in the order of millimeters. In both plots (grey) diagonal lines indicate situations with equal head difference, see also Figure 5.16.

Because of the brittle nature of masonry, it can be reasoned that the wall has also restrictions for deformations; and that, after reaching this limit, the wall can only respond to the deformations by developing cracks, which weakens the interface. Note that the maximum deformation is a summation of the multiple displacements (or elastic behaviour of the masonry) of the brick courses below and above.

For scenarios II and III the corresponding deformations are shown on top of the contour plots of the internal moment (see Figure 5.6). On the left, it shows that the line of failure, due to the exceedance of the internal moment, coincides with deformations of 4 millimeters. In this case, both walls react with their own corresponding capacity. For the second scenario (right plot of Figure 5.6) deformations of only 2 millimeters are observed within the boundaries of the analytical model. In both cases, the deformations are rather small compared to the acting moments. It is, therefore, reasoned that failure is due to the magnitude of the moments rather than the deformations.

5.2. Finite Element Modelling

The above results give reason to further research the (non-linear) behaviour of the wall. To gain this insight a new model is computed in the DIANA FEA program. The program uses finite element modeling (FEM), which can be used to force the model into the non-linear regime. Additionally, FEM allows a model with multiple dimensions, meaning that the wall can simply be constructed in a two-dimensional configuration. This gives additional insight into the cavity wall that no longer is simplified as a slender beam, but rather a 2-D plate with a window gap. The plate is divided into a vast number of small elements that are connected by so-called 'nodes'. These elements combine to create a mesh that simulates the assessed structure. For each individual element, a set of calculations is performed that also considers the properties or boundaries of the surrounding elements. Eventually, the result of the interpolation between all the elements shapes the final result for the total structure. By implementing certain non-linear material properties the wall can be investigated in its non-linear regime. The non-linear model can redistribute the forces whenever the tensile capacity is reached at certain nodes, creating cracks along the face of the plate.

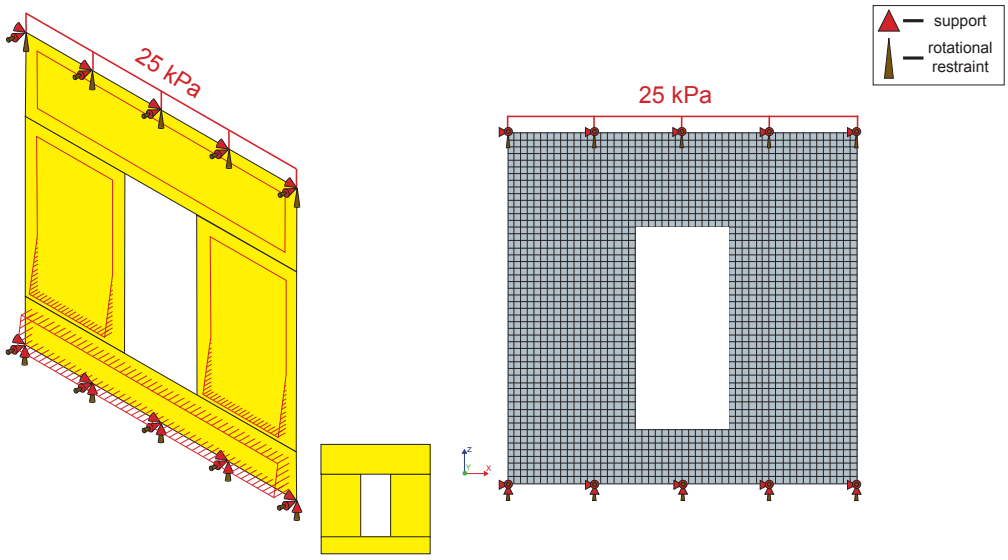

Figure 5.7: Left: Isometric view of the FEM model with the described boundaries and loads. From this figure, it should also be clear that the model was shaped by four separate sheets. Right: Front view of the mesh with the boundaries visible too. Both figures are accompanied by the same coordinate system.

5.2.1. Model description

Rather than a difficult micro-modeling approach, where the bricks and mortar are considered separately, the cavity wall is modeled as a homogenised continuum structure with combined (isotropic) masonry properties. For computational reasons, the wall is constructed with four rectangular sections as opposed to a plate with a single hole. In this configuration, the model has essentially no holes as it is the outcome of two long horizontal rectangular plates and two vertical plates at both sides of the window. The four sections are 'sewed' together in all degrees of freedom without 'healing' the input sheet; meaning that the hole that starts to form within the sewed sections is left open to simulate the window gap. The model is simply supported in all three directions at the bottom edge. At the top, the two horizontal directions are supported, recreating the (vertical) degree of freedom possible in the experimental set-up. Furthermore, in-plane rotations are restrained at both the top and bottom. In terms of loading, three separate loads are identified and implemented in the model:

1. Triangular (hydrostatic) load that is subjected on the face of the model, directed perpendicular to the wall. The load is computed as a predefined function which multiplies the hydrostatic load belonging to a water level of 1.0 meter or 9810 N. To create the load for a water level of 1.5 meters the multipliers are thus changed to 1.5 at z=0 and 0.0 at z=1.5. Note that the triangular load is re-shaped if inside water levels are accounted for. This can also be done by tweaking the multipliers from the predefined function.

2. Line load at the top edge mimicking the load that was subjected onto the wall by the springs and beam. The load has a magnitude of 2500 N/m which originates from the initial 25 kPa subjected onto the wall.

3. Self-weight of the wall. The calculations are performed by the program and use the predefined properties.

To obtain a detailed result without unnecessarily increasing the time needed for the computational progress, it is chosen to refine the model with a mesh of 52x52 elements; all having dimensions of 50x50 mm. For a quick overview of the model and the mesh, Figure 5.7 can be used.

Like the analytical model, the capacity for the wall is described by Equation 5.2. With FEM it is possible to compute when this capacity is reached. Additionally, it is shown graphically where this capacity is reached first. Likewise, for the deformations, the magnitude and locations are also given in a graphical plot, see Figure 5.8. The figure shows that at a water level of 1.7 meters, the model indicates deformations of around 5 millimeters for scenario III. Furthermore, it can be observed that the deformations are slightly skewed towards the bottom, which is a direct consequence of the triangular-shaped forcing at the bottom. Also, the DIANA FEA program recognizes the sharp corners in the window gap as a weak spot; marking the locations of the maximum moments. Note that because of the brittle nature of masonry it is almost certain that cracks will occur at the corners. Tensile forces encourage deformations and propagation at these points because stresses will concentrate at the crack tip. This phenomenon was not accounted for in the analytical model; emphasizing the importance of this model.

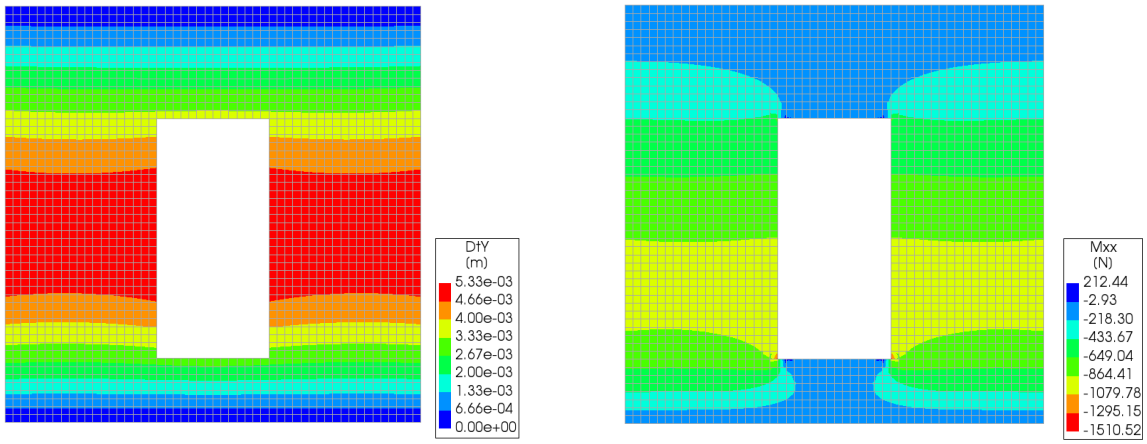

Figure 5.8: Outcomes from DIANA FEA for an outside water level of 1.7 meters. In this case capacity is coming from both leaves. Left: Deformations of the wall. Right: Bending moment distribution around the horizontal axis.

5.2.2. Limit curve: linear FEM

Using the linear version of the finite element model, already a more detailed description of the limit curve can be made that can be extended over the complete height of the cavity wall (which was not possible in the analytical model without redefining the model). From the left plot of Figure 5.9 it can be observed that the lower bound reduces to 1.35 meters (compared to 1.38 meters found by the analytical model). Further comparing the analytical model with the linear FEM, it can be seen that the curvature of the different regimes is sharper for the FEM model, whereas for the analytical model the curvature is flatter. According to the FEM model, the cavity wall is thus more 'forgiving' in the lower half of the > 100%-regime; meaning that a small amount of water inside the residence already could 'pull' the forces in a safe regime. For the analytical model, a lot more water would be required more quickly to end up in a safe regime. Both models seem to agree that exceedance of the moment capacity will happen around 1.65 meters (1.7 meters for the analytical model) for poorly functioning wall ties. Nevertheless, for well-functioning will ties the critical water level is increasing significantly to levels above 2.0 meters, albeit that for the analytical model the critical area is found outside the boundaries of the model. For both models, increasing the width of the structure to 0.27 meters leads to an upper bound of well over 3 meters in height.

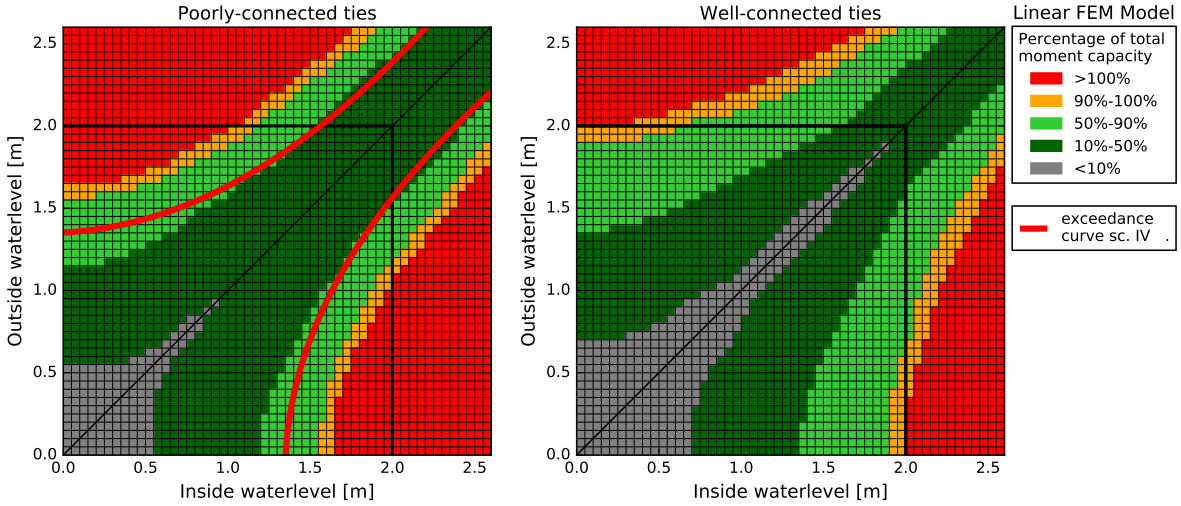

Figure 5.9: Computed results on the occurring internal moments using FEM. Left: contour plot of the behaviour of the resisting moment corresponding to poorly-connected wall ties. As with previous figures, the colours mark a certain percentage of the maximum calculated resisting moment (Eq. 5.2). Right: The contour plot corresponding to the second scenario. As to have an adequate comparison with the analytical model a square is added for both plots; marking the 2.0 m (horizontal and vertical) boundary of Figure 5.5 and Figure 5.6.

Looking at water levels above 2.0 meters the behaviour of the moments seems to reach a stable state in which the curvature of all regimes become parallel to the x=y-line. At these higher levels, the water level difference, and therefore the resulting force, decreases. Yet, the resulting force is projected closer towards the centre of the wall. This mechanism still makes the forces exceed the resisting moment. Eventually, the larger part of the forces gets transferred to the support at the top, after which the deformations and moments reduce again. For every increase in water level inside a residence, the maximum moment is decreasing, but also moving upwards. This can be seen in Figure 5.10. In this figure from left to right, the inside water level rises with the outside level at a constant value. The diagrams clearly show that the maximum moment is located at the edge of the window gap and travels upwards along this edge. Note also that the corners of the window gap are vulnerable locations and that the top corners become more prominent as the inside water level rises, while the bottom corners slowly become insignificant. This phenomenon is a direct effect of the wall's linearity. It should be questioned if this still would happen if exceedance of the tensile characteristics would lead to cracks and probably failure before the top corners will start to stand out.

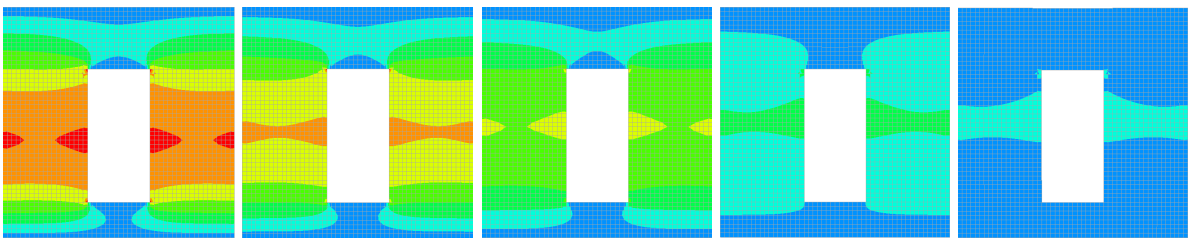

Figure 5.10: Visual demonstration of the upward movement of the internal moment. Displayed are diagrams of the wall section being fully subjected to an outside water level of 2.6 meters. The diagrams change due to an increase in inside water level (resp. 0.4m; 1.1m; 1.5m; 2.1m; 2.4m). Note that the window is not vertically centered, but rather skewed towards the bottom of the wall so that the center of the window is not identical to the center of the wall. It should also be noted that the scaling of colours is kept constant to allow for an adequate comparison. Due to the scarcity of colours, only the blue and green colours mark the sections where the moment capacity is not exceeded.

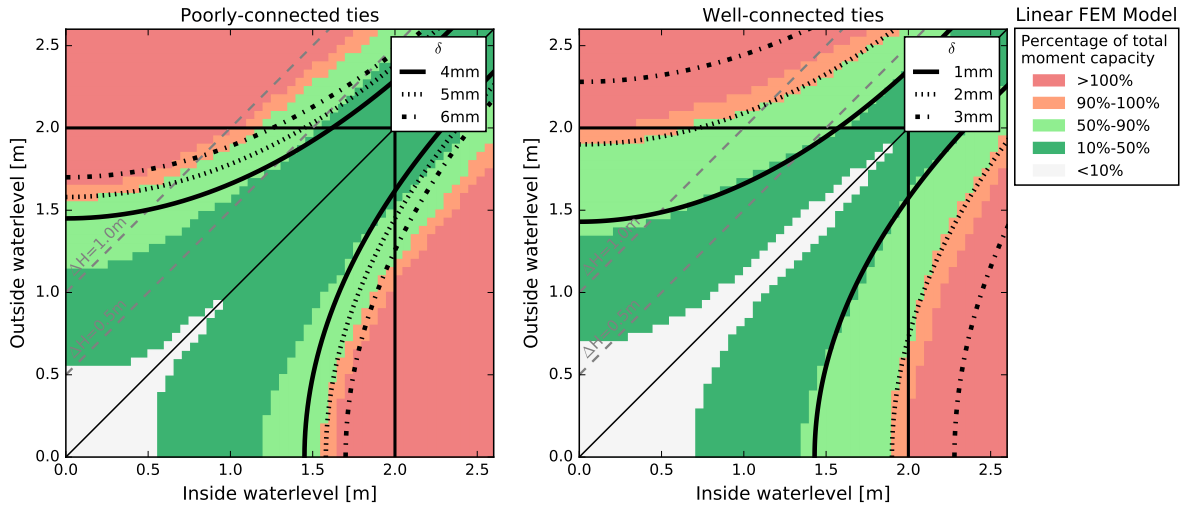

Figure 5.11: Computed results on the occurring deformations using FEM. Left: Deformations from the third scenario overlaying the earlier found momentum behaviour. Right: the deformations found by FEM for the second scenario. In both plots (grey) diagonal lines indicate situations with equal head difference, see also Figure 5.16.

Permanent damage weakens the wall and can possibly manipulate the limit curvature. Since here the permanent damage is a direct consequence of the brittleness of the masonry the occurring deformations are investigated in Figure 5.11. Note that for the left plot deformations of 4 to 6 millimeters are already visible and rapidly succeed one another. Compared to the analytical model these magnitudes also start to form for lower water levels. The curvature of the deformations differs from the moment-curvature, with great deformations slowly reaching in 'safe' moment regimes. This differs significantly from the right plot where not only the magnitudes are much lower, they also follow the same curvature as the moment does. Additionally, the distance between consecutive lines is greater compared to the third scenario on the left. For this second scenario, the outcomes of the finite element model and the analytical model are very much alike regarding the deformations.

5.3. Non linear FEM

With the notion that the homogeneous masonry properties are provided with a tensile strength and ultimate strain, a so-called total strain-based crack model is started. The model has a rotating crack orientation in which the stress-strain relations are evaluated in the principal directions of the strain vector [1]. Furthermore, the tensile curve is modeled using the linear ultimate crack strain. This option allows the strain to decay after the maximum stress is reached; whereas other options would terminate the computation or let the model stay in its elastic regime. The strain-based crack model is also favoured because of few required parameters and a fast computation time. Furthermore, it is suited for out-of-plane cracking for shell elements; which were used to create the mesh [24].

5.3.1. Limit curve: non-linear FEM

The resulting limit curves that were computed after the non-linear analysis are different than previous ones. Almost identical to the linear analysis, the internal moment and deformations gradually increased for the scenario with the poorly-connected wall ties. At an outside water level of 1.24 meters, the deformations suddenly reached in the order of multiple centimeters. With the wall ties well-connected, the model fails at 1.56 meters. As seen in Figure 5.12, for both approaches, the wall endured failure before the moment capacity was reached. It can also be seen that the line of failure has a mild slope, while the moment regimes have a steeper slope. As a consequence, the line of failure cuts into the regime where the acting moment is only half that of the wall's capacity.

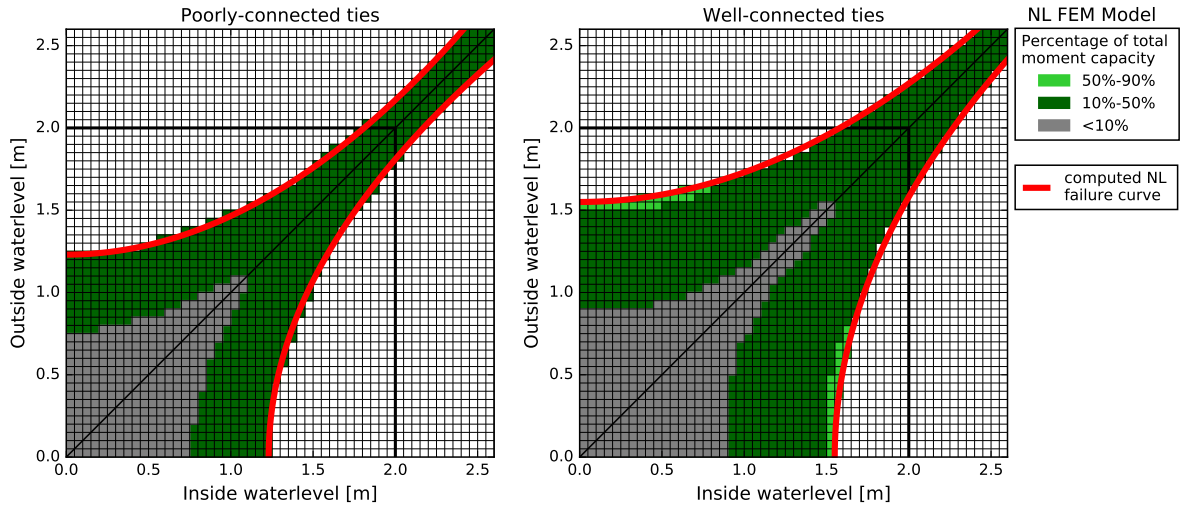

Figure 5.12: Limit curve for both scenarios for the complete structure as derived by the non linear FEM analysis. The coloured regimes indicate the state of the internal moment; with lime green indicating a factor of 0.5 - 0.9 of the maximum capacity, dark green: 0.1-0.5, and grey: <0.1. The red line indicates failure. It should be observed that for the second scenario (right), the lime green regime has just started when failure is observed. It can therefore be concluded that the resisting moment is just above half of its capacity, before failure occurs.

Both observations indicate that failure of the wall will occur due to micro-cracks and the occurring deformations. Yet, comparing the curvature and water level values with Figure 5.11 it can be concluded that the line of non-linear failure coincides with linear deformations of only 1 millimeter. This might indicate that the non-linear deformations are actually different than the values obtained in the linear analysis.

At the point where the outside water level is 1.24 meters and the inside level is a near-zero value, the wall with poorly-connected wall ties fails for the first time. At that point, the cracks that start to form in the middle section are already greater than 1.4 millimeters. The redistribution of forces to interfaces still intact no longer succeeds and as such the distribution of moments is also forming a non-linear behaviour (see Figure 5.13. It is the middle wall section that notes values greater than the moment capacity. It seems reasonable to assume that the deformations will bound the limits of the cavity wall due to its milder slope. Because of these deformations, micro-cracks start to form that quickly grow in width and activate the redistribution of forces. Nevertheless, the brittleness of masonry only allows a slight amount of forces to transfer to interfaces still unharmed, after which the moment capacity is exceeded as well.

Although the cavity wall with well-connected wall ties allows a higher water level, failure is still possible for water levels above 1.56 meters. This water level deviates significantly from the result obtained by the linear analysis. This is a consequence of modeling both walls as a single wall with an equivalent thickness. Because the stresses concentrate at the crack top, cracks propagate over the complete width, even though this width is larger than before.

From both plots, it becomes clear that the line of failure becomes stable at great water levels i.e. parallel to the diagonal. This indicates that no failure will occur ever if the water level difference is constant or below a certain level. From the Figure it is observed that failure can be avoided if the maximum head difference would be 0.2 meters. Furthermore, in those situations the resisting moment is well below 50% of its capacity.

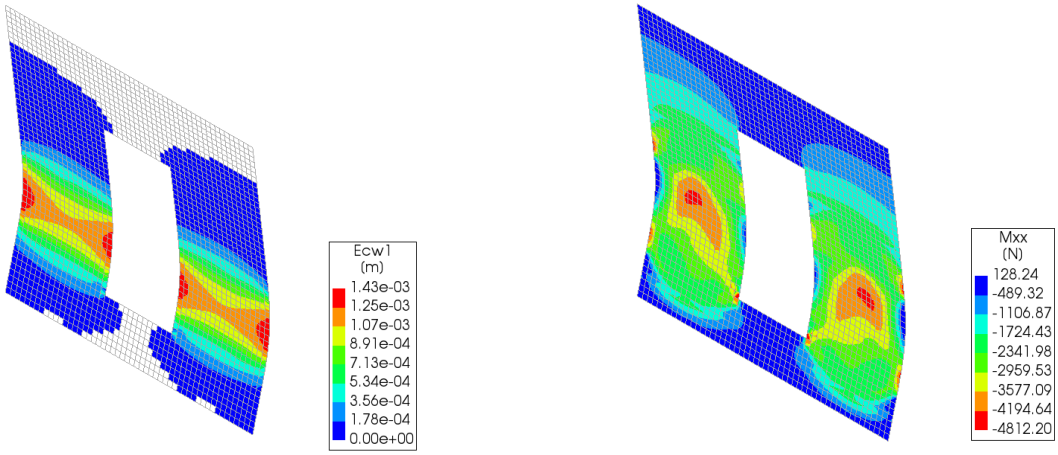

Figure 5.13: Left: results on the crack width for an outside water level of 1.24m. The cracks will form near the lower edges of the window gap. Right: results on the moment distribution for the same water level. Note that the vulnerable locations are similar to the locations where cracking will occur.

5.4. Concluding computations

In this section, final comparisons are made between the different scenarios, regarding the crack width that was obtained during the non-linear analysis using FEM. Furthermore, the deformations for all analyses are plotted together with the real observations to have a final overview of the computed models.

5.4.1. Crack width

Due to the notion of non-linearity, the masonry material can form cracks whenever the occurring (tensile) stresses are exceeded. As such, a smeared crack model is formed within the non-linear analysis. The maximum crack widths are recorded for every possible water level combination. For both the single wall scenario and the equivalent thickness scenario the water levels are translated to their corresponding momentum force. In Figure 5.14, the obtained crack widths are plotted against the moment load.

Both scenarios show the same behaviour: at first, the found cracks display values in the order of nanometers and micrometers, then at a certain point the stresses are exceeded and the crack width suddenly increases to a value of +1 millimeter, and finally, the results scatter between 0.5 and 4 millimeters. Cracks that have propagated to widths of these magnitudes have certainly dismantled the corresponding interface and as such forces can no longer be transferred through this specific interface. While the finite element model tries to compute reasonable results beyond this first point of cracking, it should be noted that the wall has already failed before the final computation and that the scattering behaviour is trivial.

As can be expected the cavity wall will fail sooner when modeled with a single wall thickness. At a value of 6814 Nm the cracks currently present start to develop widths that will result in failure of the interface. Throughout the analysis, it was shown that the first cracks started in the bottom corners of the window gap, albeit with magnitudes of only micrometers. With the water level rising also the location of the cracks with maximum width rose; much like the maximum moment did (see Figure 5.10 once more).

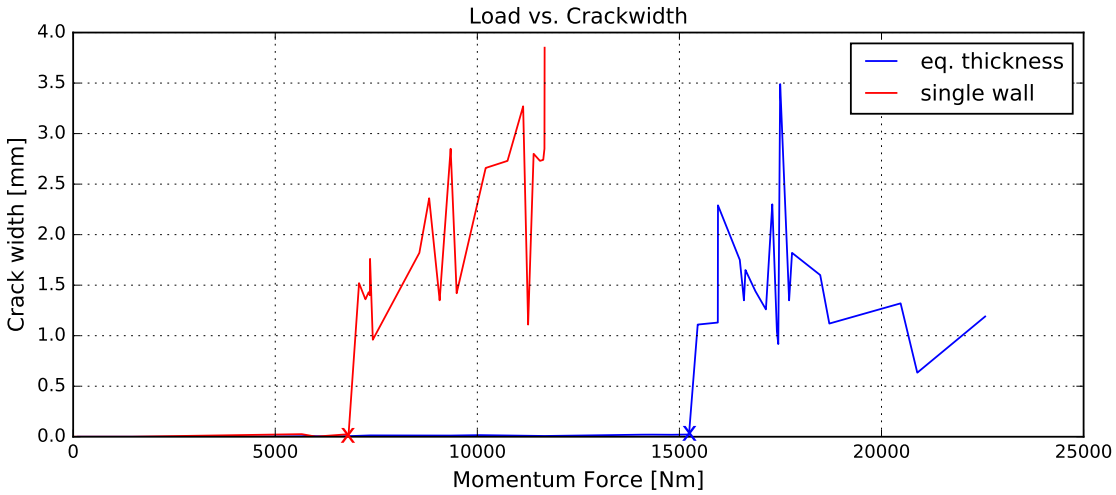

Figure 5.14: The computed crack widths plotted against the momentum force. The crack width is obtained by FEM for scenario II and scenario III, while the force is a result of the active water levels. The points of sudden increase of the crack widths are marked by an 'X'.

6814 Nm		15235 Nm	
H_{out}	H_{in}	H_{out}	H_{in}
1.15m	0m	1.5m	0m
1.2m	0.5m	1.55m	0.5m
1.7m	1.5m	1.9m	1.5m

Table 5.2: Several water level combinations that will (nearly) approach the corresponding momentum force marked by 'X' in Figure 5.14.

Forces of 15.235 Nm can be withstood when the cavity wall is modeled using an equivalent thickness accounting for both leaves of the wall. Beyond this point, the outcome is similar to the single wall. Also for this second set of results the cracks started in the window gap corners. Note that there are multiple water level combinations for both scenarios that will result in severe cracking. A small amount of combinations is provided in Table 5.2 to give the reader a sense of potentially dangerous combinations.

5.4.2. Deformations

In the previous section, it was briefly discussed that non-linear failure coincided with linear deformations of only a millimeter and with linear momentum of only half the capacity. Logically, the non-linear deformations will start to deviate from their linear counterparts when the wall will enter its non-linear regime. The point where the wall enters its non-linear regime depends strongly on the resulting force originating from the water levels inside and outside. As such, constant head differences do not lead to constant deformations, see Figure 5.15. In any case, the occurring deformations are constrained by an upper and lower bound. In this case, the second (single wall) and third scenarios (eq. thickness) mark these boundaries. The real deformations should thus be found between these two lines. In Figure 5.16 the area between the two boundaries is shaded for both the analytical results as well as the non-linear results. In which the blue areas indicate the possible deformations for a constant head difference of 0.5 meters and the red area bounds the possible deformations for a constant head difference of 1.0 meter. For the right plot, the linear FEM boundaries are also shown as dashed lines but the area for this analysis is not shaded. As expected greater deformations are observed sooner for a head difference of 1.0 meter (visible as a shift to the left).

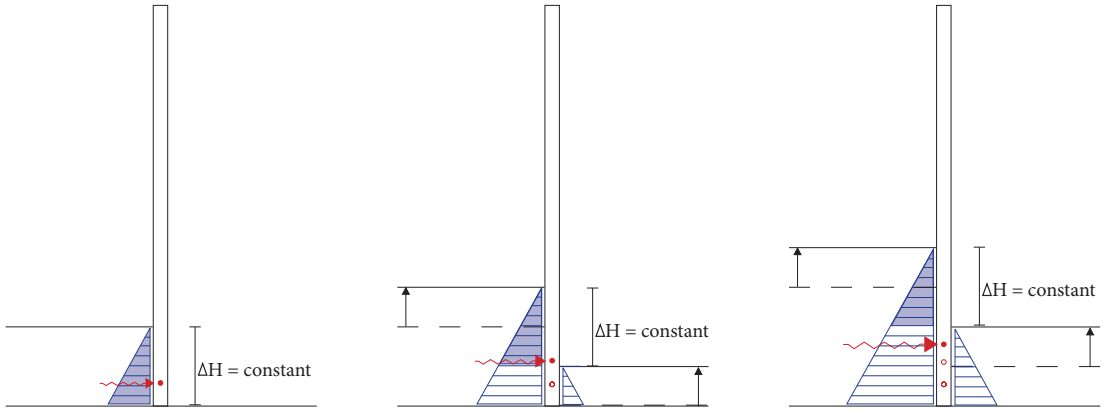

Figure 5.15: Theoretical explanation on the observed difference in deformations for identical head differences. Above three different combinations of water levels are shown that result in the same (constant) head difference for all three figures. As such the blue triangular load originating from this head difference is identical in all figures as well. Two important mechanisms can be observed: (I) The resulting force (red arrow) increases in magnitude when the identical head difference is found higher up the wall. (II) The resulting force shifts upwards; starting to deviate from the (expected) point load that acts at one-third of the water depth. Both mechanisms contribute to greater deformations, even though the head difference is identical.

On the X-axis the inside water level is noted. From both plots, it becomes clear that the deformations increase when the constant head difference 'travels' along the x-axis i.e. the same head difference results in greater deformations when located higher up the wall.

For the analytical model (left plot) there are no non-linear results. As such, the areas for both a constant head of 0.5 meters and 1.0 meter are made up by the boundaries computed in a linear analysis. For a constant head difference of 0.5 meters (blue lines) the wall will not fail. For a constant head difference of 1.0 meter (red lines) the upper bound is ended prematurely; denoted by an 'O'. At this point the moment capacity is exceeded, corresponding to a deformation of almost 4 millimeters. For completeness, all real observations recorded with a $\Delta H = 0.5$ m are plotted in the same graph left. From the real observations, 75% is located between the boundaries.

Also for the linear FEM results in the right plot, the boundaries corresponding to a constant head of 1.0 meter are ended prematurely due to exceedance of the moment capacity. Nevertheless, it should be noted that the corresponding non-linear results already ended at lower (inside) water levels denoted by 'X'. This actually means that the deformations found for the linear analysis are rather trivial and will not be reached. Further note that both upper bounds end at a deformation of 4 millimeters and both lower bounds end at a deformation of 2 millimeters; possibly indicating the limits on the allowable deformations. Above these values, cracking occurs and the wall fails.

In the right plot, it can also be seen that the non-linear deformations corresponding to $\Delta H = 1.0$m (red) start to deviate from the linear deformations at a constant inside water level i.e. at 0.1 meters. At this point, the outside level is thus 1.1 meters. The same can be seen for $\Delta H = 0.5$m (blue). For this value, the non-linear deformations start deviating at 0.4 meters i.e. an outside value of 0.9 meters. In both situations the occurring deformations and moments are well below their capacity; meaning that the non-linear behaviour is not triggered by these parameters. Due to the non-existing data for higher head differences, it cannot be concluded for sure if this observation is trivial.

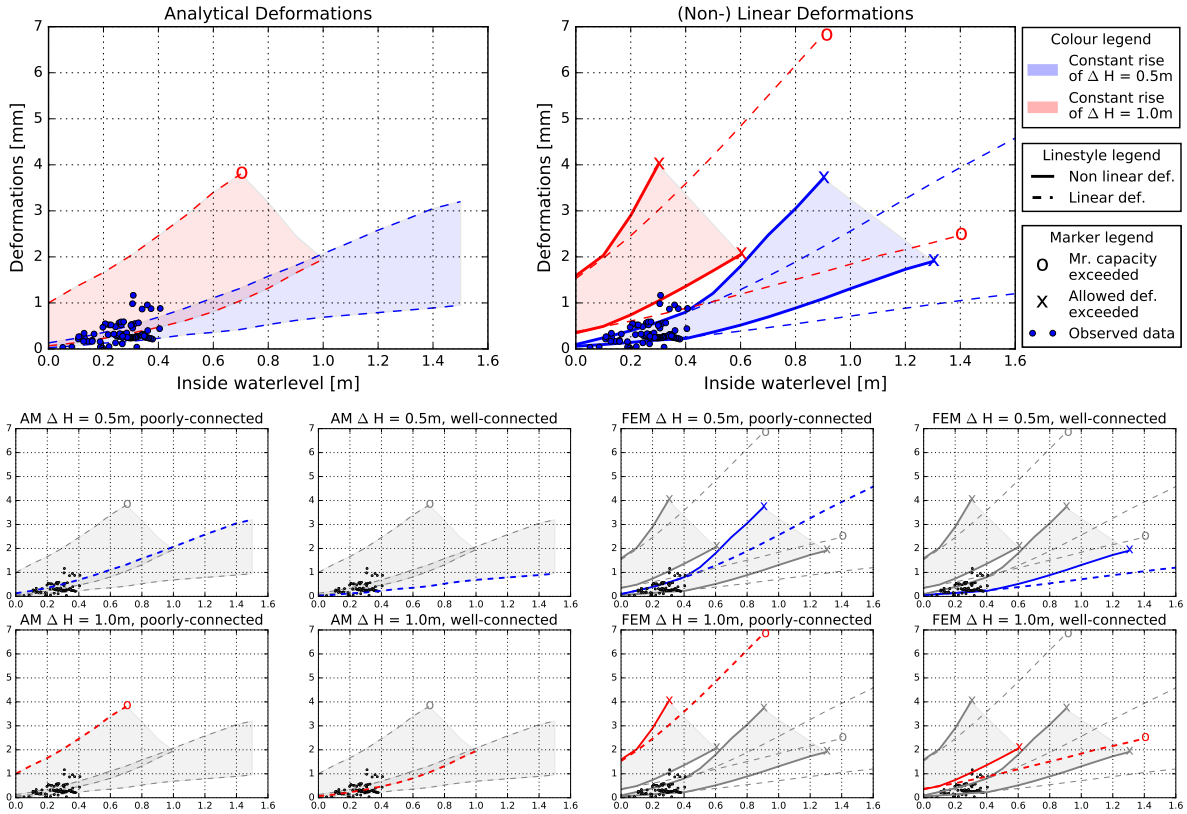

Figure 5.16: The computed deformations for both the analytical model and FEM. Left: Analytically computed upper and lower bounds regarding a constant head difference of Δ H=0.5m rising upwards along the wall (blue). In addition a similar configuration is computed regarding Δ H=1.0m (red). Right: the upper and lower bounds for Δ H=0.5m and Δ H=1.0m for the non-linear analysis. The linear FEM results are shown as dashed lines. The real observations are shown as dots. For a better overview, below the lines are shown individually depending on (I) the model, (II) the constant head difference, and (III) the behaviour of the wall ties. The single lines correspond to the diagonal slices shown in Figure 5.6 and Figure 5.11.

The real data is once again plotted; this time 88% of the points fall in between the boundaries. Furthermore, all points are situated below the x-value of 0.4, which means that the non-linear deformations are still similar to the linear values. With the maximum recorded head difference being 0.7 meters, it is almost certain that the linear regime was governed throughout the experiment.

6

Discussion

The main objective of this research is to investigate the behaviour of a cavity wall when subjected to hydrostatic forces. In this chapter, a final reflection is made on the experimental methodology and analysis. With new insights gained in the later months of the project, some assumptions and flaws can now be deemed important or irrelevant. Furthermore, the results and outcomes, treated in the previous chapter, are interpreted and compared to results from other studies.

6.1. Reflection and limitations

At the beginning of the project, it was chosen to focus the research on Dutch cavity walls only and only treat direct damages originating from wall failure in a one-way bending configuration. This focus was required to allow the project to gain a sufficiently in-depth understanding of the subject, without redundancies. Yet, it emphasizes the broad spectrum in which failure of a (cavity) wall can occur. More than once during the progress of the project, it was needed to select certain options and disregard others. The most important choices made within the scope are addressed below.

Experimental methodology

The opportunity to test a life-sized cavity wall allowed certain insights that could not be obtained by solely simulating the wall's behaviour with computations. For instance, the way the bricks were cut and placed to make room for the window gap changed the stretcher bond in certain locations. Also, the wall ties were not necessarily placed on the optimal structural position but rather on convenient spots where both wall courses were equal in height. Nevertheless, the experiment in the basin also bounded the possible flood actions. Hydrodynamic actions were certainly present in the form of wind and localised turbulence effects due to the location of the water outlet cannot be ruled out either. These phenomena could not be controlled in the basin and their effects are almost certainly negligible compared to the hydrostatic loads. However, during real flood events, it is the summation of all these flood actions that determine the failure curve of a cavity wall. Thus, the computed results are not final and will change if other flood actions are accounted for as well.

Most houses that feature a cavity wall were built in the early 1980's. Selecting the materials to resemble these types of older walls can certainly be used to replicate adequate results. Nevertheless, a virgin wall cannot produce identical outcomes as a real wall would. The wall that was constructed, therefore, consisted of available materials of which some are alternative. It should be noted though, that selecting the mortar is of greater influence for the outcomes than the selection of steel brackets. Furthermore, it can be reasoned that for out-of-plane bending, the structural properties of different brick types will not significantly affect the outcomes, while changing the brick size and orientation of the stretcher bond will.

Replacing the glass with polycarbonate material allowed the experiment to proceed safely. While glass used in windows is sufficiently safe, certain water levels will exceed its capacity after which the inside of a residence will fill up with water; reducing the hydrostatic pressure. This given fact was neglected for the sake of the experiment and while it is believed that significant water levels can be withstood, the outcomes of this project should not be applied in practice, without considering this.

Experiment
There are some flaws originating from the construction that may have affected the outcomes. While their exact influence is unknown, mentioning the flaws once more can provide an insight into the quality of the results. For one, the inner and outer leaf of the cavity wall were not perfectly aligned; a result of a tilted pillar. This means that the width of the cavity is smaller at the bottom than at the top. The wall ties placed at the bottom are thus placed further in the mortar and incline more to the right or left to prevent the ties from sticking out. From Chapter 5 it became clear that the width of the cavity wall is of great influence for the capacity. With the CaSi wall tilted there was already a (minor) eccentric load coming from the self-weight.

Unfortunately, it turned out that the cavity could not be kept dry. This affected part of the protocol and the possible outcomes. While mortar is not completely water-tight the amount of water coming in came from numerous leakages and joints that were not closed sufficiently. It became impossible to control the water levels around the wall and certain leakages became hard to trace through the wall. It was opted to keep the cavity dry and as such obtain data about the influence of the wall ties. With water only pressing against the outer leaf, the deformations of the inner leaf could (at least partly) give insight into the behaviour of the wall ties. This flaw was dealt with by addressing boundaries (see Section 5.1.4). From the results of Section 5.4.2 it can be concluded that most of the real observations do fall between the assigned boundaries. Nevertheless, for higher water levels, the dispersion of the upper and lower boundary becomes large; making it hard to find a good estimate.

6.2. Leakage rate through interface

In Section 4.4 the contribution of leakages through the window-wall interface is investigated. The results show only a minor discharge into the box; indicating that a well-mounted window can be watertight for at least 80 centimeters of water. The study further demonstrates that the location of the window (i.e. the distance from the bottom of the window to the bottom of the wall) highly influences the contribution to the rise rate inside a residence.

The results were expected, considering the similarity between water intrusion and air loss; which should be prevented for environmental reasons. From that same perspective, it can be expected that the importance of solid execution of the window-wall interface will increase in the near future; reducing possible contributions to the rise rate even further. Although the results might suggest that some amount of water can be expected to seep through the interface, findings of similar studies ([26]) make it more plausible that the recorded leakages can be traced back to an inadequate mounting of the window. This also complies with observations of the carpenter; stating that the wall should be built around the window to have a sufficiently narrow interface. The findings should, however, not be compared one-to-one with environmental studies on the air-and heat losses. The most important difference is found in the scale of which water intrusion would be considered as major. Signs of humidity would, therefore, be judged differently depending on the perspective. Nevertheless, both literature and the results show that execution is one of the most important factors that influence the possible leakages. When only regarding the interface from the flood risk perspective, the importance of the final sealant is obvious. The reason for this can be found in the weep holes that allow water to enter the cavity; bypassing earlier sealants.

The results also imply that no real contribution to the inside rise rate can be expected from the window until the glass shatters under the forces of hydrostatic pressure or other hydrodynamic flood actions. This was already assumed in earlier studies ([32]), albeit that in the same study the properties of glass are presumed to be weak; immediately forming a pathway into the residence once the water has reached the window. While the properties of (double-paned) glass do not fit in the scope of this research, it is believed that considerable water heights can be withstood. Due to the replacement of the glass pane for a polycarbonate equivalent, the results cannot confirm at what height or force the glass would shatter. It should further be noted that the reliability of the results is impacted by multiple other leakages present in the masonry work and the box. Nonetheless, by approximating the other leakages using the Toricelli method the total inflow is adequately simulated; indicating that the final results can be considered valid.

6.3. Wall deformations

The results from Chapter 4 were used to further compute the behaviour of the wall. Due to the vast similarity between this project and the previous wall experiment that was discussed in Section 1.4, the outcomes of both projects can be compared to find correlations and possible contradictions. Additionally, from other similar studies, relevant aspects are treated as well.

The earlier study on the masonry wall experiments follows a similar process of analysing the data. Both the data from that experiment and the data from the current project were obtained with the same type of sensors. It should be noted that the previous experiment included multiple configurations; adjusting the overburden and side supports [24]. Fortunately, one configuration was performed with similar conditions as the current project. A brief comparison between the deformations and moments of that specific data is shown in Figure 6.1 next to data from this year. As expected, both plots show an increase in deformation corresponding to an increase in acting moment. Another observation might suggest that the single masonry wall of previous experiments records greater deformations. While this is certainly the case, the degree at which this happens is less extreme than it would seem. The reason for this can be found in the initially recorded deformations; already starting at values of 2-3 millimeters. Note that the same observation can be made for this year's data. By vertically translating the results towards the x-axis, deformations of 2-2.5 millimeters would be shown for moments around 1.7 kNm/m for the 2020 experiments. For the current experiment, this would result in 0.5-1 millimeters.

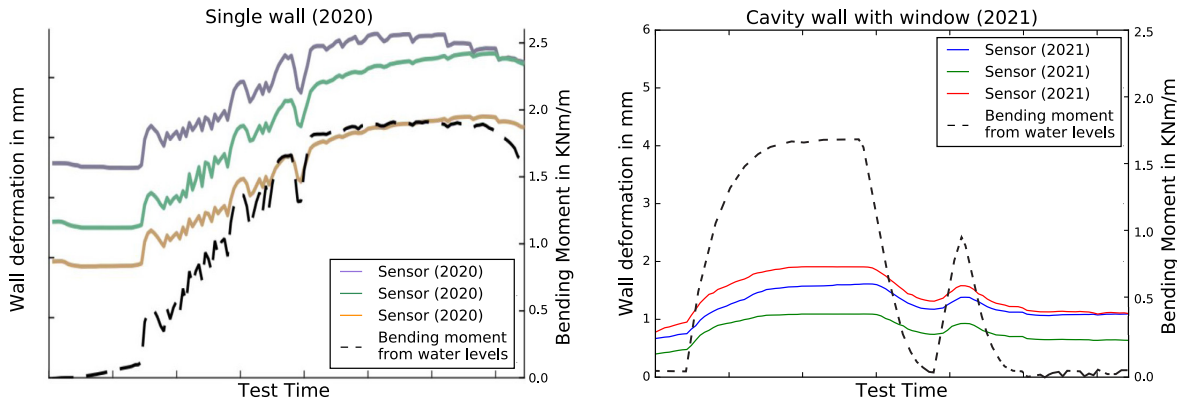

Figure 6.1: Comparison between the experiment of 2020 (left) and the current project of 2021 (right). Both (partial) results were obtained for similar conditions: 25kPa of overburden, no support from the sides, and similar bending moment values. (Left figure adapted from: Dutch Buildings Flood Fragility by Korswagen (2021)).

In line with expectations, a single leaf wall records greater deformations than a cavity wall for the same conditions; even with a window gap present. This would imply that a cavity wall is capable of transferring certain forces through the wall ties; increasing the width and the structural capacity. The difference in deformations cannot be completely attributed to the second wall, as the potentiometers had some temporary difficulties grasping the deformations. Considering the magnitudes of deformations and scale of the errors the sensors provided unstable results; mainly affected by temperature and deformations of the catchment box. Within the translation of this data into a structural stiffness, most of the influence of the errors was removed by considering the average value. It should be noted that the errors for the pressure sensors might be in the same order of magnitude as the potentiometers but the scale in which the pressures ranged was much larger; reducing the bias for these specific sensors.

Plotting the bending moment against the recorded deformations gave blurry outcomes, which is a direct consequence of the repetition within certain testing rounds. The hysteresis visible in the plots could have been related to permanent damages. Visual inspections did not reveal such damages. From the computations of Chapter 5 it is almost certain that the achieved water levels did not force the cavity wall in its non-linear regime, which argues that the great dislocation of the plot originates from errors. To account for this only the initial responses were considered, which lead to Figure 4.5. This approach resulted in a more uniform behaviour, albeit that the spread is still significant. This spread, however, cannot be fully attributed to the degradation of the wall's properties as indicated by Chapter 5's computations. Only at the final test 10, a significant adjustment was made by fully removing the spring load. The linear trend of this test did not deviate from the trends from test 7 or test 8.

Contrary to what was expected, the weakening effect of the window gap did not outweigh the strengthening effect of the additional wall leaf. This becomes clear when comparing the current results with the previous data (single leaf), see Figure 6.2. In this figure, the most prominent slopes of the force-displacement plots are shown together with the slopes from the previous experiment. The data deviates significantly, with the cavity wall showing a greater resistance against the acting moment.

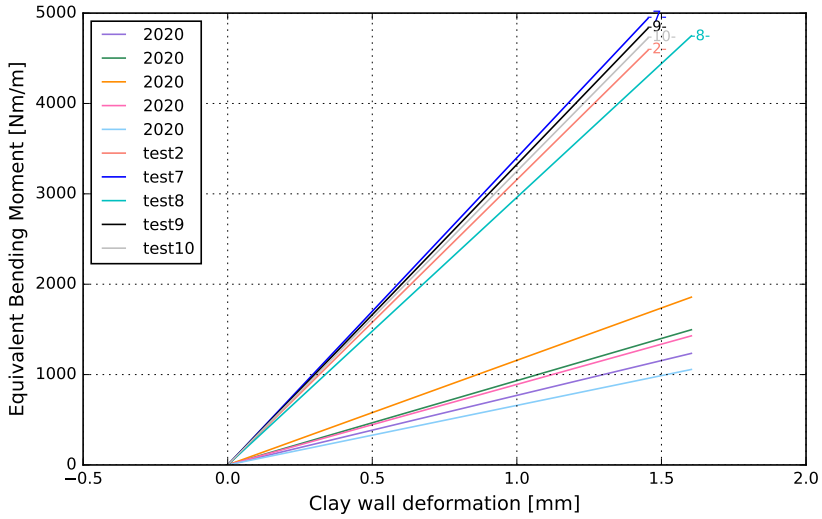

Figure 6.2: Comparison between the different slopes obtained from the force-displacement plots from both FPH experiments. (Data obtained and adapted from: Dutch Buildings Flood Fragility by Korswagen (2021)).

These findings agree with other experiments that wall ties can indeed improve the resistance capacity both in tensile and compressive configurations, albeit that this is greatly influenced by the wall tie design and thickness [28]. A similar pattern was observed by the sensor measuring close to the window. Here, an even greater resistance against bending was observed. However, no additional wall ties were fitted here. A plausible explanation for this is found in the framework that was fitted in between the walls. Around the window frame the connection between both walls is improved by the solid wooden framework; possibly increasing the collaboration between the walls.

The final computations were split into two to generate results for both well-connected wall ties and poorly-connected wall ties; resulting in a range of outside water levels that can lead to failure dependent on the wall tie behaviour. This report demonstrates a strong resemblance between the linear analyses of both the analytical model and the FEM model; which suggests that a window gap can be modeled by applying a weaker stiffness. Yet, in terms of deformations, the results start to deviate slightly. The deformations found by the FEM model are greater; possibly indicating that the stiffness was overestimated for the analytical model.

While previous research was focused on a single masonry wall, it can be expected that the resistible water levels increase for a cavity wall. Indeed this is the case for the linear models, with the results demonstrating that greater outside water levels can be withstood for the same one-way bending configuration, see Table 6.1. However, this hypothesis is contradicted by the non-linear analysis; showing similar water levels for the cavity wall as well as the single leaf masonry wall of 2020. This might be explained by the fact that, although both leaves are contributing to the resistance, failure of one wall would imply failure of the second wall too. This explanation is, however, constrained by the limited data on the wall ties. Based on the study of 2020, it can be reasoned that greater water levels can be withstood when the wall is featured with lateral constraints. This is also in line with other research; showing that having at least one restrained vertical edge contributes to a greater resistance [8]. Note that having vertical constraints changes the cracking patterns.

	2021 van Haren	2020 Korswagen		2019 Jansen
Configuration	**One-way bend. cavity wall**	**One-way bend. single leaf**	**Two-way bend. single leaf**	**two-way bend. cavity wall**
Analytical Model	1.7 m - 2.0 m	0.95 m	x	x
Failure criterion	Bending moment	Bending moment	x	x
Linear FEM	1.65 m - 2.0 m	x	0.9 m - 1.5 m	x
Failure criterion	Bending moment	x	Bending moment	x
Non linear FEM	1.3 m - 1.55 m	1 m	1.3 m	x
Design values Linear	x	x	x	1.2 m - 1.8 m
Design values + velocity (2m/s)	x	x	x	0.9 m - 1.5 m

Table 6.1: Comparison between the final results of the three relevant projects that were performed to investigate the flood fragility of modern residences. Listed in the table are the outside water levels that will lead to failure according to different models. (Data obtained and adapted from: Dutch Buildings Flood Fragility by Korswagen (2021) and from Structural damage to Dutch terraced houses due to flood actions by Jansen (2019)).

Although the influence of vertical constraints depends on the total length of the wall, for cavity walls too, it can be expected that higher water levels can be withstood when lateral constraints are present. The modeling of these constraints is beyond the scope of this project but it is believed that corner anchors used to connect differently orientated walls have some capacity in the vertical direction.

While the experiments at FPH focused on hydrostatic pressure (and debris actions for the 2020 research), other flood actions were investigated in a flume experiment in 2019. Looking at the linear models from this research, the results show little overlap with the findings of 2019. Primarily, this can be explained by the used design values for 2019. These values were chosen to match the quality and configuration of residences from 1965 to 1975. For modern residences with a cavity wall a water level of 1.8 meters was found [20]. This value corresponds well with the computations from Chapter 5. The outcome of this current research is limited by the absence of certain flood actions in the basin, which affects the resistance greatly, as is demonstrated by the addition of a hydrodynamic force in the form of a velocity forcing (2019). The velocity reduces the allowable water level by 0.3 meters, see Table 6.1 once more.

One important aspect that was not focused on in previous research was the upward moving effect of the resulting force when facing water levels at both sides of the wall. While this is a well-known structural phenomenon, the inclusion of this effect from a flood risk perspective indicates that the allowable head difference decreases for higher water levels. According to the computations, the head difference that can be countered ranges from 1.3 m for an inside water level of zero to 0.3 m when the inside water level reaches 1.4 meters. Chronologically, this requires certain changes during a flood event: If the wall has already failed for an outside water level of 1.3 meters, an inside water level of 1.4 cannot be reached anymore. Note that a second flood or an additional rise also counts as such a change. The allowable head differences computed by this current project are quite in line with a similar analysis executed in 2003. In that study, it is stated that head differences of 1.0 m - 1.5 m will imply failure [22]. When hydrodynamic flood actions like velocity are accounted for, this value can drop to an allowed difference of only 0.5 meters [22]. Similar experiments for early cavity walls in the United States report an allowed head difference of 0.9 m [42], indicating a possible difference in construction technology or improvement of the material since then.

7

Conclusions and recommendations

In this chapter, the findings of the main objectives are combined to answer the research questions as formulated in the Introduction. Other relevant remarks are noted as well. Finally, the gained experience is translated in recommendations that can be used to improve and focus future studies on the flood fragility of a (cavity) wall.

7.1. Conclusions

To answer the main research question, first, the sub-questions are treated to have a final overview of the project. For convenience, the sub-questions are repeated and treated separately.

1. What are the out-of-plane deformations of a window-featured cavity wall?
Different from a solid single leaf wall, the deformations corresponding to a cavity wall featuring a window are smaller for the same set of water levels. Whereas deformations reached values of 2 to 4 millimeters for a single leaf wall, the cavity wall displayed values of 2 millimeters at most. Note that both results were obtained for a wall with the same dimensions (1:1 ratio) and the same configuration (one-way bending i.e. no side support). This indicates that the strengthening effect of increasing the wall width is stronger than the weakening effect originating from a window gap. It was concluded that, although the deformations are imposed by the water levels, it is actually the momentum balance that describes the order of deformations. From a structural point of view, this was already known and can be simply explained with the resulting force. Nevertheless, it offers a new perspective regarding the interaction between water levels inside and outside a residence.

2. At what rate does the water infiltrate through the gap and how does the rate evolve through time?
Conventional window frames and sealants turn out to be able to prevent any significant leakages into a residence assuming that the window-wall interface is sufficiently small in width. For greater widths due to damages, the water pressure might rupture the sealant, albeit that new environmental regulations already counter such great gaps for heat loss purposes. Logically, failure of the window-wall interface only contributes to the rise rate if the outside water reaches the window. If an outside water level reaches beyond the window bottom, the discharge becomes constant as long as the inside water level has not reached the window. Eventually, the residence is filled up to the same level as the window, after which the discharge becomes a function of the changing head difference. Finally, when both levels are equal the leakage stops. It was also concluded that the discharge is dependant on the placement of the wall. In general, residences are filled up more quickly if the window is placed lower in the wall. It was expected that it would take less time to completely fill a residence affected by low outside water levels. However, this is only partly true. It was observed that the leakage

rate lowers significantly when the outside water level is only 10 centimeters higher than the window level. This is because the velocity corresponding to this head difference is rather low; taking a lot of time to fill the residence up to the window level in the first place. It should be noted that the leakage rate corresponding to the failure of the window-wall interface is only minor and can be neglected when considering more prominent pathways like the sewage system.

3. How do the moment distributions on the walls evolve by including water levels on both sides?
Because of the triangular shape of water pressure, the resulting force is defined at a third of the water depth. Considering water levels on both sides of the wall the resulting force moves slightly upwards. As long as the resulting force is transferred closer to the middle, internal moments and deformations stay large even though the head difference reduces. It is concluded that the resulting moment always decreases with ascending inside water level. Yet, this does not happen at a constant rate. This is a direct consequence of the upward movement of the resulting force. As such the behaviour of the moment distribution follows a parabolic trend. At low inside water levels, the reduction of the moment is low in comparison to the additional influence the resulting force gains by the increased height. This eventually turns around for higher water levels inside a residence; the reduced head difference implies a favourable reduction in bending moment that is no longer completely compensated by an unfavourable increase in lever arm.

4. How does the inclusion of both the window and the cavity influence the structural stages of the wall during a flood?
Both the analytical model and the FEM model produce useful results, albeit that the FEM model is more accurate. Depending on how the wall ties are behaving, an upper and lower bound are found considering a single wall for the upper bound and a wall with an equivalent thickness of 16 centimeters for the lower bound. The computations show that the wall reaches its non-linear stage somewhere around 1 meter of outside water level. At that level, the first micro-cracks are observed and the computed deformations start deviating from their linear counterparts. In terms of deformations, the failure curve corresponds to non-linear deformations of 4 millimeters for the upper bound and 2 millimeters for the lower bound. At those limits the interface cracks; leading to non-linear failure for outside water levels between 1.3 and 1.6 meters. It should be emphasised that modeling the cavity wall as a single wall in terms of cracking is somewhat wrong considering the propagation of a crack. A crack can only propagate through one interface, while a cavity wall consists of two walls and thus also two different interfaces. Nevertheless, a cavity wall subjected to one-way bending and loaded with a vertical compressive stress of 25 kPa can withstand water levels up to 1.30 meters and does not fail for head differences below 0.25 meters.

Research question: How does the presence of a window affect the stability of a cavity wall during floods and how does it influences the rise rate of water inside the building?
A cavity wall benefits greatly from its width (compared to a single leaf wall). This becomes obvious from the recorded deformations that are significantly lower than the deformations recorded for a single leaf. In addition, the wall ties transfer a certain amount of forcing towards the other leaf, which has a favourable effect on the capacity. Nevertheless, the window introduces a weak spot in terms of structural resistance. The stiffness of the wall is affected by the window gap. Considering water levels at both sides of the wall, the upward movement of the resulting force will slowly transfer towards this vulnerable wall section. The window gap also marks the start of the cracking stage, with micro-cracks starting out in the lower window corners and rapidly dismantling various masonry interfaces. It can be expected that the cracks will form a pathway for the water to enter the residence. Before the cracking stage, however, the window-wall interface can be considered as a sealed interface, with no contribution to the inside rise rate. The position of the window does not change this.

7.2. Recommendations

Considering the results and computations of this research it can be advised to allow (at least some) water to enter the house. In that way, the resulting force originating from the hydrostatic pressures is decreased or even diminished. Note that this still leaves room for other flood actions to affect the failure of a wall or building. For low water levels outside (<1.0 m) it can be tried to keep the residence dry as this will not lead to failure and thus won't outweigh the financial consequences of water damages inside a residence. A well-known advice is to prevent water from flowing in through the sewage system by placing sandbags in the toilet. It should also be reasoned that the walls with structural purpose are constrained at the sides as well. This will increase the water levels that can be withstood, although at some point it will not be safe to keep the residence dry anymore.

From a hydraulic point of view, it would be too soon to adapt the flood risk assessment based on these initial experiments. There are still multiple aspects that should be studied in greater depth before it can be determined if adaption is even needed. For one, the inclusion of several common hydrodynamic flood actions acting on a cavity wall at the same time should be studied, like wave actions and flow velocities. This will tell the real survivability of a cavity wall during a flood event. Based on those outcomes it should be reasoned whether or not it is safe to retreat to the next floor. This also might affect the individual risk of a person during a flood event. It should, therefore, be investigated to which extent the 'new' risk is acceptable for different areas and cities and see if those numbers outweigh the dangers of horizontal evacuation.

Based on the above, potential tests and research should investigate:

1. The influence of wall ties. For this, it must be guaranteed that the cavity can be kept dry. The cavity closers used in this project worked very well. A better understanding of the wall ties can be used to improve the boundaries set in this research.

2. Debris actions on cavity walls. Because the calcium silicate wall is designed to bear the structural loading damages on the outer leaf might not lead to immediate failure.

3. Various flood actions at once. It is needed to find the behaviour of a cavity wall subjected to this buildup of forces. It should be investigated for what levels the wall will collapse and if these levels can be sufficiently reduced by letting water inside the residence.

4. How the various definitions of risks will be affected by the findings of the above investigations. This might lead to a change in evacuation strategies in major cities.

Based on structural interest, the following aspects can be added to the existing experiment at FPH:

1. The point at which the water levels will exceed the stresses of ordinarily used glass. This would eventually mean that a residence will fill up anyway and that the resulting force will not reach until the middle of a wall.

2. The behaviour of a wall with a 'repaired' section. With time certain damages are repaired with more modern and possibly stronger materials. It might be possible that this virgin piece will change certain outcomes.

3. Walls with different stretcher bonds. Especially modern houses show a great variation of bonds. Some reduce the joint lengths significantly, which would lead to a lower resistance against vertical stresses.

Bibliography

[1] Manual: DIANA Finite Element Analysis. 47.5 total strain crack models. `https://dianafea.com/manuals/d105/Diana.html`. Accessed: October 10th, 2021.

[2] L. Barnes, J. Hauser, L. Heikes, A.J. Hernandez, P.T. Richard, K. Ross, G.H. Yang, and M. Palmquist. *Experimental and Quasi-Experimental Research*. Colorado State University, 2012.

[3] N. Van Den Bossche, W. Huyghe, J. Moens, A. Janssens, and M. Depaepe. Airtightness of the window-wall interface in cavity brick walls. *Elsevier*, 45:32–42, 2012.

[4] Bouwbesluit. artikel 2.18. hoogte lid 3. Technical report, Ministerie van Binnenlandse Zaken en Koninkrijkrelaties, 2012.

[5] W.C. Brade. *Theoretisch en practisch bouwkundig handboek*. A.J. van Weelden, 1827.

[6] T. Bristogianni, F. Oikonomopoulou, C. Justino de Lima, F. Veer, and R. Nijsse. Structural cast flass components manufactured from waste glass: diverting everyday discarded glass from the landfill to the building industry. *Heron*, 63(1/2):57–102, 2018.

[7] J.J. Brooks. *Concrete and Masonry Movements*. Buttersworth-Heinemann, 2015.

[8] Lang-Zi Chang, F. Messali, and R. Esposito. Capacity of unreinforced masonry walls in out-of-plane two-way bending: A review of analytical formulations. *Elsevier Structures*, 28:2431–2447, 2020.

[9] P.A. Claisse. *Civil Engineering Materials*. Buttersworth-Heinemann, 2016.

[10] L.K. Clausen. Potential dam failure: Estimation of consequences and implications for planning. Technical report, School of Geography and Planning at Middlesex Polytechnic, 1989.

[11] B.J. Crowder-Moore, T.A. Weston, and J.D. Katsaros. Performance testing of flashing installation methods for brick mold and nonflanged windows. *ASTM*, 3:133–152, 2006.

[12] M. Delghust, A Janssens, and J. Rummens. Retrofit cavity-wall insulation: performance analysis from in-situ measurements. *Research on building physics*, 1:297–304, 2010.

[13] J. Van Elk and D. Doornhof. Groningen earthquakes structural upgrading: data documentation exposure database v5. Technical report, Arup, 2018.

[14] M. Escarameia and A. Karanxha. Quentifying the flood resilience properties of walls in typical uk dwellings. *Institution of building services Engineers*, 2007.

[15] J. Ferrand et all. Wetting effect on torricelli's law. *Physical review letters*, 117:248002, 2016.

[16] A.P.A. Faiyas, S.J.F. Erich, H.P. Huinink, and O.C.G. Adan. Understanding the water absorption from mhec modified glue mortar into porous tile: Influence of pre-drying. *Construction and Building Materialse*, 217:363–371, 2019.

[17] C.J.W.P. Groot and J. Gunneweg. Or 1 -historische metselwerk: kwaliteitseisen restauratiebaksteen. *TU Delft*, 2007.

[18] D. Hoffmann and K. Niesel. Quantifying the effect of air pollutants on renderings and also moisture transport phenomena in masonry including its constituents. Technical report, Federal Institute for Materials Research and Testing, 1995.

[19] J.P. Ingham. *Geomaterials Under the Microscope*. Academic Press, 2013.

[20] L. Jansen, P.A. Korswagen, J.D. Bricker, S. Pasterkamp, K.M. de Bruijn, and S.N. Jonkman. Experimental determination of pressure coefficients for flood loading of walls of dutch terraced houses. *Elsevier*, 216, 2020.

[21] I. Kelman. *Physical Flood Vulnerability of Residential Properties in Coastal, Eastern England*. PhD thesis, University of Cambridge, 2002.

[22] I. Kelman and R. Spence. A limit analysis of unreinforced masonry failing under flood water pressures. *Masonry Int.*, 16.2:51–61, 2003.

[23] I. Kelman and R. Spence. An overview of flood actions on buildings. *Elsevier Engineering Geology*, 73:297–309, 2004.

[24] P. Korswagen. Dutch buildings flood fragility: masonry wall experiments at flood proof holland. Technical report, Delft University of Technology, 2021.

[25] P.A. Korswagen Eguren. Structural damage to masonry housing due to earthquake-flood multihazards. Master's thesis, Delft University of Technology, 2016.

[26] S. Van Linden and N. Van Den Bossche. Watertightness performance of face-sealed versus drainend window-wall interfaces. *Elsevier Building and Environment*, 196, 2021.

[27] B. Maaskant, S.N. Jonkman, and M. Kok. Analyse slachtofferaantallen vnk-2 en voorstellen voor aanpassingen van slachtofferfuncties. Technical report, Deltares, 2009.

[28] A. Martins, G. Vasconcelos, and A. Campos Costa. Experimental study on the mechanical performance of steel ties for brick masonry veneers. *Taylor and Francis*, Brick and block masonry: trends, innovations and challenges, 2016.

[29] K.M. Mosalam, G. Ayala, R.N. White, and C. Roth. Seismic fragility of lrc frames with and without masonry infill walls. *Journal of Earthquake Engineering*, 01:693–720, 1997.

[30] C.V.R. Murty and Sudhir K. Jain. Beneficial influence of masonry infill walls on seismic performance of rc frame buildings. *12th world conference on earthquake engineering*, 2000.

[31] Rijkswaterstaat. Watersnoodramp 1953. `https://www.rijkswaterstaat.nl/water/waterbeheer/bescherming-tegen-het-water/watersnoodramp-1953/index.aspx`. Accessed: January 28th, 2021.

[32] W. Roos. Damage to buildings. Technical report, Delft Cluster, 2003.

[33] C.T. Salzano, F.J. Masters, and J.D. Katsaros. Water penetration resistance of residential window installation options for hurricane-prone areas. *Elsevier*, 45:1372–1388, 2010.

[34] S.B. Singh, P. Munjal, and N. Thammishetti. Role of water/cement ratio on strength development of cement mortar. *Journal of Building Engineering*, 4:94–100, 2015.

[35] K. Slager and D. Wagenaar. Standaardmethode 2017 schade en slachtoffers als gevolg van overstromingen. Technical report, Deltares, 2017.

[36] R. Stenvert. *Biografie van de Baksteen 1850-2000*. WBooks, Zwolle, 2012.

[37] J.R. Sterrenburg. Hoge wandliggers in kalkzandsteen. Master's thesis, Eindhoven University of Technology, 2007.

[38] M. Stewart. *Surface Production Operations*. Gulf Professional Publishing, 2016.

[39] C.F.F. Thijssen. *Bouwconstructieve analyse van naoorlogse meergezinshuizen in de non-profit huursector*. Delft University Press, 1990.

[40] B.F. Tjeerdsma, M. Boonstra, A. Pizzi, P. Tekely, and H. Militz. Characterisation of thermally modified wood: molecular reasons for wood performance improvement. *Holz als Roh-und Werkstoff*, 56:149–153, 1998.

[41] Trouw. Tienduizenden op de vlucht voor water. `https://www.trouw.nl/nieuws/tienduizenden-op-de-vlucht-voor-water~ba4c65cf/`. Accessed: 30 oktober, 2020.

[42] USACE. Flood proofing tests: tests of materials and systems for flood proofing structures. Technical report, United States Army Corps of Engineers National Flood Proofing Committee, 1988.

[43] L. Westrik. Building strength and flood fatalities. Technical report, Delft University of Technology, 2020.

Acknowledgements

As with all projects and experiments, the final product would not be as it is without the help of others. I therefore would like to thank Ton and Maria Belen for reintroducing me to the concrete lab and the effort of trying to transport the materials towards the basin. Many thanks also to the masons Oscar and Wil for not only creating the wall I envisioned but for sharing their ('Haagse') life lessons and wonderful diverse playlist too. I would also like to thank Ruben for his help precisely creating and mounting the window frame and Giorgos for preparing the sensors and teaching me basic electrical engineering.

Here I would also like to show my appreciation for the supervision, support, and ideas of my committee members. Guus, a big thanks for introducing me to the project and your involvement in my thesis, even when it took a turn outside your expertise. I am very grateful for your help, shaping and structuring the report. Jan, I am most thankful for your insightful suggestions and your everlasting fascination that kept me eager to investigate the wall in greater detail. Bas, I appreciate your involvement mid-project; finally, fulfilling all the requirements for my committee. Your questions helped me realise the importance of viewing the results from different perspectives and keep a focus on the real-life impact of a flood. Jeremy, many thanks for chairing the committee and all your effort to attend the meetings that were way out of your timezone. Your enthusiasm and feedback shaped this report for the better.

A special thanks is reserved for my daily supervisor Paul, with whom I share the same birthday. I have said it before: it is quite exceptional to see your supervisor with a sledgehammer; demolishing a wall, handling a wheelbarrow with gunk, and stacking bricks, sandbags and mortar. Paul, thanks a lot for helping me out during the experiments and computations, challenging me from start to finish, and doing so with a laugh and a burger.

And in these special times a final thanks to my committee for all your patients when internet connections failed, when slideshows did not work, and when poor microphones prevented the communication.

In the spirit of promises made and promises kept I would also like to thank Paulina and Iris for reading and reviewing my work. Finally, I want to thank friends and family for the much appreciated (coffee) breaks and interest in the project.

M. van Haren
Delft, November 2021

A

Appendix: Mortality functions

In 2017 Rijkswaterstaat ordered to improve the standard model for the determination of damages and fatalities due to floods. The proposed changes on the thresholds and inclusion of the transition zone were added [35]. Although it was concluded that the criteria for the breach zone are hard to meet, it is assumed, nevertheless, no survivors remain near the breach (100-200m), therefore the mortality in the different zones is described by:

$$F_{D,B} = 1 \tag{A.1}$$

$$\text{if } (h \cdot v \geq 7m^2/s) \text{ and } (v \geq 2m/s) \tag{A.2}$$

After the breach zone, the water enters an area where it can rise quickly; mortality is then defined as:

$$F_{D,S}(h) = \Phi_N(\frac{ln(h) - \mu_N}{\sigma_N}), \text{ with } \mu_N = 1.46 \text{ and } \sigma_N = 0.28 \tag{A.3}$$

$$\text{if } (h \geq 2.1 \text{ and } w \geq 4) \text{ and } (h \cdot v < 7m^2/s \text{ and } v < 2m/s) \tag{A.4}$$

Before the water enters the area with minor rise rates, first a transition zone is defined, where mortality is calculated using:

$$F_D = F_{D,O} + (w - 0.5)\frac{F_{D,S} - F_{D,O}}{3.5} \tag{A.5}$$

$$\text{if } (h \geq 2.1 \text{ and } 0.5u \geq w \geq 4) \text{ and } (h \cdot v < 7m^2/s \text{ and } v < 2m/s) \tag{A.6}$$

Finally, when the water has reached a vast area where rise rates are regarded low, the mortality is calculated via:

$$F_{D,O}(h) = \Phi_N(\frac{ln(h) - \mu_N}{\sigma_N}), \text{ with } \mu_N = 7.60 \text{ and } \sigma_N = 2.75 \tag{A.7}$$

$$\text{if } (w < 0.5) \text{ or } (h < 2.1 \text{ and } w \geq 0.5) \text{ and } (h \cdot v < 7m^2/s \text{ and } v < 2m/s) \tag{A.8}$$

Note that a lognormal distribution is used in some of the definitions and that apart from the depth, h, and flow velocity, v, also the rise rate in the first 1.5 meters, w, is considered one of the characteristics still.

B

Appendix: Specification on materials

	Component	Name	Dimensions	Manufacturer
Wall	fired-clay brick	EUROA WF VORMBAK	Waal	Wienerberger
Wall	Calcium-Silicate brick	Kalkzandsteen CS16	Amstel	Calduran
Wall	Mortar	Remix BM2 versie 2	-	Remix
Wall	Wall ties	Spouwanker universeel L.	200x30x3,6	Gebr. Bodegraven BV
Wall	L-shaped bracket	Stalen latei verzinkt	90x90x3x980	NEHOBO
Wall	Ceramic window sill	Raamdorpel verglaasd bruin	160x105x20	Hornbach
Window	Window frame	Meranti kozijnhout A profiel	66x110x1950	Konsta
Window	Window frame	Meranti kozijnhout A profiel	66x110x2750	Konsta
Window	Window frame	Meranti kozijnhout C profiel	66x110x1050	Konsta
Window	Plexiglass	Polycarbonaat 8mm	700x1500	Plexideal.nl
Window	Secondary framework	Vuren balk geschaafd	44x69	Konsta
Window	Silicone sealant	SikaHyflex 250 Facade	-	Sika
Other	Screws	HECO-FIX-plus	3,5x40	HECO
Other	Silicone sealant	Tixophalte seal and fix	-	Shell
Other	Catchment box plates	Constructieplaat OSB-III 4-zijdig	2440x59x18	Hornbach
Other	Two-component epoxy	Sikadur	3:1	Sika
Other	Weep closers	Spuitmondjes	-	Handson
Other	box reinforcement	Verbindingsplaat	100x 15	-
Window	box framework	Vuren balk geschaafd	44x69	Konsta
Sensors	PVC Tubes	Elektrabuis grijs	3/4"	Pipelife
Sensors	PVC Tubes	Elektrabuis creme	5/8"	Pipelife
Sensors	PVC glue	Bison hard PVC Lijm	-	Bison

C

Appendix: Designs

As a reminder, the dimensions and most important assumptions made for the design of the wall and the window frame are listed below as bullet points. The blueprint for the wall can be seen in Figure C.1 and the window is shown in Figure C.2. Furthermore, the blueprint for the catchment box is provided in Figure C.3.

C.1. Cavity wall

1. The height of the fired-clay brick including a joint was assumed to be 60 millimeters (50+10).
2. The height of the CaSi brick including a joint was assumed to be 80 millimeters (72+8).
3. The total height of the designed cavity wall was 2630 millimeters. This was reached by 44 courses of clay bricks and 3 courses of CaSi bricks.
4. Both the fired-clay brick and CaSi brick have a width of 10 millimeters.
5. The width of the cavity was designed to be 70 millimeters. This was done to allow for some tolerances at the edges of the steel rig.
6. In each successive course the bricks were staggered by half a stretcher, creating a stretcher bond.
7. The length of a brick used in the wall may not exceed the minimum of 10 millimeters i.e. the header dimension. The Casi bricks near the window should be cut shorter to allow a header at the edge.

C.2. Window

1. The ordinary profiles have sections of 67x114 mm.
2. The glass should be replaced by polycarbonate plexiglass for safety reasons.
3. The window should be mounted in the gap using a secondary framework made of pinewood.
4. There may not be any screws in the bottom profile to guarantee water tightness.
5. The profiles are treated with a primary layer of paint. The duration of the experiment does not require the profiles to be treated with another layer of paint to prevent decay.

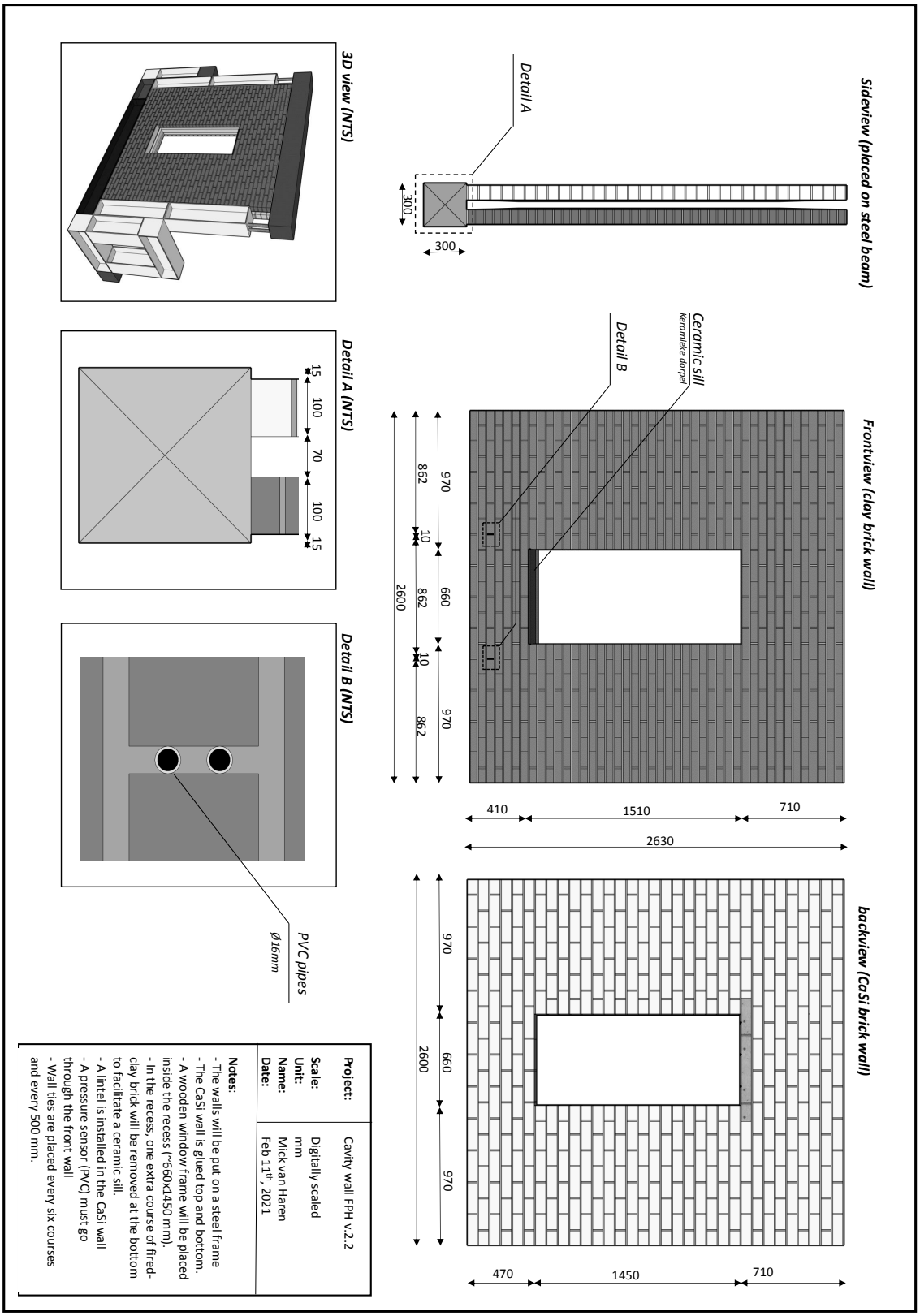

Figure C.1: Blueprint illustration of the cavity wall built at the Flood Proof Holland Basin with details A and B. The dimensions are noted in millimeters and the figures are scaled digitally.

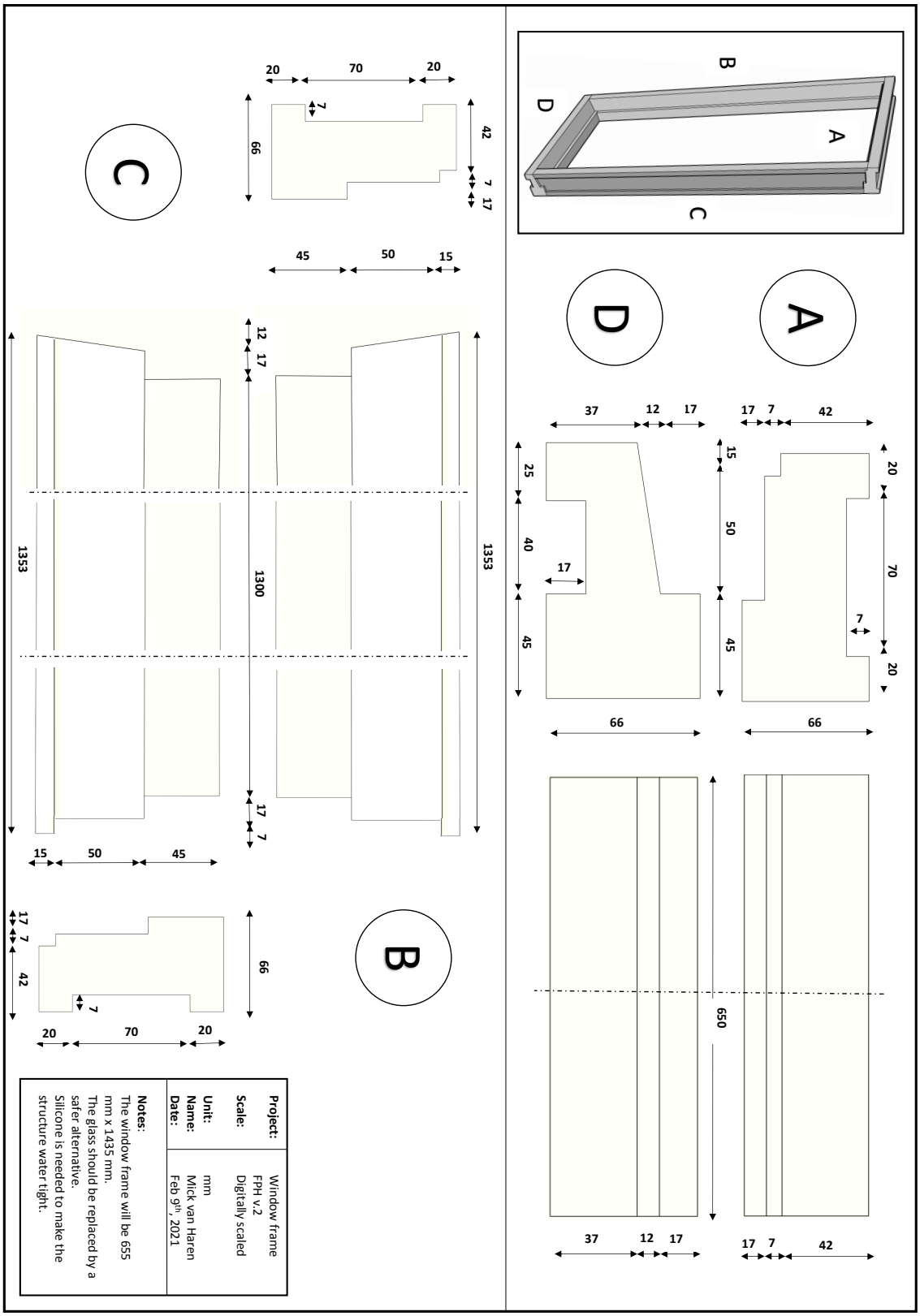

Figure C.2: Blueprint illustration of the window frame placed in the cavity wall at the Flood Proof Holland Basin. The dimensions are noted in millimeters and the figures are scaled digitally.

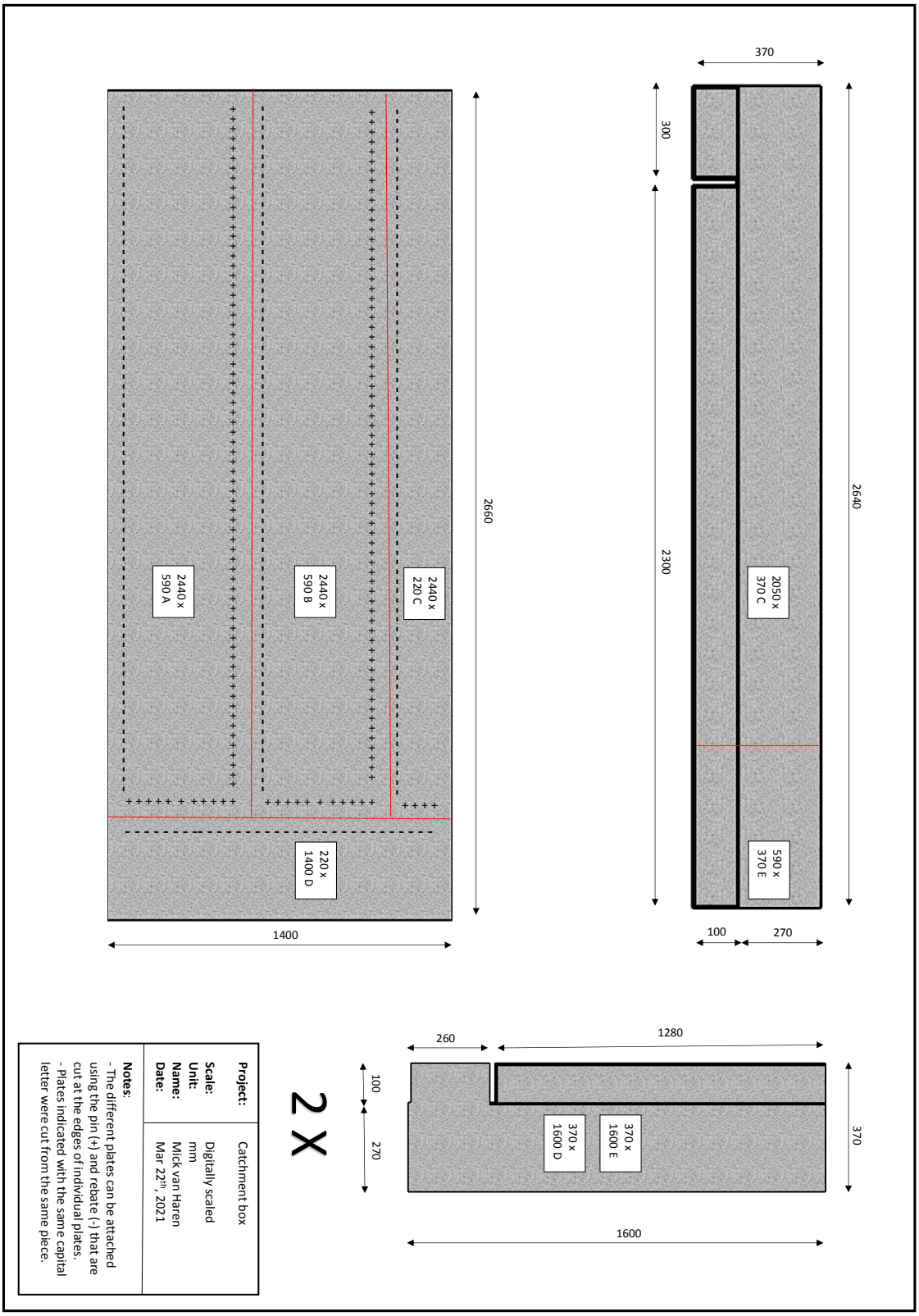

Figure C.3: Blueprint illustration of the catchment box needed for the experiments to control the water level at the backside of the wall at the Flood Proof Holland basin. The dimensions are noted in millimeters and scaled digitally.

C.3. Construction report of the cavity wall

Construction of the wall began in the early morning of March 18^{th}, 2021. Two weeks earlier the first course of CaSi bricks was glued to the bottom part of the steel rig, see left Figure C.4. The two-component epoxy glue was used to prevent the wall from sliding of the rig and to create sufficient bonding between the wall and the steel beam. The first course was laid down on the edge of the bottom beam; diverging from the 15 millimeters required by the current design. During preparations the right pillar was found to be tilting slightly out-of-plane. In fact, the pillar was inclined with 1.36 degrees, which resulted in 5.7 centimeters offset at the top. This meant the pillars would not cover the clay wall completely. The design was therefore altered. By moving the cavity wall slightly backwards and by lowering the cavity thickness, the top of the rig was able to support the wall properly.

The masons started by stringing a horizontal wire between both steel pillars. They also measured the width of the window and set up vertical wires as well. The mortar was mixed with water on-site indicating a possible deviation from the prescribed mixture recipe. This modification on the recipe could either be deliberate to account for weather conditions or accidental. To establish this deviation, if any, nine couplets were constructed and left to harden next to the wall.

Next, the masons started the first part of the CaSi brickwork. The bricks were placed 5 millimeters from both pillars to make sure the wall was not constrained by the lateral columns. The masons cut the bricks with their trowel (Dutch: troffel) and placed the bricks on top of the mortar. After eight courses they removed the surplus mortar dripping out of the joints and prepared the next round of brickwork.

The masons were only given minor instructions on where to place the wall ties in order for them to place the ties like they normally would, see Figure C.5. After 24 courses, the concrete lintel was placed and by noon the CaSi wall was finished. By then it was observed that the wall was constructed with reference to the pillars instead of leveled by a ruler. The CaSi wall therefore was built with a small inclination identical to the tilted pillar.

Because of the weather conditions the steel top beam was lowered onto the CaSi wall and glued with the same two-component epoxy glue to make sure the wall would not fall over and was restrained top and bottom, see Figure C.4 centre.

Figure C.4: Left: the first course of calcium silicate bricks. Centre: two-component epoxy glue at the top of the wall. Right: Existing gap between the steel beam and the clay wall.

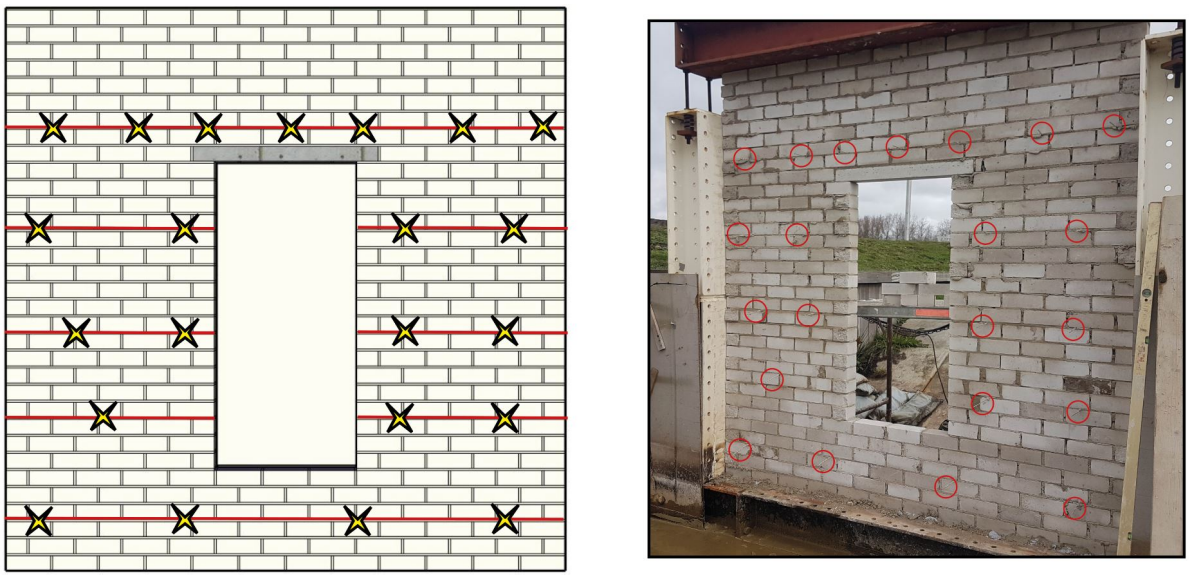

Figure C.5: Copy of Figure 3.3: Illustration of the placement of the wall ties.

The next day the clay wall was constructed. It was less cloudy than the previous day and the sun shone brighter (see Figure E.2 in Appendix E), which could have affected the mortar mixture. Again, nine couplets were constructed and left in the basin so they would resemble the properties as much as possible.

It was important to make sure the clay courses reached the same height as the CaSi courses to guarantee a tight fit for the window frame. The first joints were therefore made thicker. In these joints the PVC pipes were placed. Again the surplus mortar was removed after ten-or-so courses, after which the next round was prepared. The second wall was constructed using a ruler, which resulted in a smaller cavity thickness at the bottom and a greater thickness at the top. As a result the clay wall could not be attached to the 'tilted' steel beam at the top, see right Figure C.4. (This problem was later dealt with by installing an unevenly-cut wooden beam to fill the gap. Wooden slats were then placed against the wooden beam to form a C-shaped top piece that surrounds the top course of the bricks. The final piece was attached to the steel top beam; locking the wall into place.)

Because of the smaller cavity thickness at the bottom, the wall ties would exceed the maximum penetration depth here. The ties were bend in horizontal direction as a solution for this problem.
A steel bracket was placed at the same height as the lintel to assure a solid connection with the window frame.

Afterwards the interface between the wall and the steel rig was filled with a silicone substance to make sure water cannot enter the cavity or the other side of the wall via this artificial pathway. The silicone was placed at both sides of the cavity wall up until a height of 130 centimeters.

C.4. Construction report of the window frame

After construction of the wall the window gap was re-measured and the profiles were cut. Screws were used to attach the lateral profiles to the top and bottom. Since the cavity was smaller at the bottom than at the top, the distance between the two walls at the lower part of the window was also smaller than the at the top of the window gap. This would be a problem for the secondary framework that was designed to fit inside the cavity. Another problem arose when it turned out the split

of the cut bricks was placed inwards. This technique resulted in smooth edges at the visible sides of the wall, but inside the cavity the surface was irregular.

To make sure the secondary framework would fit, the inner surface of both walls was polished with a grinder first. The surface at the top was polished to a lesser extent to make up for the difference in cavity thickness. Between the lintel and the steel bracket, the secondary framework was wedged and at the bottom no framework was present, since there the sills would be placed.

The window frame was then planed to make up for some slightly displaced bricks. The window frame was placed from inside to outside i.e. pushed through the CaSi wall. The frame was placed 75 millimeters inwards of the brick wall, which is customary for this kind of windows. A total of eight screws were placed in pre-tapped holes in the lateral profiles and top profile only (three at each side and two at the top). No screws should penetrate the bottom profile because this would break the exterior moisture barrier. With tightening of the screws the secondary framework was pulled into the rebate (Dutch: sponning) of the profiles; locking the window frame in the cavity, see Figure C.6. The polycarbonate plexiglass was placed in the frame with silicone. Another layer of silicone was applied to place the grills. The grills were nailed onto the profiles and the final edges were once more treated with silicone.

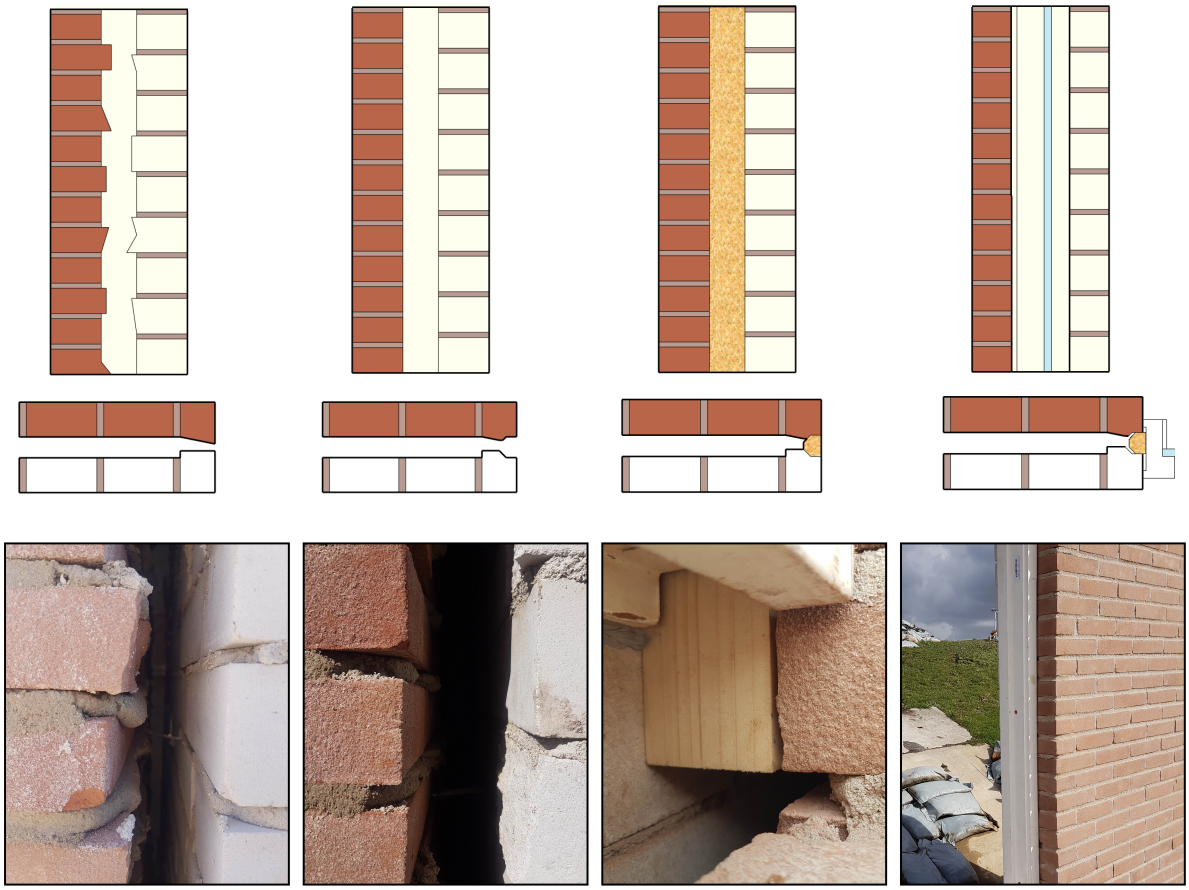

Figure C.6: Copy of Figure 3.4: Illustration of the method of placement for the secondary framework. Top: Side view of the wall. Bottom: Top view of the wall. The grinder could only reach a couple of centimeters inside the cavity. The corners of the wooden framework were sanded to mitigate the problem. The framework was pulled into the rebate by tightening of the screws.

Because the maximum water level that can be realised in the basin will not reach the top of the window frame, the watertight sheet (Dutch: loden slab) was not accounted for. This sheet is a customary material to drain the water at the top; preventing the water to accumulate on top of the window frame.

A few weeks later the ceramic sills were placed. First mortar was mixed and placed on the free course of bricks. Next, the sills were installed individually. The sills were locked in the rebate of the bottom profile, pulled forward, and then tapped downwards. The joints between the sills were filled with the same mortar (Figure C.7).

Commonly, window frames are already present at site once construction of a wall starts. In that way the mason can place the bricks right against the frame and a tight interface exists. While the order of construction for this experiment is thus atypical, it was tried to recreate the tight interface by filling the gaps in the interface with mortar.

Figure C.7: Placement of the ceramic sills. Underneath the window profile a rebate is present in which the flange of the sill can be locked. Left picture: the situation before placement of the sills. Right picture: sill placement. Note also the small rebate in the sill itself, which is present to allow rainwater to drop in front of the wall instead of seeping over the wall.

D

Appendix: Specification on sensors

Below additional specifications can be found on the potentiometers and the pressure sensors as well as the Measurement and Control Unit.

D.1. Potentiometers

The potentiometers will measure any deflection by inward-or outward movement of the pin. The measurments are thus limited by the length of this pin; deflections greater than this 'stroke length' cannot be measured. The potentiometers used, have a maximum stroke of 38 millimeters. A similar version of the potentiometers used, Model No. 13FLP50A, can be seen in Figure D.1. General specifications of these potentiometers can be found in Figure D.2.

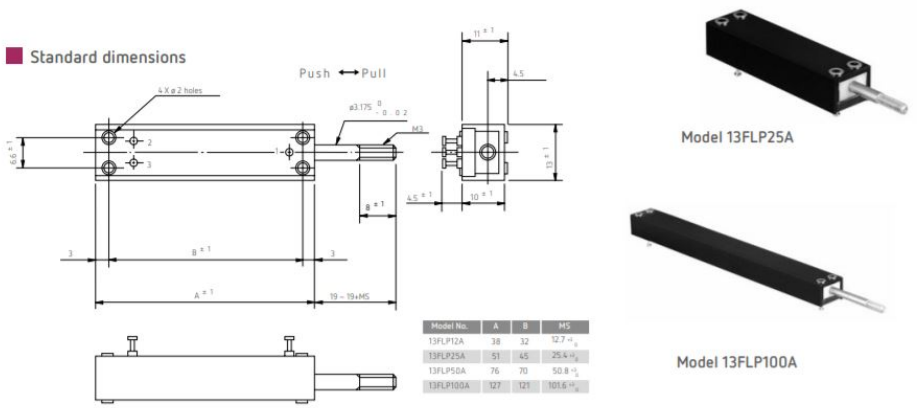

Figure D.1: Standard dimensions of comparable potentiometers. While the sensors are not identical to the ones used at FPH, it still gives useful insights.

D.2. Pressure Sensors

The pressure sensors were placed in front of the wall, behind the wall (inside the catchment box, and inside the cavity. For the latter a tube was placed inside the fired-clay brick wall to connect the third pressure sensor to the cavity. During installation, the tube system was filled with water before the final placement of the sensor. This was done to remove the air inside the tube that otherwise would have been trapped between the water and the sensor itself.
Specifications on the relative pressure senors (model No. 24PC-XXH6D) can be found in Figure D.3 and Figure D.4.

General Specifications

Model No.		13FLP12A	13FLP25A	13FLP50A	13FLP100A
Standard Resistance Values		500,1k,2k,5k,10k (Ω)	500,1k,2k,5k,10k (Ω)	1k,2k,5k,10k,20k (Ω)	1k,2k,5k,10k,20k (Ω)
Total Resistance Tolerance		±20% (K)			
Independent Linearity Tolerance	Standard Class	±2.0%	±1.5%	±1.0%	±0.7%
	Precision Class	±1.0%	±0.7%	±0.5%	±0.3%
Resolution		Essentially Infinite			
Output Smoothness		Within 0.1% against input voltage			
Contact Resistance Variation		Within 2% C.R.V.			
Power Rating		0.2W	0.4W	0.7W	1.2W
Electrical Stroke		12.7±0.5mm	25.4±0.5mm	50.8±0.5mm	101.6±0.5mm
Mechanical Stroke (MS)		12.7 $^{+3}_{0}$ mm	25.4 $^{+3}_{0}$ mm	50.8 $^{+3}_{0}$ mm	101.6 $^{+3}_{0}$ mm
Insulation Resistance		Over 1,000M Ω at 500V.D.C.			
Dielectric Strength		1 minute at 500 V.A.C.			
Friction		Within 0.5N (50gf)			Within 1.0N (100gf)
Stopper Strength		Approx. 20N (2kgf)			
Resistance Temperature Coefficient		±400p.p.m./°C			
Mass		Approx. 10g	Approx. 15g	Approx. 25g	Approx. 35g

Figure D.2: Specifications on comparable potentiometers. The stroke length is most comparable to model No. 13FLP50A. (obtained from: https://www.althensensors.com/sensors/linear-position-sensors/linear-potentiometers/4882/13flp-series-linear-potentiometer/)

Characteristic	Min.	Typ.	Max.	Unit	Note
Supply voltage	2.5	10	12	Vdc	–
Input resistance	4	5	6	kOhm	–
Output resistance	4	5	6	kOhm	–
Time response	–	–	1	ms	2

Characteristic	Parameter
Operating temperature range: without EPDM seals with EPDM seals	 -40 °C to 85 °C [-40 °F to 185 °F] -20 °C to 85 °C [-4 °F to 185 °F]
Storage temperature range	-55 °C to100 °C [-67 °F to 212 °F]
Soldering terminal temperature/time	315 °C [599 °F] max./10 s max.
Vibration	10 G at 20 Hz to 2000 Hz
Shock	100 G for 11 ms
Life	1 million cycles min.

Figure D.3: Specifications on the pressure sensors.
Note: the absolute ratings are the extreme limits the device will withstand without damage.
Note 2: Time required for the output to increase from 10% to 90% of span in response to a step change in input pressure from the specified min. to max. operating pressure.

Characteristic	Operating Pressure Range														Unit	Note
	0 psi to 0.5 psi		0 psi to 1 psi		0 psi to 5 psi		0 psi to 15 psi		0 psi to 30 psi		0 psi to 100 psi		0 psi to 250 psi			
	Typ.	Max.	Typ.	Max.	Typ.	Max.	Typ.	Max.	Typ.	Max.	Typ.	Max.	Typ.	Max.		
Span	–	35 ±10	–	45 ±15	–	115 ±30	–	225 ±60	–	330 ±90	–	225 ±69	–	212 ±68	mV	1
Null offset	–	0 ±30	–	0 ±30	–	0 ±30	–	0 ±30	–	0 ±30	–	0 ±30	–	0 ±30	mV	2
Linearity (Best Fit Straight Line, P2>P1)	±0.2	±1.0	±0.2	±1.0	±0.2	±1.0	±0.2	±1.0	±0.2	±1.0	±0.2	±1.0	±0.2	±1.0	%span	3
Null shift (0 °C to 25 °C, 25 °C to 50 °C)	±1.0	–	±1.0	–	±1.0	–	±1.0	–	±1.0	–	±1.0	–	±1.0	–	mV	4
Span shift (0 °C to 25 °C, 25 °C to 50 °C)	±5.0	–	±5.0	–	±5.0	–	±5.0	–	±5.0	–	±5.0	–	±5.0	–	%span	5
Repeatability and hysteresis	±0.5	–	±0.5	–	±0.5	–	±0.5	–	±0.5	–	±0.5	–	±0.5	–	mV	6
Overpressure	–	20	–	20	–	20	–	45	–	60	–	200	–	250	psi	7

[1]Span is the algebraic difference between the output signal measured at the upper and lower limits of the operating pressure range, where Port 2 (P2)>Port 1 (P1).

[2]The output signal obtained when zero pressure is applied to all available ports.

[3]The maximum deviation of product output from a straight line fitted to the output measured over the specified operating pressure range, calculated according to BFSL. The straight line is fitted along a set of points that minimizes the sum of the square of the deviations of each of the points ("least-squares" method).

[4]The maximum deviation in offset due to changes in temperature over the compensated temperature range, relative to offset measured at a reference temperature of 25 °C.

[5]The maximum deviation in span due to changes in temperature over the compensated temperature range, relative to full-scale span measured at a reference temperature of 25 °C.

[6]Repeatability is the maximum difference between the output readings when the same pressure is applied consecutively, under the same operating conditions, with pressure approaching from the same direction within the specified operating pressure range. Hysteresis is the maximum difference between output readings when the same pressure is applied consecutively, under the same operating conditions, with pressure approaching from opposite directions within the specified operating pressure range.

[7]Overpressure is the maximum pressure that may safely be applied to the product for it to remain in specification once pressure is returned to the operating pressure range. Exposure to higher pressures may cause permanent damage to the product. Unless otherwise specified, this applies to all available pressure ports at any temperature within the operating temperature range.

Figure 1. Circuit Diagram

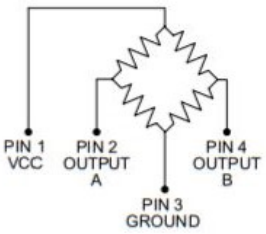

Output "A" increases as P2 pressure increases.

Output "B" deceases as P2 pressure increases.

Symbol	Description
Vcc	supply
OUTPUT A	bridge positive output
GROUND	ground
OUTPUT B	bridge negative output

Figure D.4: Further specifications on the pressure sensors and their operating pressure range.
(obtained from://www.farnell.com/datasheets/2002508.pdf)

D.3. Measurement and Control Unit

The Control Unit converts the direct voltage input with ratio-metric analog to digital conversion. The input is sampled at a rate of 1Hz with 24-bit precision. Because both types of sensors require a different set of cables, the wiring is complex. Additionally to make the most out of the configuration, multiple wires are shared by the potentiometers. To give an overview on the cable management, the individual cables and their corresponding sensors are shown in Figure D.5, D.6, and D.7.

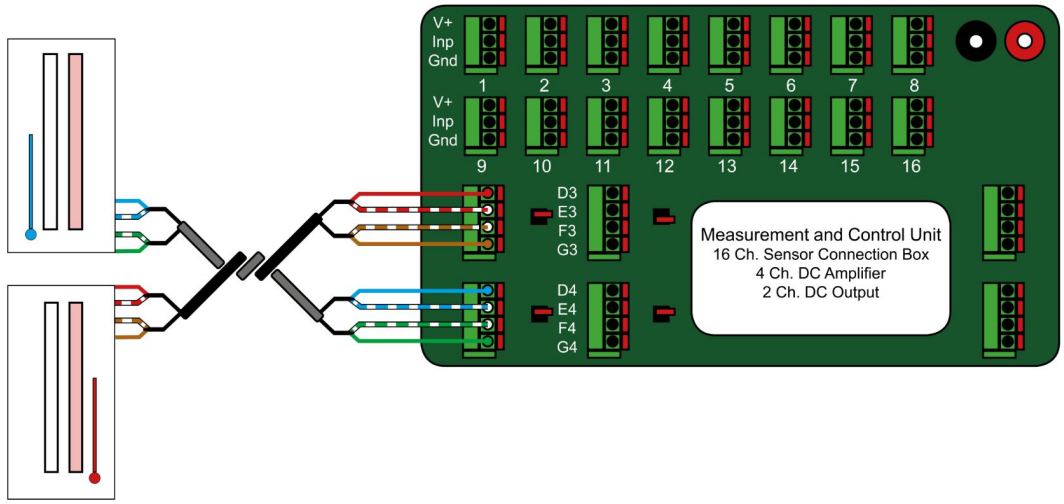

Figure D.5: Detail on wiring of the sensors. Cable 1 features the wires for pressure sensor 1 (front of the wall) and pressure sensor 2 (inside the catchment box).

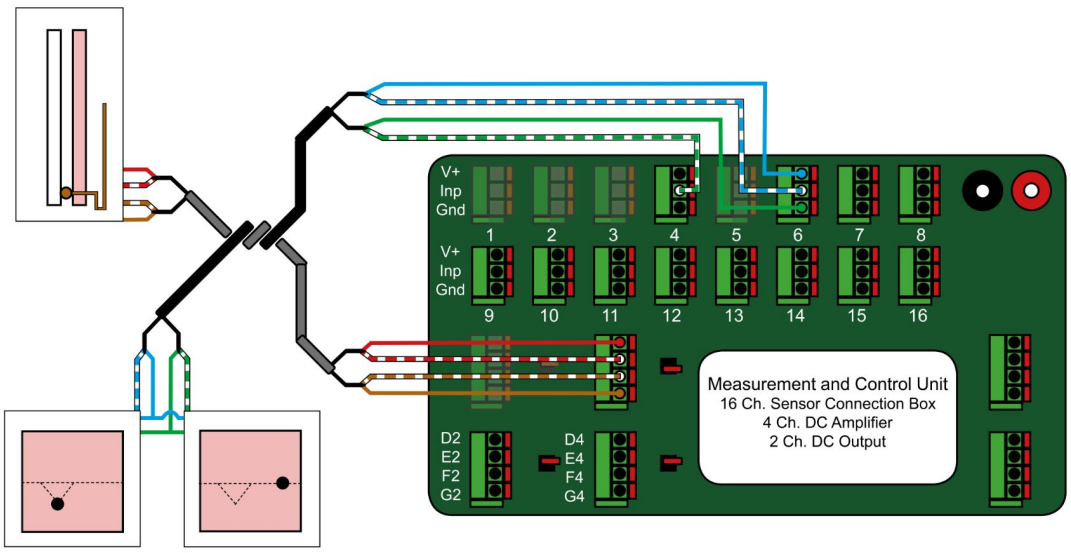

Figure D.6: Detail on wiring of the sensors. Cable 2 features the wires for pressure sensor 3 (inside the cavity) and potentiometers 5 and 6 (both at the clay wall).

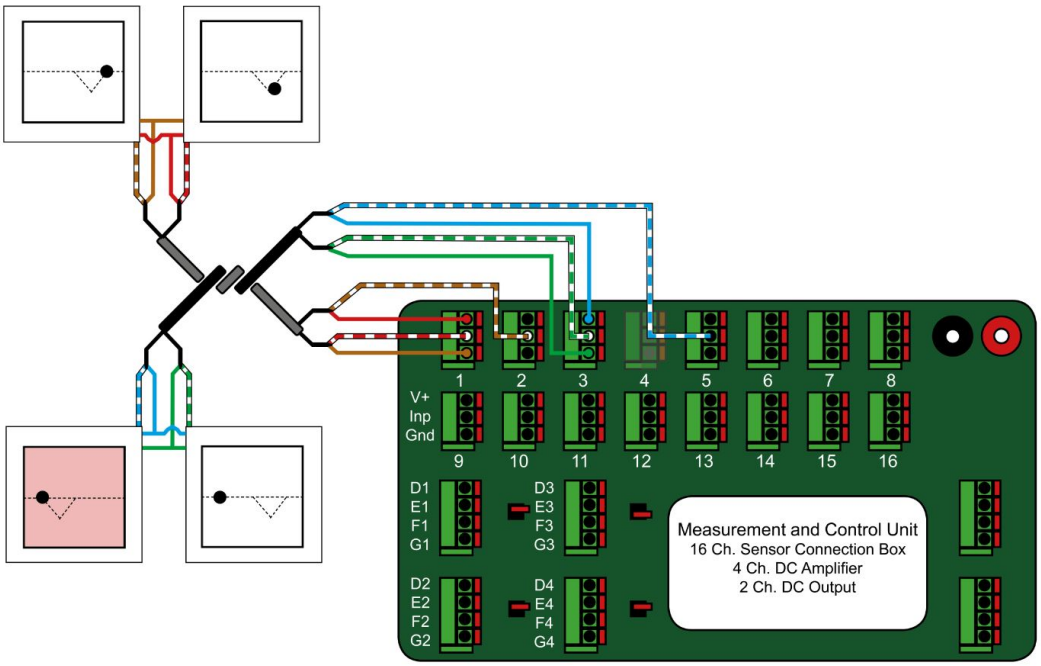

Figure D.7: Detail on wiring of the sensors. Cable 3 features the wires for potentiometers 1,2, and 3 (all at the CaSi wall) and potentiometer 4 (at the clay wall).

D.4. Sensitivity of potentiometers

The potentiometers are sensitive to small deflections and can measure any movement in the order of micrometers. Since displacements of the wall are in the order of millimeters the sensors can describe the displacements in sufficient detail. Errors that are in the same order of magnitude blur the actual displacement of the wall. It is important to know the magnitude of such occurring errors and to understand the behaviour of the sensors. For that matter the recordings were kept running in-between test days. Note that in-between those test days the basin was drained and that any displacement occurred in the absence of hydraulic pressure.

The behaviour of the sensors shows a sinusoidal trend with periods with magnitudes of around 80.000 seconds, which is close to the length of one day. Phenomena like wind gusts are therefore ruled out because these will not act on such duration scales. It is therefore chosen to compare the data with the hourly temperature and sunshine duration. These meteorological phenomena tend to have the same sinusoidal trend. On top of that, temperature variations are well-known biases. The results can be found in Figure D.8. As expected the temperature has an effect on the sensors as they show a positive correlation. The sunshine duration shows a negative correlation, which is maybe due to the fact that the wall itself is also sensitive to temperature variations; the sensors therefore record the behaviour of the wall instead of their own behaviour. Interference of temperature variations can thus lead to maximum errors of around 2 millimeters, albeit in large periods.

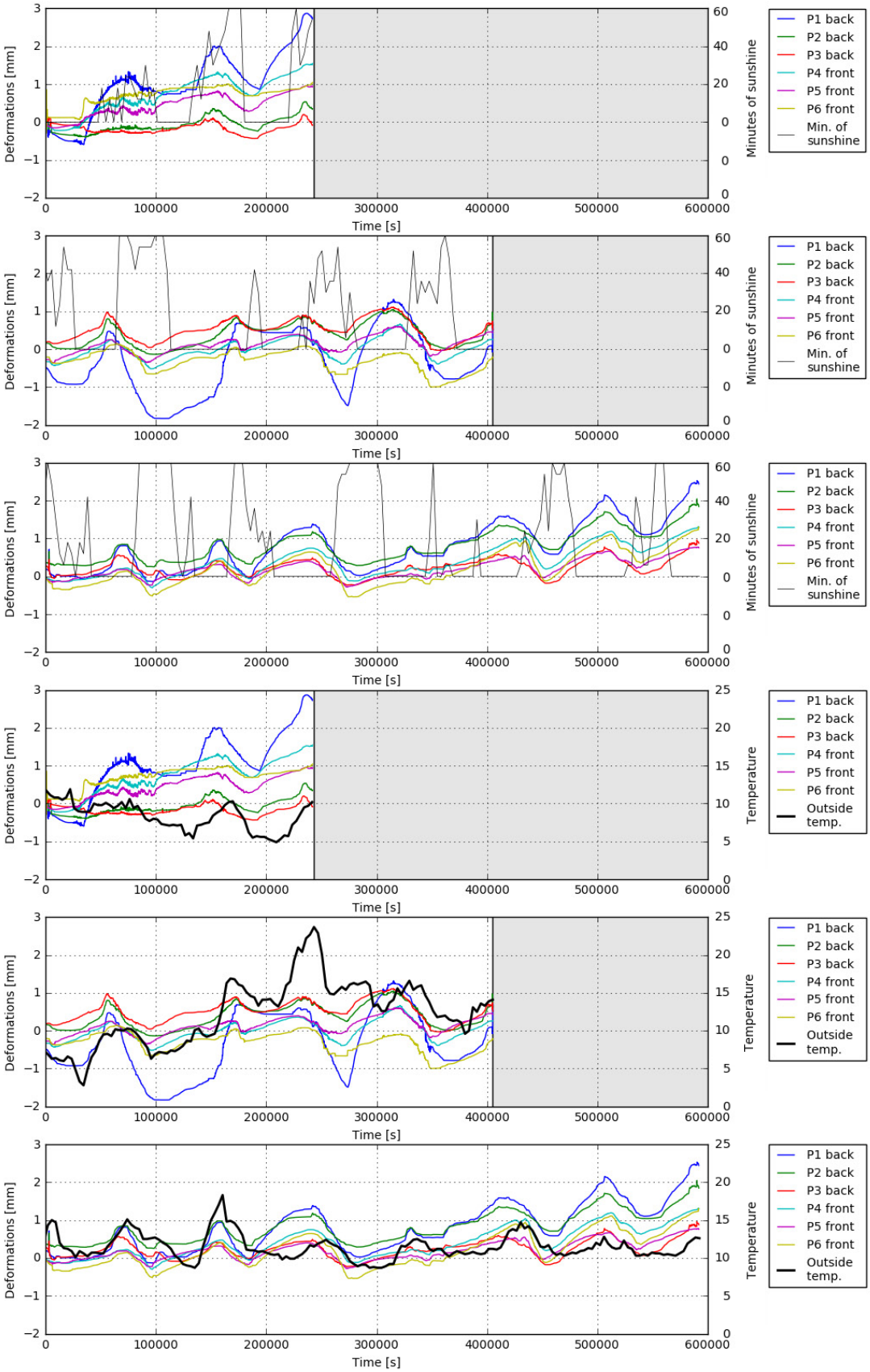

Figure D.8: Graphical representation of the deformations measured throughout the days where no experiments took place. The deformations (left axis) are plotted next to the sun duration and temperatures (right axis). Note that the deformations where measured every 30 seconds and the sun duration and temperature only once per hour. The meteorological data therefore coincides with the first measurement of that specific hour. Top and fourth: from May 3^{rd}, 2021 to May 6^{th}, 2021; Second and fifth: from May 6^{th}, 2021 to May 11^{th}, 2021; Third and bottom: from May 11^{th}, 2021 to May 18^{th}, 2021.

E

Appendix: Meteorological data

The Flood Proof Holland basins are situated in an open area; meaning the set-ups there are subjected to the climate conditions. To gain insight in the conditions during the first stages of the wall-hardening, relevant data from two nearby weather stations is extracted from the public database. The two stations are located at Hoek van Holland and Rotterdam; with FPH situated in-between these stations. Although the basin itself will have its own micro climate, it is expected that this will not deviate significantly from the climate itself. Since the obtained data does not show great differences between the two stations, the general climate conditions at FPH are assumed to be similar to Hoek van Holland and Rotterdam.

E.1. KNMI data

From the weather stations precipitation-,temperature, and windspeed data is extracted. This then will show the conditions at various stages of the wall i.e. during construction and testing of the wall. For convenience, the abbreviations used in the database are listed below.

1. Precipitation
   RH: Daily precipitation amount
   RHX: Maximum hourly precipitation amount

2. Temperature
   TG: Daily mean temperature
   TN: Minimum temperature
   TX: Maximum temperature

3. Windspeed
   FG: Daily mean windspeed
   FXX: Maximum wind gust

In Figure E.1 the start of construction is shown by the first red dashed line. The second red line marks the 28^{th} day of hardening. The start and end of the first measuring campaign are shown by green solid lines; during this period the movement of the wall has been constantly measured, with intermediate tests as the only interruption. Afterwards two more tests were performed which are visible by the additional green lines.

During the hardening stage precipitation at the start was limited. At the second half of the 28 days it started raining more often, which could have affected the mortar. Nevertheless, the mortar already had a significant period of hardening without precipitation affecting its mixture.

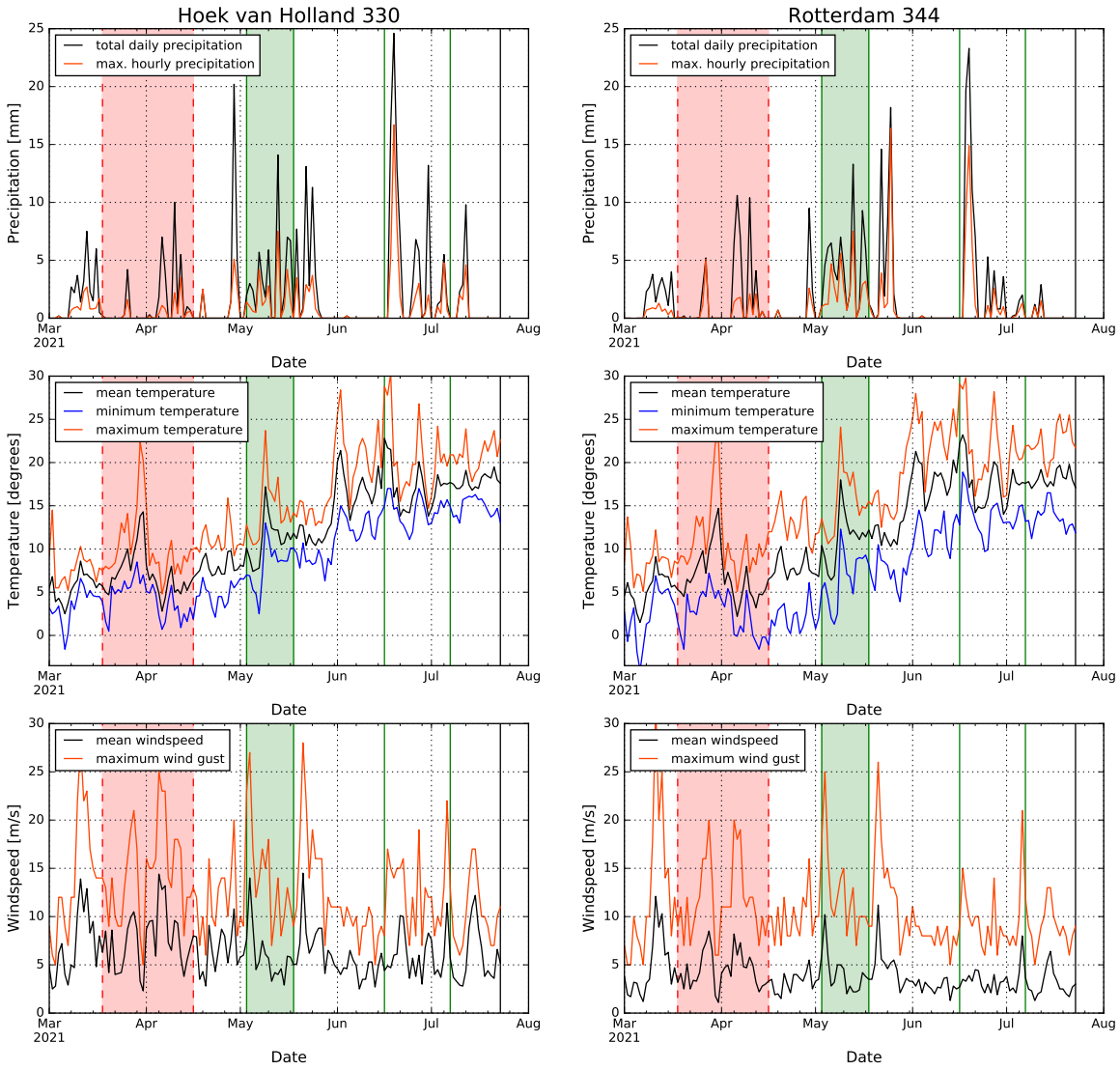

Figure E.1: Meteorological data of two nearby stations at Hoek van Holland (station 330) and Rotterdam (station 344). This data is obtained from the public data base of the Royal Netherlands Meteorological Institute (KNMI). The red dashed lines mark the start of construction and the end of the 28th day of hardening. The green solid lines mark the start and end of the first measurement campaign and the additional measuring afterwards.

From the temperature data it is deducted the wall was hardening during a more-or-less constant period of time. Afterwards the temperature gradually increased due to seasonal effects. The average temperature during the hardening stage was 6.9 degrees; 10.6 degrees during the day and 3.4 degrees during the night. At the end of march one outlier is recorded.

The wind speed can act just like the water as a pressure when faced against the wall. Especially near the coast wind speeds can reach great numbers. From the recordings these great numbers are not visible with only a few peaks reaching above 25 m/s (90 km/h). The gusts could have affected the recorded deformations when pointed in the right direction. However, the duration scales of the sinusoidal trends in Figure D.8 do not match the duration scales of the wind gusts. There is no way of identifying the 'accidental' extra forcing of the wind. Note though that the wall was situated in the corner of a 1.5 meter deep basin. During testing the wind only could have reached the top half of the wall.

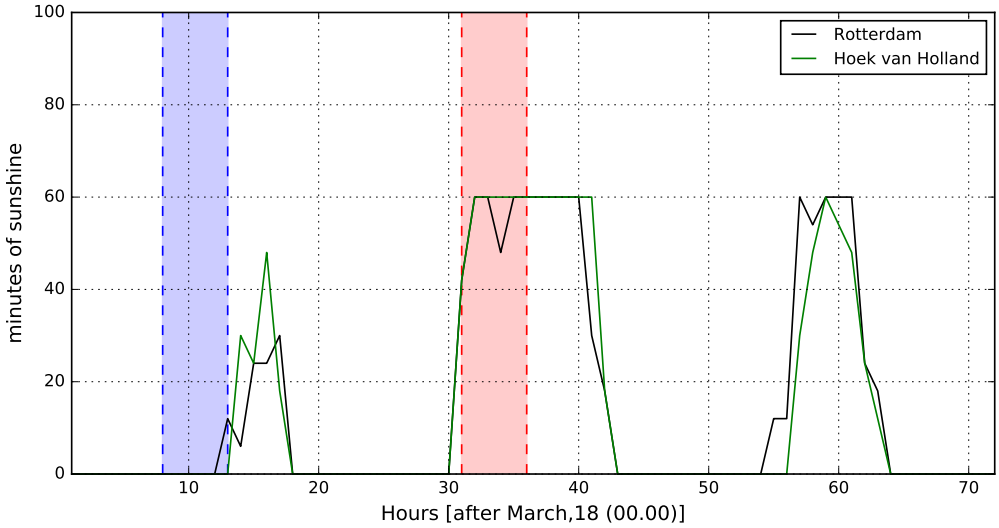

Figure E.2: Sunshine during the first 72 hours of hardening. This data is obtained from the public data base of the Royal Netherlands Meteorological Institute (KNMI). It shows the sunshine data of two nearby stations at Hoek van Holland (station 330) and Rotterdam (station (344). The blue area marks the actual construction of the CaSi wall. Likewise, the red area marks the actual construction of the clay wall.

Additionally, the sunshine during construction and the first 72 hours of hardening are regarded in a more detailed manner. Figure E.2 shows the number of minutes the sun shone during that specific hour. Logically, at night the number of sunshine minutes is zero. The maximum number of minutes the sun can shine during an hour is 60 minutes. According to Figure E.2 it was cloudy when the CaSi wall was constructed, while the sun shone bright during the clay wall construction. This can indicate a difference in the hardening rate of the mortar, because water could have been evaporated.

F

Appendix: Correlation matrices

F.1. Computation of correlation matrices

The main reason to convert the water levels to their equivalant bending moments is to obtain a better relationship that can explain the deformations in a more adequate way. For that matter the correlation matrices for every test is computed using a Nonparametric Bayesian Network (NPBN) in the Uninet program. Uninet uses the Spearman's rank correlation coefficient, ρ, to assess the relationship between two variables. If high values for bending moments corresponds with (or are close to) the same ranks as for the high values in deformations, the relationship is strong i.e. ρ = (-) 1. The values for the deformations are computed by averaging the recordings of sensors 2 and 3 for the CaSi wall and sensors 4 and 5 for the clay wall, since these sensors were situated on the same height and have not been relocated. According to the tables below: the deformations of the CaSi wall have the strongest relationship with the deformations of the clay wall. This is rather logical since the walls are attached to each other and influence each others behaviour. Obvious relationships aside, it can be deducted that for 70% of the tests the bending moment and deformations of the CaSi wall have a stronger relationship. For the clay wall this is even 90%.

Furthermore, it becomes evident that the water level differences and bending moments are strongly related, although this is more obvious for the clay wall variables.

Test 1	Waterlevel diff. CaSi	Bending M. CaSi	Deform. CaSi	Waterlevel diff. Clay	Bending M. Clay	Deform. Clay
Waterlevel diff. CaSi	*1*	0.923	-0.204	0.987	0.735	0.152
Bending M. CaSi	0.923	*1*	-0.285	0.911	0.805	0.291
Deform. CaSi	-0.204	-0.285	*1*	-0.202	-0.237	-0.431
Waterlevel diff. Clay	0.987	0.911	-0.202	*1*	0.932	0.134
Bending M. Clay	0.735	0.805	-0.237	0.932	*1*	**0.576**
Deform. Clay	0.152	0.291	**-0.431**	0.134	0.576	*1*

Test 2	Waterlevel diff. CaSi	Bending M. CaSi	Deform. CaSi	Waterlevel diff. Clay	Bending M. Clay	Deform. Clay
Waterlevel diff. CaSi	*1*	0.952	0.548	0.906	0.929	0.474
Bending M. CaSi	0.952	*1*	**0.533**	0.863	0.931	0.487
Deform. CaSi	0.548	0.533	*1*	0.499	0.516	0.234
Waterlevel diff. Clay	0.906	0.863	0.499	*1*	0.932	0.515
Bending M. Clay	0.929	0.931	0.516	0.932	*1*	**0.562**
Deform. Clay	0.474	0.487	0.234	0.515	0.562	*1*

Test 3	Waterlevel diff. CaSi	Bending M. CaSi	Deform. CaSi	Waterlevel diff. Clay	Bending M. Clay	Deform. Clay
Waterlevel diff. CaSi	*1*	0.841	0.417	0.736	0.751	0.649
Bending M. CaSi	0.841	*1*	0.608	0.623	0.656	0.689
Deform. CaSi	0.417	0.608	*1*	0.313	0.337	0.67
Waterlevel diff. Clay	0.736	0.623	0.313	*1*	0.982	0.722
Bending M. Clay	0.751	0.656	0.337	0.982	*1*	**0.752**
Deform. Clay	0.649	0.689	**0.67**	0.722	0.752	*1*

Test 4	Waterlevel diff. CaSi	Bending M. CaSi	Deform. CaSi	Waterlevel diff. Clay	Bending M. Clay	Deform. Clay
Waterlevel diff. CaSi	*1*	0.623	0.195	0.787	0.662	0.654
Bending M. CaSi	0.623	*1*	**0.726**	0.496	0.99	0.826
Deform. CaSi	0.195	0.726	*1*	0.156	0.698	0.541
Waterlevel diff. Clay	0.787	0.496	0.156	*1*	0.559	0.623
Bending M. Clay	0.662	0.99	0.698	0.559	*1*	**0.847**
Deform. Clay	0.654	0.826	0.541	0.623	0.847	*1*

Test 5	Waterlevel diff. CaSi	Bending M. CaSi	Deform. CaSi	Waterlevel diff. Clay	Bending M. Clay	Deform. Clay
Waterlevel diff. CaSi	*1*	0.548	-0.077	0.705	0.676	0.112
Bending M. CaSi	0.548	*1*	0.563	0.393	0.622	0.677
Deform. CaSi	-0.077	0.563	*1*	0.055	0.164	**0.923**
Waterlevel diff. Clay	0.705	0.393	-0.055	*1*	0.811	0.154
Bending M. Clay	0.676	0.622	0.164	0.811	*1*	0.417
Deform. Clay	0.112	0.677	**0.923**	0.154	0.417	*1*

Test 6	Waterlevel diff. CaSi	Bending M. CaSi	Deform. CaSi	Waterlevel diff. Clay	Bending M. Clay	Deform. Clay
Waterlevel diff. CaSi	*1*	0.594	0.271	0.877	0.835	0.548
Bending M. CaSi	0.594	*1*	**0.381**	0.525	0.773	0.644
Deform. CaSi	0.271	0.381	*1*	0.240	0.322	0.228
Waterlevel diff. Clay	0.877	0.525	0.240	*1*	0.883	0.546
Bending M. Clay	0.835	0.773	0.322	0.883	*1*	**0.729**
Deform. Clay	0.548	0.644	0.228	0.546	0.729	*1*

Test 7	Waterlevel diff. CaSi	Bending M. CaSi	Deform. CaSi	Waterlevel diff. Clay	Bending M. Clay	Deform. Clay
Waterlevel diff. CaSi	*1*	0.756	0.399	0.631	0.745	0.489
Bending M. CaSi	0.756	*1*	0.617	0.483	0.765	0.583
Deform. CaSi	0.399	0.617	*1*	0.258	0.449	**0.684**
Waterlevel diff. Clay	0.631	0.483	0.258	*1*	0.832	0.497
Bending M. Clay	0.745	0.765	0.449	0.832	*1*	0.601
Deform. Clay	0.489	0.583	**0.684**	0.497	0.601	*1*

Test 8	Waterlevel diff. CaSi	Bending M. CaSi	Deform. CaSi	Waterlevel diff. Clay	Bending M. Clay	Deform. Clay
Waterlevel diff. CaSi	*1*	0.571	0.760	0.972	0.970	0.730
Bending M. CaSi	0.571	*1*	0.249	0.556	0.562	0.229
Deform. CaSi	0.760	0.249	*1*	0.739	0.735	**0.983**
Waterlevel diff. Clay	0.972	0.556	0.739	*1*	0.997	0.708
Bending M. Clay	0.970	0.562	0.735	0.997	*1*	0.704
Deform. Clay	0.730	0.229	**0.983**	0.708	0.704	*1*

Test 9	Waterlevel diff. CaSi	Bending M. CaSi	Deform. CaSi	Waterlevel diff. Clay	Bending M. Clay	Deform. Clay
Waterlevel diff. CaSi	*1*	0.784	0.396	0.880	0.876	0.694
Bending M. CaSi	0.784	*1*	0.372	0.693	0.739	0.649
Deform. CaSi	0.396	0.372	*1*	0.352	0.358	0.691
Waterlevel diff. Clay	0.880	0.693	0.352	*1*	0.967	0.699
Bending M. Clay	0.876	0.739	0.358	0.967	*1*	**0.774**
Deform. Clay	0.694	0.649	**0.691**	0.699	0.774	*1*

Test 10	Waterlevel diff. CaSi	Bending M. CaSi	Deform. CaSi	Waterlevel diff. Clay	Bending M. Clay	Deform. Clay
Waterlevel diff. CaSi	*1*	0.859	0.683	0.636	0.683	0.661
Bending M. CaSi	0.859	*1*	0.672	0.550	0.626	0.639
Deform. CaSi	0.683	0.672	*1*	0.441	0.485	**0.790**
Waterlevel diff. Clay	0.636	0.550	0.441	*1*	0.957	0.579
Bending M. Clay	0.683	0.626	0.485	0.957	*1*	0.630
Deform. Clay	0.661	0.639	**0.790**	0.579	0.630	*1*

G

Appendix: Plots bending moment vs. recorded deformation

Below all plots are presented showing the relationship between the computed bending moment and the recorded deformation per test per wall. In the plots below the results of sensor P2 and sensor P3 are averaged just as the results of sensor P4 and sensor P5 are. Sensor P1 and sensor P6 were placed closer to the window. For completeness these sensors are still shown.

As the effect of the wall ties is unknown it is not clear if part of the bending moment transferred to the other wall section and influenced the corresponding deformations. As such the behaviour of the other wall is plotted in the same graph as well.

G.1. Clay wall

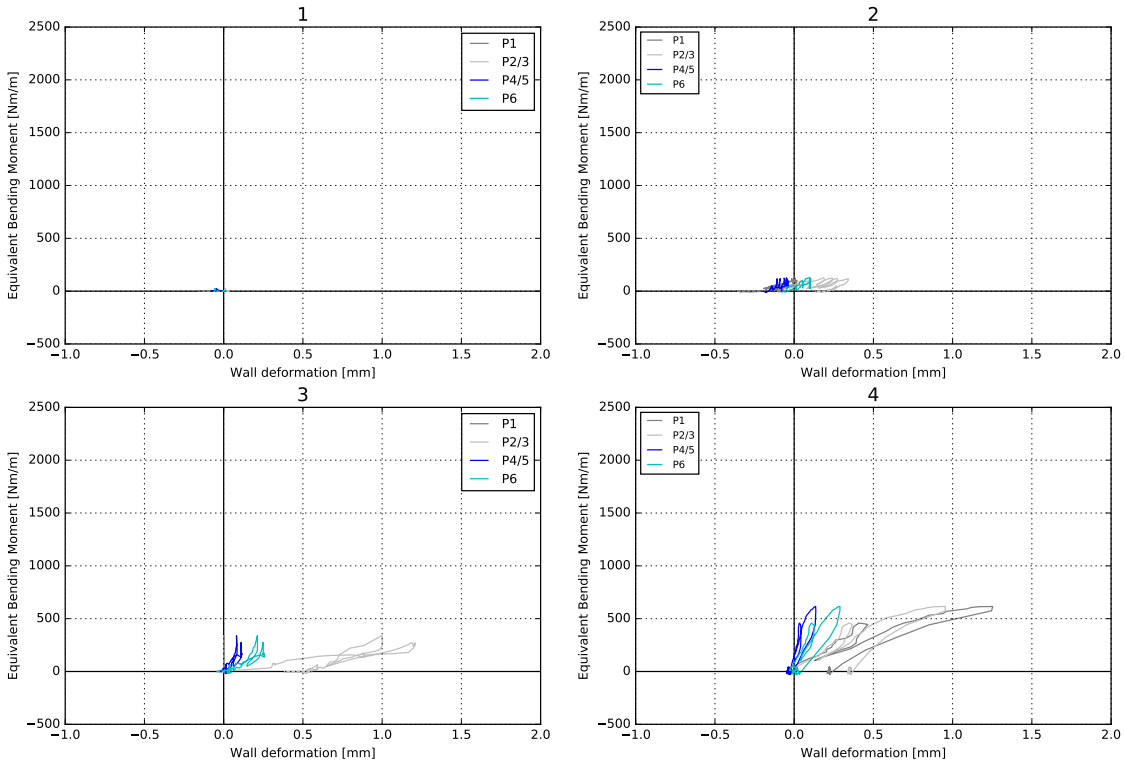

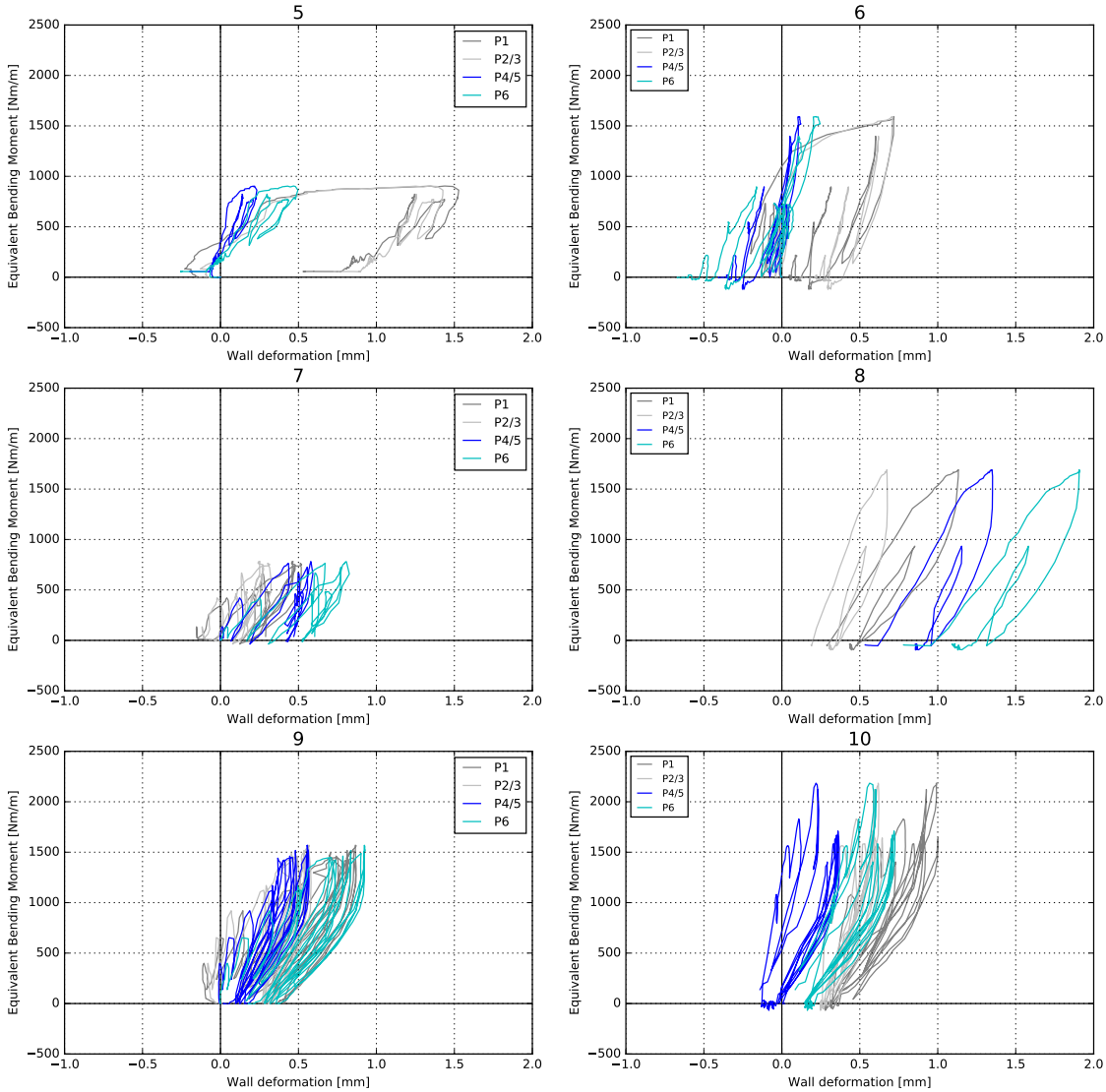

Figure G.1: The equivalent bending moment plotted against the clay wall deformations. The plots clearly show hysteresis. Note that sensor P6 that was placed close to the window records greater displacements, but also has a greater start value.

G.2. Calcium silicate wall

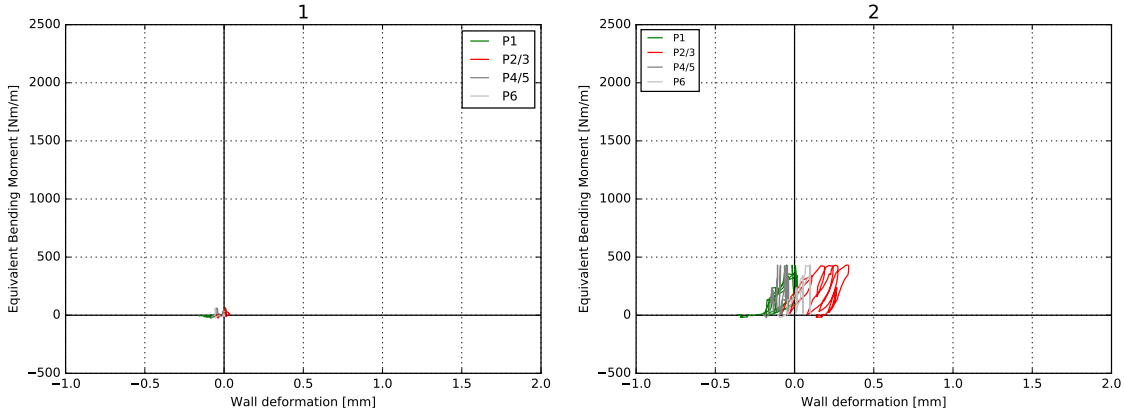

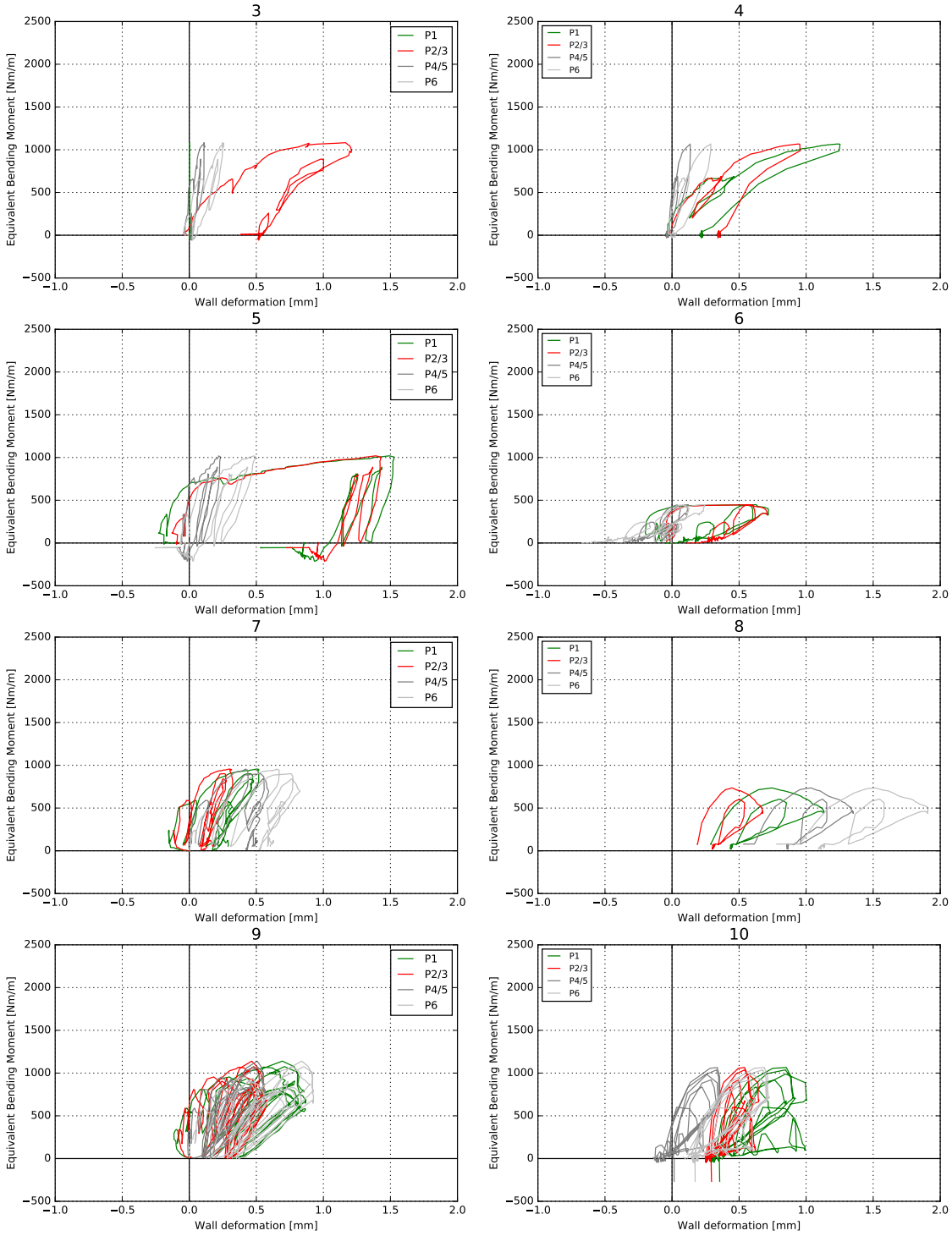

Figure G.2: The equivalent bending moment plotted against the CaSi wall deformations. The plots clearly show hysteresis. Note that sensor P1 that was placed close to the window records greater displacements, but also has a greater start value. In graph 3 the deformations recorded by sensor P1 were not thrust-worthy and as such were removed from the plot.

H

Appendix: Results bond wrench tests

H.1. Complete lab results

Of every brick type one of the nine specimen broke during transport and two specimens broke during installation. For the calcium silicate couplets this meant that six specimens delivered sufficient result; for the clay bricks the same holds as well. The couplets were all measured and weighted leading to the density of the individual couplets. After the test the weight of the brick pulled off , either with or without the mortar attached, was measured too. Further data provided the maximum force that has been subjected to the couplet specimens and the computed bond strength. Since the crack width was measured and kept at a constant rate, the tensile fracture energy could also be computed. For both types of couplets the results are listed in Table H.1 and Table H.2.

Although the couplets were produced by the same mason, from the total weights it can be deducted that the clay couplets were constructed more uniformly with a standard deviation of only 20 grams; for the CaSi couplets this value is 100 grams. Because of the slight differences in weight the density of the CaSi couplets was also slightly deviating. From the weight pulled off it can be concluded whether or not the mortar was pulled of the bottom brick or top brick, since the mortar apparently adds an average weight of 352 grams to the CaSi top brick and 365 grams to the clay top brick (Figure H.1); these values also indicate that the mortar layer in both types of bricks is similar.

Specimen	**Density [kg/m3]**	**Total Weight [kg]**	**Weight pulled off [kg]**	**Max. subjected force [N]**	**Bond strength [MPa]**	**Tensile fracture energy [N/mm]**
CS_A	1898.8	6.095	2.835	-	-	-
CS_B	1845.8	5.925	2.780	8.66	0.005	0.0004
CS_C	1842.7	5.915	3.090	8.29	0.005	0.0014
CS_D	1831.8	5.880	3.270	-	-	-
CS_E	1908.1	6.125	3.080	10.97	0.007	0.0008
CS_F	1828.7	5.870	3.195	5.65	0.002	0.0006
CS_G	1883.2	6.045	2.840	12.48	0.009	0.0010
CS_H	1869.2	6.000	3.220	9.78	0.006	0.0007
Average	*1863.51*	*5.98*	-	*9.31*	*0.006*	*0.0008*
st. deviation	*30.75*	*0.099*	-	*2.36*	*0.003*	*0.0003*
c.o.v.	*0.017*	*0.017*	-	*0.254*	*0.470*	*0.4149*

Table H.1: Most important lab results of the tested CaSi couplets

Specimen	Density [kg/m3]	Total weight [kg]	Weight pulled off [kg]	Max. subjected force [N]	Bond strength [MPa]	Tensile fracture energy [N/mm]
Clay_A	1580.1	3.65	1.630	-	-	-
Clay_B	1569.3	3.625	2.005	156.61	0.17	0.009
Clay_C	1593.1	3.68	2.005	14.94	0.01	0.001
Clay_D	1593.1	3.68	1.630	-	-	-
Clay_E	1597.4	3.69	2.030	34.46	0.03	0.001
Clay_F	1590.9	3.675	1.645	328.75	0.37	0.046
Clay_G	1584.4	3.66	1.685	29.51	0.03	0.001
Clay_H	1588.7	3.67	1.650	169.90	0.19	0.012
Average	*1587.1*	*3.67*	-	*91.77*	*0.13*	*0.012*
st. deviation	*8.43*	*0.02*	-	*109.75*	*0.14*	*0.017*
c.o.v.	*0.005*	*0.005*	-	*1.19*	*1.02*	*1.49*

Table H.2: Most important lab results of the tested Clay couplets

Although the previous parameters indicate a sufficient uniform set of couplets, the mechanical properties do not. While the maximum force that has been subjected onto the couplets looks uniform on the calcium silicate bricks, the values deviate a lot from the ones obtained from the clay specimens. Here outliers of 328.75 N were recorded before the couplet broke, leading to a standard deviation of 109.75 N. Inherently, this leads to bond strengths and fracture energy values that are significantly different depending on the type of brick. Note the coefficient of variation is almost 0.5 for the bond strength (CaSi) and the bond strength of the clay couplets record a c.o.v. of 1.

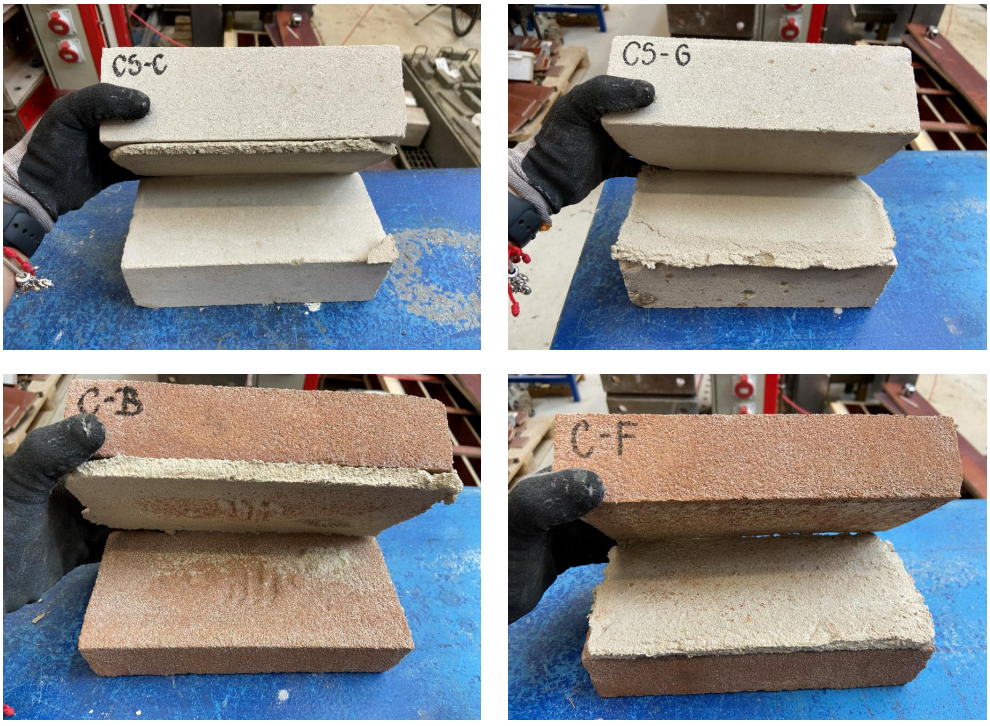

Figure H.1: Various pictures of failure mode A where the top brick was pulled of the mortar and failure mode B where the top brick and mortar were pulled of the bottom brick.

Appendix: Analytical model script

I.1. Main script for two sided water level

```
restart;
u4 := diff(u(x), x$4) = q0*c;
u0 := dsolve(u4); u0 := u(x)=(1/24)*q0*c*x^4+(1/6)*B1*x^3+(1/2)*B2*x^2+B3*x+B4;
u0; diff(u0, x); diff(u0, x$2); diff(u0, x$3); diff(u0, x$4);
uw4 := diff(uw(x), x$4) = q0*c;
uw0 := dsolve(uw4); uw0 := u2(x)=(1/24)*q0*c*x^4+(1/6)*B5*x^3+(1/2)*B6*x^2+B7*x+B8;
uw0; diff(uw0, x); diff(uw0, x$2); diff(uw0, x$3); diff(uw0, x$4);
w4 := diff(w(x), x$4) = q0*(a+b+c)-q0*(a+b+c)*x*(1/(a+b+c));
w0 := dsolve(w4);
w0; diff(w0, x); diff(w0, x$2); diff(w0, x$3); diff(w0, x$4);
v4 := diff(v(x), x$4) = 0;
v0 := dsolve(v4); v0 := v(x) = (1/6)*c1*x^3+(1/2)*c2*x^2+c3*x+c4;
v0; diff(v0, x); diff(v0, x$2); diff(v0, x$3); diff(v0, x$4);
z4 := diff(z(x), x$4) = 0;
z0 := dsolve(z4); z0 := z(x) = (1/6)*c5*x^3+(1/2)*c6*x^2+c7*x+c8;
z0; diff(z0, x); diff(z0, x$2); diff(z0, x$3); diff(z0, x$4);

eq1 := 0 = subs(x = 0, rhs(u0));
eq2 := subs(x = 0, rhs(diff(u0, x$1)))*ka = ei*subs(x = 0, rhs(diff(u0, x$2)));
eq3 := subs(x = a+b+c, d*rhs(diff(v0, x$1)))*kc =
-ei*subs(x = a+b+c+d, rhs(diff(v0, x$2)));
eq4 := subs(x = a+b+c+d, rhs(v0)) = 0;
Interface1 := ei*subs(x = a, rhs(u0)) = eired*subs(x = a, rhs(uw0));
Interface2 := ei*subs(x = a, rhs(diff(u0, x$1))) =
            eired*subs(x = a, rhs(diff(uw0, x$1)));
Interface3 := ei*subs(x = a, rhs(diff(u0, x$2))) =
            eired*subs(x = a, rhs(diff(uw0, x$2)));

Interface4 := ei*subs(x = a, rhs(diff(u0, x$3))) =
            eired*subs(x = a, rhs(diff(uw0, x$3)));
Interface5 := subs(x = a, rhs(uw0)) = subs(x = a, rhs(w0));
Interface6 := subs(x = a, rhs(diff(uw0, x$1))) = subs(x = a, rhs(diff(w0, x$1)));
Interface7 := subs(x = a, rhs(diff(uw0, x$2))) = subs(x = a, rhs(diff(w0, x$2)));
```

```
Interface8 := subs(x=a, rhs(diff(uw0, x$3))) = subs(x=a, rhs(diff(w0, x$3)));
Interface9 := subs(x = a+b, rhs(w0)) = subs(x = a+b, rhs(v0));
Interface10 := subs(x = a+b, rhs(diff(w0, x$1))) =
            subs(x = a+b, rhs(diff(v0, x$1)));
Interface11 := subs(x = a+b, rhs(diff(w0, x$2))) =
            subs(x = a+b, rhs(diff(v0, x$2)));
Interface12 := subs(x = a+b, rhs(diff(w0, x$3))) =
            subs(x = a+b, rhs(diff(v0, x$3)));
Interface13 := eired*subs(x=a+b+c, rhs(v0)) = ei*subs(x=a+b+c, rhs(z0));
Interface14 := eired*subs(x = a+b+c, rhs(diff(v0, x$1))) =
               ei*subs(x = a+b+c, rhs(diff(z0, x$1)));
Interface15 := eired*subs(x = a+b+c, rhs(diff(v0, x$2))) =
               ei*subs(x = a+b+c, rhs(diff(z0, x$2)));
Interface16 := eired*subs(x = a+b+c, rhs(diff(v0, x$3))) =
               ei*subs(x = a+b+c, rhs(diff(z0, x$3)));

k_rot:=?:  EI:=?: waterheightIN:=?:  waterheightOUT:=?:
q0:=9.81*10"^(3):bottomheight:=0.42: topheight:=0.71:

solution := solv({eq1,eq2,eq3,eq4,Interface1,Interface2,Interface3,
Interface4,Interface5,Interface6,Interface7,Interface8,Interface9
Interface10,Interface11,Interface12,Interface13,Interface14,Interface15,
Interface16}, {B1,B2,B3,B4,B5,B6,B7,B8,_C1,_C2,_C3,_C4,c1,c2,c3,c4,c5,c6,
c7,c8})

ud0 := evalf(subs(a=waterheightIN, b=waterheightOUT-waterheightIN,
subs(a=bottomheight, b=waterheightIN-a, c=waterheightOUT-waterheightIN,
d=2.6-waterheightOUT-topheight, e=topheight, ka=k_rot, kc=k_rot, ei=EI,
eired = [1 .. 4]), rhs(u0)));
uwd0 := evalf(subs(a=waterheightIN, b=waterheightOUT-waterheightIN,
subs(a=bottomheight, b=waterheightIN-a, c=waterheightOUT-waterheightIN,
d=2.6-waterheightOUT-topheight, e=topheight, ka=k_rot, kc=k_rot, ei=EI,
eired = [5 .. 8]), rhs(uw0)));
wd0 := evalf(subs(a=waterheightIN, b=waterheightOUT-waterheightIN,
subs(a=bottomheight, b=waterheightIN-a, c=waterheightOUT-waterheightIN,
d=2.6-waterheightOUT-topheight, e=topheight, ka=k_rot, kc=k_rot, ei=EI,
eired = [8 .. 12]), rhs(w0)));
vd0 := evalf(subs(a=waterheightIN, b=waterheightOUT-waterheightIN,
subs(a=bottomheight, b=waterheightIN-a, c=waterheightOUT-waterheightIN,
d=2.6-waterheightOUT-topheight, e=topheight, ka=k_rot, kc=k_rot, ei=EI,
eired = [12 .. 16]), rhs(v0)));
zd0 := evalf(subs(a=waterheightIN, b=waterheightOUT-waterheightIN,
subs(a=bottomheight, b=waterheightIN-a, c=waterheightOUT-waterheightIN,
d=2.6-waterheightOUT-topheight, e=topheight, ka=k_rot, kc=k_rot, ei=EI,
eired = [16 .. 20]), rhs(z0)));

W := piecewise(x < 0, 0, 0<=x and x<a,ud0/(0.1e-2*EI), a<x and x<=b,
ud0/(0.1e-2*EI), b < x and x <= c, wd0/(0.1e-2*EI), c < x and x <= d,
vd0/(0.1e-2*EI), d < x and x <= e, zd0/(0.1e-2*EI), x > 2.6, 0);
```